

Artificial Intelligence-Based Condition Monitoring Techniques for Powertrains in Electric Vehicles

Wangjie Lang

PhD

University of York
Physics, Engineering and Technology
September 2023

Abstract

With the rapid development and wide application of electric vehicles (EVs), condition monitoring and fault diagnosis of EV motors have become key tasks to ensure the reliability and safety of EVs. The aim of this study is to propose an integrated approach to achieve accurate monitoring of electric vehicle motor status and timely diagnosis of faults. This research utilizes a variety of data-driven methods including few-shot learning and graph neural networks to improve the reliability and efficiency of these systems. The first segment explores the use of AI in fault detection and diagnosis (FDD), particularly in Permanent Magnet Synchronous Motors (PMSMs). By employing a hybrid few-shot learning network that amalgamates model-driven and data-driven methods, the research addresses the limitations in acquiring sufficient quality data for fault diagnosis. It particularly focuses on detecting Voltage Source Inverter (VSI) open-circuit faults, enhancing diagnostic certainty through attention-based vision transformer models. The second part delves into vibration analysis, a vital aspect of motor condition monitoring. It introduces an attention-based spatial-spectral graph convolutional network (ASSGCN) aimed at reducing the number of required sensors while maintaining accurate vibration signal reconstruction. The model investigates the spectral features and spatial configurations of the vibration signals, predicting them at different sensor sampling points effectively. Lastly, the research presents a spatial-spectral-based inductive graph neural network specifically designed to tackle the challenges of high evaluation accuracy with fewer vibration sensors. This algorithm aggregates and extracts features of sensor graph signals and employs convolutional networks for reconstructing vibration signals at virtual sensor points. Collectively, these approaches contribute to the reduction of operational costs, enhancement of system reliability, and improvement of fault diagnostic accuracy. Experimental verifications have been carried out on a 21 kW IPMSM testing rig equipped with Brüel & Kjær's vibration sensing technology, confirming the efficacy of the proposed methods. These techniques pave the way for more efficient, reliable, and cost-effective condition monitoring and fault detection in electric motor systems across various applications.

Key words: Electric vehicle; Fault diagnosis; Data-driven algorithm; Vibration signal

Table of Contents

Abstract.....	2
Table of Contents.....	3
List of Tables.....	6
List of Figures.....	7
Acknowledgements.....	9
Declaration.....	10
List of Publications.....	11
Nomenclature.....	12
Chapter 1 Introduction.....	14
1.1. Motivation.....	14
1.2. Dissertation Outline.....	16
Chapter 2 Review of Artificial Intelligence-based Technique for Condition Monitoring of EV Motors	18
2.1. Introduction.....	18
2.2. Electric Motor and fault types.....	22
2.3. Traditional Fault monitoring techniques.....	25
2.4. Feature Extraction in.....	28
2.5. Fault Classification.....	34
2.5.1. Support vector machine (SVM) based approach.....	34
2.5.2. MLP/KNN/RF-based approach.....	38
2.5.3. Convolutional Neural Network (CNN).....	41
2.5.4. Recurrent neural network (RNN).....	45
2.5.5. Generative Adversarial Network (GAN).....	47
2.5.6. Deep Belief Network (DBN).....	50
2.5.7. Autoencoder.....	53
2.6. Other AI-based approaches.....	59
2.6.1. Adaptive neuro-fuzzy system (ANFIS).....	59
2.6.2. Compressed sensing.....	61

Table of Contents

2.6.3.	Infrared thermography and temperature estimation strategy	62
2.6.4.	Transfer learning.....	64
2.6.5.	GA-based approach.....	64
2.6.6.	Artificial Ant System (AAS) and dictionary learning.....	65
2.7.	Discussion And Future Development.....	67
Chapter 3 Hybrid Model for Inverter Fault Diagnosis of EV Powertrain.....		70
3.1.	Introduction	71
3.2.	Open-circuit Fault Analysis in PMSM Drive System.....	74
3.3.	The Proposed Model-Data-Hybrid-Driven Method	77
3.3.1.	Luenberger Observer for the diagnosis variables.....	77
3.3.2.	Transformer-Based Machine Learning Model.....	78
3.3.3.	Mechanism of the hybrid method	83
3.4.	Experimental verification	84
3.4.1.	Model-Based Residual Analysis	86
3.4.2.	Model Optimization of Network Hyperparameters	89
3.4.3.	Analysis of feature extraction capability under restricted data	92
3.5.	Conclusion	95
Chapter 4 Artificial Intelligence Neural Network Based Virtual Vibration Sensor Reconstruction in EV Powertrain		96
4.1.	Introduction	96
4.2.	Motor Vibration Analysis.....	100
4.2.1.	Stator Structure Vibration Model.....	100
4.2.2.	Stator vibration modal analysis	103
4.3.	Spectral-spatial Graph Model for Vibration Signal Reconstruction.....	104
4.3.1.	Spectral-Spatial Attention Module	106
4.3.2.	Spectral-Spatial Convolution Module.....	107
4.3.3.	Sensor Cluster Adjacency Matrix Construction	109
4.3.4.	Overall structure and training strategy.....	109
4.4.	Experimental setup and validation	110
4.4.1.	Data Preprocessing and Description	112
4.4.2.	Prediction performance with multiple operation conditions.....	114

Table of Contents

4.5. Conclusion 121

Chapter 5 The Study of Sensor Distribution Patterns and Random Masking Based on Vibration Sensor Reconstruction 122

5.1. Introduction 123

5.2. Signal Reconfiguration Kriging Problem Migration 126

5.2.1. Modal Experiment Analysis 127

5.2.2. Transfer Path Analysis 128

5.2.3. Kriging Problem Description 131

5.3. The Multiscale-ssgen Model 132

5.3.1. TPA-based Inertance Adjacency Matrix Construction 133

5.3.2. Attention-based Feature Fusion Module 135

5.3.3. Spatial-Spectral (SS) Diffusion Graph Convolution 137

5.3.4. Training Strategy 138

5.4. Experimental Verification 139

5.4.1. Data Description 139

5.4.2. Accuracy of Reconstruction Performance with Different Operating Conditions 141

5.4.3. Performance Comparison Under Different Sensor Organization Numbers 143

5.4.4. Various Sensor Distribution Discussion 145

5.5. Conclusion 147

Chapter 6 Conclusions and Future Work 148

6.1. Conclusion 148

6.2. Future Work 151

Reference 152

List of Tables

TABLE 2-1 Highlight of Feature Extraction Method.....	30
TABLE 2-2 Highlight of Classical Machine Learning Method.....	39
TABLE 2-3 Highlight of Deep Learning.....	56
TABLE 2-4 Highlight of Other AI-Based Method.....	66
TABLE 3-1 The Parameters of The Experimental PMSM.....	84
TABLE 3-2 Faulty State and Label.....	85
TABLE 3-3 Fault Diagnosis Accuracy Under Different Network Structures and Hyperparameters.....	90
TABLE 3-4 Fault Diagnosis Accuracy Under Different Network Structures and Hyperparameters.....	90
TABLE 3-5 Performance Comparison with Different Models.....	91
TABLE 4-1 Experimental Setup Parameters.....	111
TABLE 4-2 Comparison of Results.....	114
TABLE 4-3 Comparison of Results.....	115
TABLE 4-4 Experimental Accuracy and Computational Burden.....	118
TABLE 4-5 Comparison Results.....	119
TABLE 5-1 Modal Experimental Analysis.....	128
TABLE 5-2 Experimental Setup Parameters.....	139
TABLE 5-3 Experimental Conditions Description.....	140
TABLE 5-4 Experimental Results.....	143
TABLE 5-5 Experimental Results.....	144

List of Figures

Fig. 2-3. General flowchart of FDD techniques.....	22
Fig. 2-4. Typical faults: (a) Stator winding short-circuit (WSC). (b) Rotor crack fault (CRF) [226].	23
Fig. 2-5. Flowchart of traditional Machine learning and Deep learning.....	34
Fig. 2-6. The optimal hyperplane for binary classification by SVM.....	35
Fig. 2-7. The structure of KNN.	39
Fig. 2-8. The basic structure of the random forest.	40
Fig. 2-9. The basic structure diagram of CNN.	42
Fig. 2-10. The basic structure diagram of RNN.	45
Fig. 2-11. The basic structure diagram of GAN.	48
Fig. 2-12. The basic structure diagram of DBN.....	52
Fig. 2-13. The basic structure diagram of AE.....	54
Fig. 2-14. The entire process test bench.	63
Fig. 3-1. Current loop in healthy and fault conditions.....	75
Fig. 3-2. Responses in the faulty half of a fundamental period.....	75
Fig. 3-3. Structure of transformer encoder.....	76
Fig. 3-4. Flowchart of model-data-hybrid-driven diagnosis method.....	79
Fig. 3-5. The experimental platform.....	83
Fig. 3-6. Dynamic responses under load change between 3 N.m and 6 N.m (a) phase A estimate and actual current. (b) phase A residuals.....	84
Fig. 3-7. Three phase residuals under different fault states (a) fault T1 state. (b).....	84
Fig. 3-8. Phase A estimate and actual current under different fault states (a) fault T1 state. (b) fault T1&T4 state. (c) fault T1&T3 state.....	85
Fig. 3-9. Accuracy and loss curve in training and testing process.....	86
Fig. 3-10. Performance comparison with classical few-shot learning methods with 5 steps adaptations.....	87
Fig. 3-11. (a) Confusion matrix of Vit for the diagnosis of each category. (b) Confusion matrix of the proposed method for the diagnosis of each category.....	93
Fig. 4-1. Classification of vibration analysis methods [22].	99
Fig. 4-2. Shell micro-element segment.....	101
Fig. 4-3. The basic frame of the proposed algorithm.	104
Fig. 4-4. Graph data for sensor cluster distribution.	105
Fig. 4-5. The framework of the proposed ASSGCN.....	106
Fig. 4-6. The spectral-spatial correlation diagram of the vibration signal.....	110
Fig. 4-7. Experimental setup.	111
Fig. 4-8. Sampling dataset of 10 sensor distribution points in the frequency domain.	112
Fig. 4-9. Measured and reconstructed value of OCF under the condition of 6000rpm without load.	116
Fig. 4-10. Measured and reconstructed value of acceleration response under the condition of	

6000rpm without load.....	116
Fig. 4-11. Measured and reconstructed value of acceleration response under the condition of 8200rpm with a load of 48N.	116
Fig. 4-12. Measured and reconstructed value of OCF under the condition of 8200rpm with a load of 48N.	117
Fig. 4-13. Spectrum of OCF under the condition of 6000rpm without load for sensor point 1 and point 10.....	119
Fig. 4-14. Spectrum of OCF under the condition of 8200rpm without load for sensor point 9 and point 10.....	119
Fig. 4-15. Curve of MAE training loss with different epochs.....	120
Fig. 5-1. Diagram of vibration monitoring	126
Fig. 5-2. Stator transfer path diagram.	127
Fig. 5-3. Source-path-contribution flowchart of the motor system.....	129
Fig. 5-4. Diagram of data-driven for signal reconstruction in vibration testing.	133
Fig. 5-5. Diagram of different sensor distribution.....	135
Fig. 5-6. Different adjacency information.....	136
Fig. 5-7. Multiscale feature fusion module.....	137
Fig. 5-8. Experiment rig.....	140
Fig. 5-9. SPC diagram in collecting data.....	141
Fig. 5-10. Measured and reconstructed value of acceleration response under the condition of 8200rpm without load.....	141
Fig. 5-11. Spectrum of acceleration response under the condition of 8200rpm without load for sensor point 9 and point 10.....	142
Fig. 5-12. Predicted error in different sensor numbers.....	145
Fig. 5-13. Heatmap for different sensor distribution and operating conditions.....	147

Acknowledgements

First of all, I would like to thank my main supervisor, Dr. Hu Yihua. He gave me valuable guidance on my academic path, turning me from a clueless student into an independent scientific researcher. At the same time, he gave me care and encouragement in life. I am grateful for his valuable comments and suggestions on my research as well as my life and career. I am honored to be his doctoral student, and I hope to live up to his high expectations and beliefs through my achievements. Secondly, I would also like to thank my second major supervisors, Dr. Mohammad Nasr Esfahani and Dr. Hamed Ahmadi, for their strong support and academic guidance.

I would also like to thank my family, my father and mother, who have always given me unrequited support and love, allowing me to move forward on my academic path without hesitation. During many dark times in my academic career, their encouragement helped me regain my confidence. In addition, I would also like to express my gratitude to my girlfriend, Ms. Wang Xuan. I am so grateful for her patience, tolerance, companionship, and warm love. I wouldn't have gotten to this point without her accompany. Wish her success in her academic pursuits as well. Many thanks to my collaborator Dr. Quanfeng Li for providing necessary support and advice. Special thanks also go to my talented and lovely colleagues and friends, especially Mr. Mei Shangming, Mr. Zhang Xiaotian, Mr. Liu Hongzuo, Mr. Nie Yu, Mr. Alexander and Mr. Zhang Zeliang, with whom I had many fruitful discussions and pleasant time.

Finally, I would like to express my sincere thanks to the Department of Electrical Engineering, University of York for their support. Special thanks to Ms. Camilla Danese for her grace, patience and kindness. And thanks to the friends I met along the way. I wish you all the best.

Declaration

I declare that this thesis is a presentation of original work and I am the sole author. This work has not previously been presented for an award at this, or any other, University. All sources are acknowledged as References.

Main contents in Chapter 2 have been submitted to IEEE Transactions on Transportation Electrification. Title is “Artificial Intelligence-Based Technique for Fault Detection and Diagnosis of EV Motors: A Review ”(Published)

Main contents in Chapter 2 have been submitted to IET book Title is “Artificial Intelligence-Based Technique for Fault Detection and Diagnosis of EV Motors: A Review ”(Published)

Main contents in Chapter 3 have been submitted to IEEE Transactions on Transportation Electrification. Title is “A Hybrid Model Based Siamese Network Residual Analysis for Inverter Fault Diagnosis of EV Powertrain ”

Main contents in Chapter 4 have been submitted to IEEE Transactions on Industrial Electronics. Title is “ASSGCN Model Based Vibration Signal Reconstruction in Motor Vibration Testing ”(Accepted)

Main contents in Chapter 5 have been submitted to IEEE Transactions on Industrial Electronics. Title is “Inductive Graph Neural Network for Virtual Vibration Sensor Reconstruction in PMSM Powertrain ”

List of Publications

- [1] **W. Lang**, Y. Hu, C. Gong, X. Zhang, H. Xu and J. Deng, "Artificial Intelligence-Based Technique for Fault Detection and Diagnosis of EV Motors: A Review," *IEEE Transactions on Transportation Electrification*, vol. 8, no. 1, pp. 384-406, March 2022, doi: 10.1109/TTE.2021.3110318.
- [2] **W. Lang**, Y. Hu, Z. Zhang, G. Chen, J. Si and H. Wen, "A Hybrid Model Based Siamese Network Residual Analysis for Inverter Fault Diagnosis of EV Powertrain" *IEEE Transactions on Transportation Electrification* (Under Review)
- [3] **W. Lang**, Y. Hu, Q. Li, A. Wireko-Brobby and M. Alkahtani, "ASSGCN Model Based Vibration Signal Reconstruction in Motor Vibration Testing," *IEEE Transactions on Industrial Electronics* (accepted)
- [4] **W. Lang**, Y. Hu, Q. Li and Y. Salamah "Inductive Graph Neural Network for Virtual Vibration Sensor Reconstruction in PMSM Powertrain," *IEEE Transactions on Industrial Electronics* (Under Review)
- [5] Y. Hu, **W. Lang**, X. Zhang "AI Techniques in EV Motor and Inverter Fault Detection and Diagnosis" *IET book* (Under Production)

Nomenclature

T	Kinetic energy
U	Potential energy
φ	Energy consumed by damping
K	Stiffness matrix
C	Damping matrix
M	Mass matrix
F_1	Excitation force
Y	Displacement
n	Number of stator slots
m_c	Mass of a slot
p_m	Electromagnetic force
f_1, f_2	Shear forces
ρ_1, ρ_2	Densities
R_1, R_2	Radius
a, b	Lengths
$\zeta_1, \zeta_2, \zeta_3$	Damping ratios
dm_1	Mass of shell micro-element segment
$f_i(t)$	Excitation force at the i^{th} source point
$H_{m,i}(t)$	Transfer function between the i^{th} source point and the m^{th} receiver point
R_j	j^{th} output of the system
F_i	i^{th} input to the system
H_{ij}	Transfer function from F_i to R_j
Z_i	Observed value at discrete point (X_i, Y_i)
Z_o	Estimated value at point (X_o, Y_o)
λ_i	Weight factor
$\epsilon_k^2(Z_o)$	Kriging error
Var	Variance
Cov	Covariance
μ_{ij}	Semi-variance function
L	Inductance
ω_e	Electrical Angular Speed
R_s	Stator Resistance
i_d, i_q	Direct and Quadrature Axis Currents
u_d, u_q	Direct and Quadrature Axis Voltages
ψ_f	Flux linkage due to magnets
$x(t), u(t), y(t)$	State, Control, and Output Vectors
A, B, C, D	State space matrices

Declaration

K	Feedback gain
e, \dot{e}	Error and its derivative
pos	Position
PE	Position Encoding
d_{model}	Dimension of the Model
Q, K, V	Query, Key, Value in attention mechanism
d_k	Dimension of Key space in attention mechanism
W^O, W^Q, W^K, W^V	Weight matrices in attention mechanism
$E_w(x_i, x_j)$	Distance of input sample features
$TE(x)$	Transformed encoder output
$L(y, w, x_i, x_j)$	Loss function
$P(x_i, x_j)$	Similarity output
FC	Fully Connected layer
$Sigm$	Sigmoid function
ViT	Vision transformer

Chapter 1 Introduction

1.1. Motivation

The importance of an electric vehicle motor is a key component of the electric vehicle. Unlike traditional fuel vehicles, electric vehicles rely on a battery-driven electric motor to generate power to run the vehicle. Electric vehicle motors have a high energy conversion efficiency, which provides higher energy utilization compared to internal combustion engines. This makes electric vehicles more efficient, reduces energy waste and environmental pollution, and is important for combating climate change and improving air quality. Electric vehicle motors use electrical energy as a power source, which can be supplied by a variety of renewable energy sources, such as solar and wind. Therefore, electric vehicle motors can reduce dependence on finite fossil fuels and promote energy sustainability. Electric vehicle motors can be precisely controlled and regulated according to driving needs. Through electronic control systems, drivers can achieve precise control of power output, acceleration and braking force, improving driving safety and comfort. However, electric vehicle motors face a number of problems and challenges during use. One of the key issues is the condition monitoring and fault diagnosis of electric motors. As electric motors operate under high loads, high rotational speeds and different operating environments, they may suffer from various faults and damages, such as insulation breakdown, bearing wear and excessive temperatures. Therefore, accurate monitoring of motor status and timely diagnosis of faults are important tasks to ensure the reliability and safety of electric vehicles.

The main objective of this study is to address the challenges of motor condition detection due to insufficient sensor data or positional bias and cost constraints. Data-driven artificial intelligence-based algorithms are developed to reconstruct motor vibration data and perform fault diagnosis and correction. The overview of this research can be summarized as follows:

To review the application of artificial intelligence techniques to motor fault diagnosis: Different fault detection and diagnosis methods are analyzed. The mainstream feature

extraction methods are reviewed, and the application of AI techniques in motor fault diagnosis is described in a larger part, and the three parts of traditional machine learning, deep learning algorithms and hybrid algorithms are reviewed through the theoretical framework. In the deep learning section, almost all the algorithms are based on Artificial Neural Networks (ANN), which are developed and changed to achieve different purposes. The overview work provides a comprehensive understanding of data-driven based algorithms at this stage and lays the foundation for subsequent algorithm development.

To present a hybrid model for VSI open-circuit fault diagnosis: An observer is used to obtain motor fault current residuals as input samples for fault information. A Siamese network based on few-shot learning is constructed for VSI open-circuit fault diagnosis. Current signals in fault states contain uncertain components due to torque pulsations and inputting them as features into the diagnostic model leads to unnecessary redundant diagnosis. By using the residual values as input signals, the uncertain current components can be removed, resulting in better diagnostic performance. Due to the limited experimental conditions, the problem of sparse samples is solved by constructing a few-times learning based on the concatenated network framework. The adopted attention-based algorithm is able to extract global features in the signal and obtain higher output classification performance. However, considering that the variation of system parameters affects the diagnostic performance, the robustness of the hybrid model under the variation of system parameters needs to be further investigated.

To propose an Attention-based Spatial-Spectrogram Convolutional Network (ASSGCN) model to reduce the number of sensors required for motor vibration signal reconstruction: It offers significant cost and time savings for vibration testing in electric powertrain applications. By reducing the number of sensors required, the overall monitoring cost can be reduced without compromising the effectiveness of fault detection and prediction. The proposed ASSGCN model offers a promising solution for reducing vibration testing costs, increasing efficiency and improving the overall understanding of motor vibration characteristics.

To propose an algorithm based on a graphical neural network model combined with multi-scale information fusion: It is proposed for reconstructing the virtual sensor information at the

periphery of the motor stator in vibration testing. The proposed model is capable of mining nonlinear patterns and features in the motor vibration signals. The reconstruction accuracy is improved by learning the complex interactions between nodes and utilizing the connection information between sensors. The effect of the number and distribution of sensors on the reconstruction accuracy may show variability under different operating conditions is explored. The analysis results can be used as virtual sensor signals to provide a reference for evaluating different motor states, thus reducing the cost of installing vibration sensors and improving the efficiency of vibration monitoring.

The challenges of motor condition monitoring in electric vehicles mainly include: 1. Sensor selection and arrangement: selecting appropriate sensors and arranging them correctly on the motor to obtain accurate and reliable motor operating parameters and performance data. 2. Data processing and analysis: processing and analyzing a large amount of data on motor vibration, temperature, current, etc., extracting key features, and performing fault diagnosis and prediction. 3. Through motor condition monitoring and fault diagnosis technology, timely monitoring, fault diagnosis and preventive maintenance of electric vehicle motors can be realized to improve the reliability, safety and maintenance efficiency of electric vehicles, and promote the further development and popularization of electric vehicle technology.

1.2. Dissertation Outline

The dissertation consists of seven chapters. An outline of the structure is organized as follows:

Chapter 1 introduces the motivation of this study. Besides, the main objectives and a brief introduction of the research contents are illustrated.

Chapter 2 reviews the application of AI techniques in motor fault detection and diagnosis (FDD) in recent years is reviewed. AI-based FDD is divided into two main steps: feature extraction and fault classification. The application of different signal processing methods in feature extraction is also discussed. In particular, the application of traditional machine learning

and deep learning algorithms in fault classification is described in detail.

Chapter 3 designs a combined model and data-driven few-shot learning network is proposed to detect voltage source inverter (VSI) open-circuit faults in PMSMs. This method uses the residual obtained from the observation data and the actual measurement data as the original sample to eliminate the influence of harmonics, thereby improving the quality of the input data and reducing the uncertainty of diagnosis. Then, combined with the Siamese network framework, an attention-based visual transformer (ViT) model is applied to explore the association of global features of input samples instead of local features of input samples through signal dimension transformation.

Chapter 4 designs an Attention-based Spatial Spectral Graph Convolutional Network (ASSGCN) model is proposed to reconstruct the vibration signal of a motor by reducing the number of sensors. The three spectral features of the vibration signal are modeled separately, and the correlation of the operating condition force (OCF), acceleration, and vibration impedance matrix is studied and analyzed in the spatial dimension. Through dynamic correlation analysis of spatial configuration and spectral response, the proposed ASSGCN model predicts vibration signals at different sensor sampling points.

Chapter 5 designs a spatial spectrum-based inductive graph neural network for mining the spatial connectivity and spectral correlation of vibration sensor-based clusters. The algorithm efficiently aggregates and extracts sensor map signal features near the target location and reconstructs the vibration signal of the virtual sensor through a convolutional network.

Chapter 6 is the conclusion part. The main contributions of this study are summarized. The future work that can be carried out to further improve the condition monitoring and fault diagnosis technology for preventive maintenance of electric vehicle motors.

Chapter 2 Review of Artificial Intelligence-based Technique for Condition Monitoring of EV Motors

As a bridge for power transmission, the motor drive system plays a crucial role in the safety of electric vehicles. Meanwhile, in order to improve the efficiency and stability of the drive system, more and more research based on artificial intelligence technology is devoted to the fault detection and diagnosis of motor drive system. Therefore, this chapter reviews the application of AI technology in motor fault detection and diagnosis in recent years. AI-based fault detection and diagnosis (FDD) is mainly divided into two steps: feature extraction and fault classification. The application of different signal processing methods in feature extraction is discussed. The application of traditional machine learning and deep learning algorithms in fault classification is particularly detailed. In addition, the characteristics of all the techniques reviewed are summarized. Finally, recent advances, research gaps and future challenges in motor fault monitoring and diagnosis are discussed.

2.1. Introduction

FDD is a condition detection technique that can be used to identify the operating condition of an electric motor, detecting early faults, and making predictions. The purpose of this technology is to detect faults and distinguish different types of faults to make decisions in advance to prevent the occurrence of hazards. In addition, modern industrial technology has been developed significantly, electric motors have been widely used in different areas of industrial systems, e.g. more electric aircraft, electric ships, especially playing a key role in the powertrain of electric vehicles. Fig. 2-1 illustrates the basic architecture of an electric vehicle drive system. The conventional powertrain of an electric vehicle consists of electrical and mechanical systems. The electrical part includes the electric motor, the battery management

unit, the power electronic devices, and the controller module, while the mechanical part includes the transmission and the wheels.

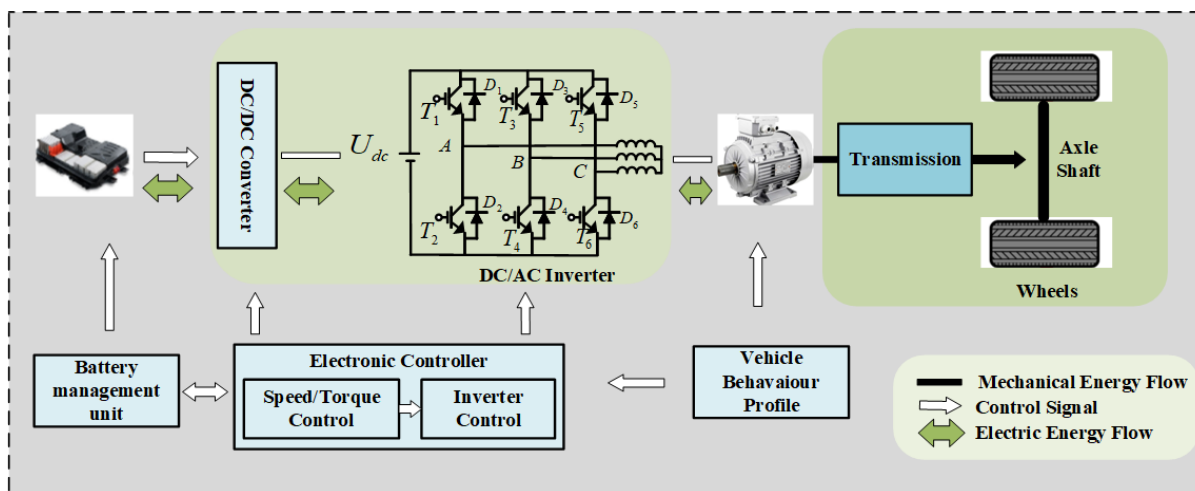


Fig. 2-1. The basic structure of the motor drive system.

Therefore, the motor is the most important component in the conversion of electrical energy to mechanical energy. The operational status and related parameters of the electric machine motor can be monitored and acquired in real-time through an online system. However, as the operating time increases, the possibility of motor failure under different operating conditions rises, threatening the reliability and safety of electric vehicles. Fig. 2-2 indicates the experimental rig for the application of motor drive system FDD techniques, which includes the motor, controller, load, sensors, etc.

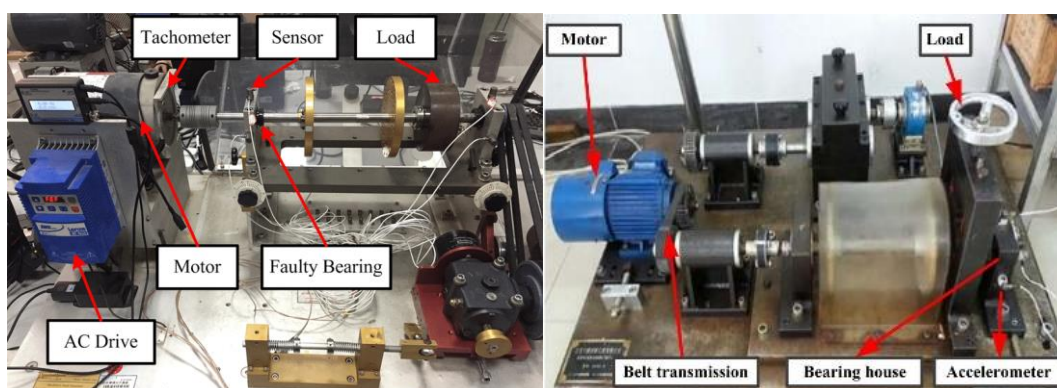


Fig. 2-2. The example of experimental rigs [42][106].

Electric motors suffer from several types of faults [1]. Generally, the two common forms of faults are the rotor and bearing faults in electric motors. The failure of one component of a

motor will lead to a chain reaction, which can fail or even paralysis of the entire equipment system [2]. Therefore, it has become imperative to enhance the safety and reliability of motor drive systems. The effective diagnosis of electrical or mechanical faults in electric motors is necessary [3-6]. For non-invasive motor fault detection and diagnosis techniques, different signals can be analyzed, including temperature analysis, vibration analysis, infrared analysis, current and voltage analysis, electromagnetic field analysis, ultrasonic analysis, etc. Vibration analysis [7-9] and motor current signature analysis (MCSA) [10] [11] are two of the most popular research in this field. Stator current analysis is known for providing non-invasive condition monitoring for EV motors [12-14]. Accurate detection of potential or existing motor faults is an essential measure to maintain safe machine operation. Among the theoretical approaches that have been studied, the technical strategy of motor fault diagnosis in different external environments and operating conditions is a guarantee of improving the reliable operation of the electric machine, however there are certain limitations [15] [16].

In general, the motor FDD techniques are divided into model and data-based methods. Model-based methods for motor fault detection are common in industrial applications. The simplest approach is based on input and output signal processing. If the output of the motor is outside the normal range of variation, the motor is considered faulty or about to fail. Mathematical models are used to describe the output amplitude, phase, frequency, and correlation with the source of the fault, and then these quantities are processed to determine the location and cause of the fault [17]. Moreover, classical methods based on state estimation or process parameter estimation are also commonly used for motor fault detection [18]. The advantage of these methods is that they can drill down in the basic dynamic characteristics of the motor system for real-time diagnosis, but an accurate mathematical model of the motor is required. Therefore, such methods are difficult to implement when the motor system model is uncertain or nonlinear.

In recent years, the data-based approach has gained popularity due to its high practicality. It is a suitable method for incorporating artificial intelligence into FDD. Fig. 2-3 illustrates the general flowchart of FDD techniques.

AI-based FDD is divided into two main steps: 1. Feature extraction. 2. Fault classification. In signal-based feature extraction engineering, the time domain signal is usually converted to the frequency domain signal by discrete Fourier transform. Simultaneously, time and frequency signal analysis become extremely important when the motor is under dynamic and transient conditions. Short-time Fourier transforms (STFT), Hilbert transforms (HT), wavelet transform (WT) and other signal processing techniques have been widely proposed. Furthermore, time-domain FDD analysis is the best choice when using minimal computational resources to process extremely complex and intermittent signals. In addition, AI-based fault classification methods include machine learning, deep learning, fuzzy neural networks, genetic algorithms, and hybrid algorithms, which can address issues that cannot be solved by traditional fault diagnosis methods [19].

Artificial intelligence is the key point of data-driven technologies. Artificial intelligence-based studies have been extensively carried out in industry applications. Especially in electrical system predictive maintenance, using machine learning algorithms to predict equipment failures can help reduce downtime and reduce repair costs [34]. Artificial neural networks use activation functions to predict interactions between artificial neurons. The related weights and biases are used to model the biological neural system. Nonlinear characteristics can be extracted and combined using artificial neural networks, which can be employed to perform classification and regression tasks in the motor drive system. In [20], artificial neural networks (ANN) were applied to track and diagnose external faults in three-phase induction motors. The data of stator voltage, current, and motor speed were used to train the network. Furthermore, the identification and diagnosis of induction motor faults implemented in supervised and unsupervised neural networks have been achieved in [21], as well. The application of neural networks in the classification of partial discharges in motor insulation was studied in [22], where the fault of an induction motor is determined by the imbalance of the inductor current. [23] investigated the state estimation of induction motors based on classical machine learning algorithm with nonlinear state estimators, which is based on stator current and rotor angular velocity measurements. In addition, deep learning (DL) can model and obtain accurate

classification and predictions for complex fault types. Machine fault diagnosis has been effectively implemented using several common deep architectures, including Autoencoder (AE), Recurrent neural network (RNN), Generative Adversarial Network (GAN), Convolutional Neural Network (CNN), and Deep Confidence Network (DBN). Research on artificial intelligence-based techniques is significant for providing valuable research directions, but there is no comprehensive overview of the application of artificial intelligence-based techniques in motor fault detection and diagnosis. It is important to investigate the contributions of different scholars in this field.

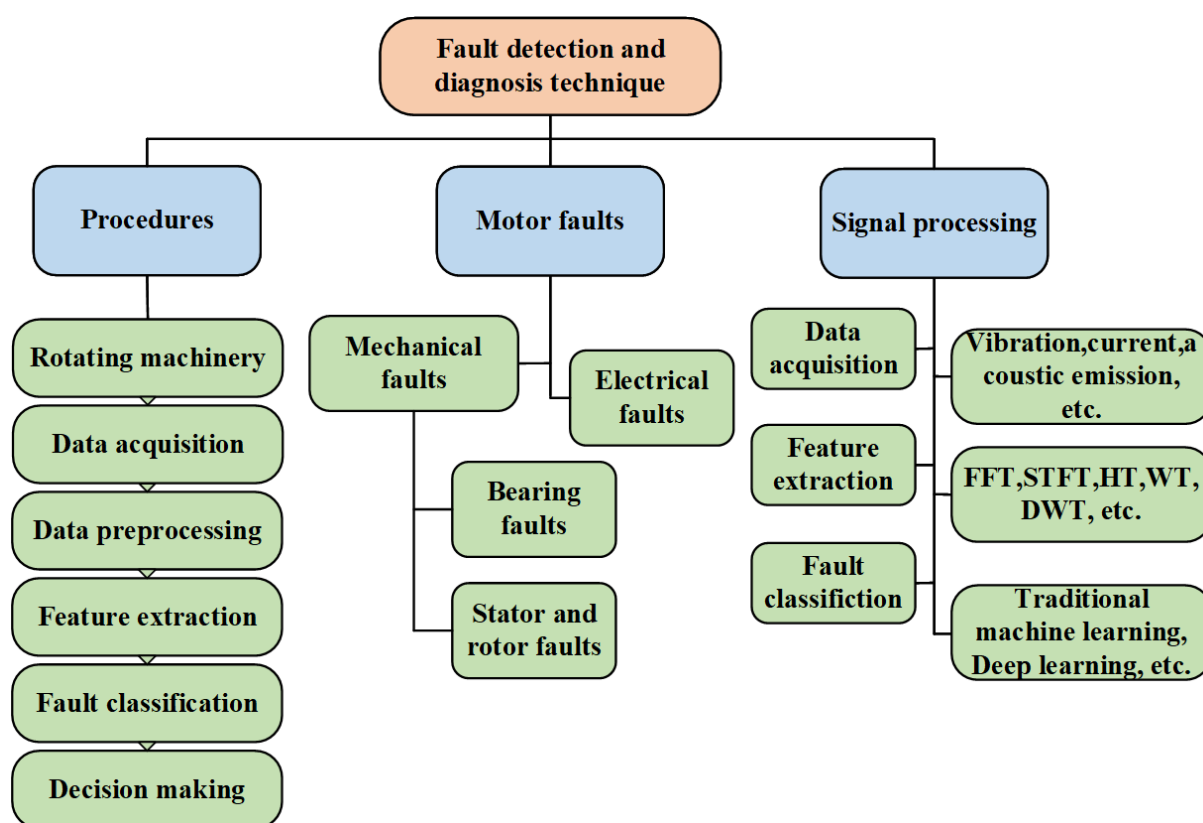


Fig. 2-3. General flowchart of FDD techniques.

2.2. Electric Motor and fault types

In the advanced powertrain system, induction motors (IMs) and permanent magnet synchronous motors (PMSMs) are the two major types of electric vehicle motors. Induction motors are widely used in industry and are characterized by stator and rotor made of laminated

silicon steel sheets and encapsulated with aluminum caps at both ends. Between the stator and the rotor, there are no mechanical elements in connection with each other, the structure is simple with reliable operation. IMs are more efficient and appropriate for high-speed operation than DC motors of the same power. The principle of operation is to generate an induction current in the rotor through the rotating magnetic field of the stator to produce electromagnetic torque, no magnetic field is generated in the rotor, therefore, the rotor speed is less than the synchronous speed. Therefore, it is also called the asynchronous motor. Due to the complex mechanical structure of DC motors which restricts the overall vehicle performance, synchronous motors are gradually becoming popular drive motors. The rotor of PMSMs produces a fixed direction magnetic field, and the stator rotating magnetic field drags the rotor magnetic field to rotate, so the rotor speed is equal to the synchronous speed. PMSM has the advantages of high efficiency, high starting torque, and high power factor.

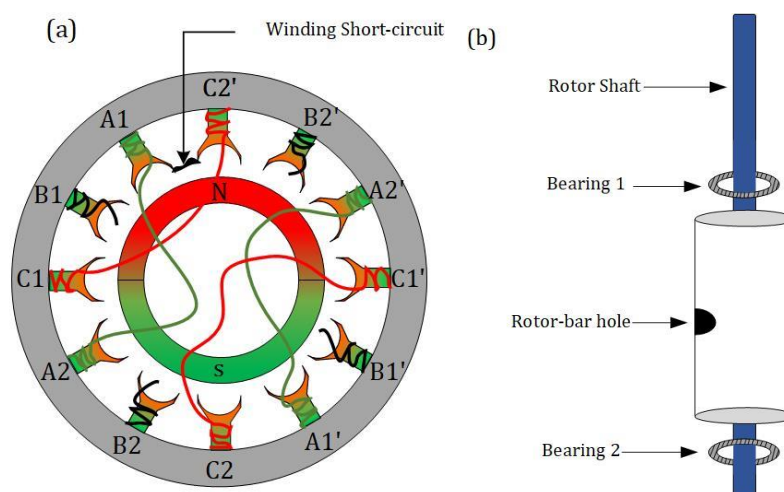


Fig. 2-4. Typical faults: (a) Stator winding short-circuit (WSC). (b) Rotor crack fault (CRF) [226].

Electric motors and drives are affected by many different types of faults: 1) Stator faults can be classified as stator open circuit and the short circuit which lead to stator imbalance and increased resistance connections. Loose electrical parts or poor connections can cause heat and eventually fire. 2) Rotor electrical faults, which include rotor open phase, rotor imbalance due to short circuits or increased resistance connections and broken bars or cracked end rings in induction motors, and rotor magnetic failures such as demagnetization in permanent magnet

synchronous machines. 3) Rotor mechanical faults such as bearings damage, bent shaft, eccentricity, and misalignment. 4) Faults of the power electronic components in the motor drive system. Fig. 2-4 illustrates the two typical faults of stator winding short-circuit (WSC) and rotor crack fault (CRF).

Listed below are the main categories of faults that can be detected with the MCSA. The frequency caused by each type of fault depends on the specific characteristics of the motor and the operating conditions.

Stator winding fault: Most winding faults result from the growth of uncorrected turn-to-turn defects. Long-term thermal aging and eventually insulation failure are the major causes of turn-to-turn defects. It may result in the opening, shorting, or grounding of one or more winding circuits, excessive heating, and machine failure.

Bearing faults: Bearing faults can be caused by several factors. i) Due to the huge output load torque, there is a high vibration in the rotor, which leads to large fatigue stress. ii) Incorrect bearing installation. iii) High parasitic currents in the bearing directed by shaft voltage cause lubrication to deteriorate. iv) Heat transferred to the shaft, resulting in friction and pollution. Bearing faults eccentricate the rotor, resulting in imbalanced magnetic forces and increased bearing stresses. Because the shaft dynamics are impacted by the distorted air gap between the stator and rotor, as well as variations in bearing stiffness, bearing failure is one of the reasons for excessive motor vibration.

Air-gap eccentricity occurs when the air gap distance between the rotor and the stator is not uniform. The two types of abnormal air-gap eccentricity are static and dynamic abnormal air-gap eccentricity. In the case of static eccentricity, the location of the minimal radial air gap is constant, but in the case of dynamic eccentricity, the position of the minimal air gap follows the rotation of the rotor. When the rotor bars retreat or approach the stator magnetic fields, the current in the stator varies.

Broken rotor bar faults: Broken rotor bars are caused by faults in the rotor bars and end rings (BRB). Frequent starting under rated voltage, thermal imbalance, overload at the beginning (thermal stress), and unbalanced magnetic tension are all potential causes of BRB. These faults

induce localized heating or arcing in the rotor, as well as vibration from the expansion and bending of the rotor.

2.3. Traditional Fault monitoring techniques

Motor current signature analysis (MCSA) is a condition monitoring approach for diagnosing electric motor issues. The idea was first presented in the early 1970s for use with inaccessible motors in nuclear power plants and motors located in dangerous regions. It has rapidly gained recognition in the industry in recent years. Motors are operated under load and evaluated online without stopping production under regular operating circumstances. MCSA can be used as a preventative maintenance technique to identify typical motor faults before they become serious, which prevents costly catastrophic faults, production interruptions and extend motor life. MCSA is an electrical signature analysis (ESA) approach that may be used to assess electric motors, generators, power transformers, and other electrical equipment. The MCSA is used to detect faults by monitoring the stator current of the motor. Only one of the three-phase supply currents of the motor is typically monitored with a single stator current monitoring device. The MCSA employs the motor stator winding as a transducer to acquire signals (induced currents) from the rotor while also revealing information about the condition of the stator. A current sensor (clamp-on probe, current transformer) with a resistive shunt at its output senses the motor current and records it in the time domain. Ideally, the motor current should be a pure sine wave. However, the motor current contains numerous harmonics. The motor current signal is further modulated by the different electrical and mechanical faults present in the motor, resulting in extra sideband harmonics. Faults in motor components cause abnormalities in the magnetic field, affecting the mutual and self-inductance of the motor. In the motor supply current spectrum, they appear as sidebands around the line (power, grid) frequencies. Motor faults can be diagnosed, and their severity can be validated based on fault characteristics. Due to the frequency range of interest for MCSA is generally 0-5 kHz, Nyquist's theorem states that a sampling rate of at least 10,000 times per second is required.

MCSA is the best choice for motors under steady-state conditions and rated loads since the current changes are influenced by both the fault and the power supply. The impact of eccentricity and the bearing faults can be reduced using a rapid current controlled inverter. Three effects are present in the faults. 1) the pulse repetition frequency, which is determined by the rotation frequency; 2) the vibration caused by the pulse; 3) a rise in the total noise level. The most accurate method is to use sensor signals to detect the existence of these faults. As the sensor is close to the fault location, the relationship between the fault and the sensed variable becomes clear. However, in addition to MCSA, many different fault diagnosis methods have been proposed.

One of the essential condition monitoring approaches is oil and lubrication analysis. Online (particle counting, temperature and viscosity monitoring, etc.) and offline (oil filter analysis for flow and cleanliness characteristics) methods are both utilized to test and analyze lubricant samples. Lubrication analysis aims to retain oil quality and ensure that the components involved operate in the best possible environment. Lubrication analysis is generally done offline, with samples being examined and tested. Furthermore, when oil filters become overly dirty owing to component wear, they might be a reliable sign of faults. Acoustic emission (AE) analysis is carried out using sensors that capture the sound generated by the machine using a sound level meter. The pressure levels and vibrations are converted into voltage signals using devices with antialiasing and high sampling rates. The types of data collected by acoustic emission analysis and vibration analysis are the same. The acoustic signal obtained is oscillatory. The acoustic signal characteristics vary depending on the faults of the rotating machinery. The noisy background might introduce additional components and impair the accuracy of fault identification of the monitored component, which is the major drawback of the AE condition monitoring method. The most widely used approach for condition monitoring is vibration analysis. Any change or malfunction in any of the mechanical components will cause the vibration profile to alter. Monitoring the vibration frequency can reveal whether a component is faulty or not. The disadvantages of vibration analysis are measurement errors due to improper sensor mounting, crystal overheating, and expensive proximity probes. Thermal

field issues in motors are of great concern, and accurate temperature calculations are critical to the design and operation of motors. In addition, accurate thermal modeling of motors is essential for condition monitoring of the motors. Motor losses can result in high temperatures, which can cause severe thermal stress. There is thermal stress in the rotor end ring and bar, which is most likely to cause motor faults. Therefore, analyzing the effect of faults on the performance characteristics of the motor through the temperature rise of the motor can provide guidance to prevent accidents in operation and maintain safety. However, thermal analysis relies heavily on the accuracy of the sensors and measurements. The analysis of air gap or stray flux measurements can directly indicate the asymmetry of the radial or axial flux of the motor generated by fault-induced anomalies. Researchers have developed methods based on the analysis of external magnetic fields. Non-invasive examination and simplicity implementation are two of the main advantages of this approach. The drawbacks of these approaches stem from the complexity of simulating the magnetic field, which is strongly dependent on the electromagnetic behavior of the stator yoke and the motor housing, both of which have significant shielding effects. One of the main reasons flux monitoring has not received as much attention as MCSA is because it fails to provide remote monitoring. However, it is a low-cost alternative method that can compensate for the reliability and variety of fault detection in the limitations of electrical, mechanical, and thermal monitoring. Initially based on the detection of modes associated with the current Park's vector representation, Park's vector approaches have been effectively utilized for condition monitoring of electromechanical systems. The extended Park's vector method relies on spectral analysis of the AC level of the current Park's vector mode, while by averaging the current Park's vector method, converter power switching faults are detected when the vector mode is not zero. The major risks of converter diagnostics are load dependency and susceptibility to transients. The phase currents are normalized by the modulus of the Parks' vector, and the absolute value of the phase derivative of the absolute Park's vector is utilized as the detection variable in the power converter self-diagnosis based on the Parks' vector technique. Multiple faults can be diagnosed with extra signal processing and variables.

2.4. Feature Extraction in

The basic task of feature extraction is to find out the most effective features for fault recognition from plenty of features, achieving the compression of the feature space dimension, i.e., to obtain a set of "fewer but more precise" classification performance with a low probability of classification error. Motor current monitoring is an effective fault detecting technique since the stator current waveform data obtained from a defective motor differs from that collected from a standard motor. Most research on this technique uses different algorithms to decompose and interpret stator current waveforms, including Fourier analysis, linear discriminant analysis, wavelets, neural networks, and other predictive analysis approaches [24-27]. Time and frequency information is used in time-frequency domain strategies to capture transient characteristics [28]. Envelope analysis is a common technique for detecting and diagnosing bearing faults, which is traditionally determined based on analytically determined peaks. The FFT method is effectively implemented in the spectral analysis of the envelope signal [29]. However, the Fourier spectrum of vibration signals generally excludes the descriptive time-varying patterns of the acquired signals. Therefore, FFT fails to meet fault diagnosis requirements in real-time application [30]. In addition, most methods analyze vibration signals in the time or frequency domain. Vibration monitoring is considered a reliable approach to assess the overall health of a rotor system. The frequency-domain analysis is attractive due to the more detailed information provided about the machine status [31]. However, fault detection is performed by comparing the indirect measurements of external forces based on the dynamic behavior of the machine. The difficulty in fault detection lies in classifying many frequency lines present in the vibration spectrum to extract useful information related to the health status of the motor. Several studies have used dynamic signal analyzers to measure the variance of the spectrum over time to solve this issue [32]. [33] developed an intelligent FFT analyzer that selects multiple frequencies in the spectrum as features and generates a reference model under healthy conditions, which is then compared to the monitoring characteristics for fault detection.

Furthermore, the Hilbert transform (HT) is presented as a method for extracting and estimating the envelope of the vibration signal to get the local energy at each instantaneous frequency. As a result, this technique may be used to characterize the energy-frequency distribution of the vibration signal. It is beneficial to extract the characteristics of nonlinear signals [34] [35]. Due to the adaptive and unexpected nature of vibration signals, conventional methods must be based on reliable motor models and cannot be used effectively for vibration signal diagnosis.

The short-time Fourier transform (STFT) is a popular signal feature extraction approach for converting quasi-steady-state vibration data into a continuous spectrum for neural network model training [36]. Faults can be detected based on the change in the expected value of the vibration spectrum modeling error. However, many potentially unstable frequencies must be tracked since there is no precise method exists for predicting which form of failure will occur. Moreover, vibration spectra often contain puzzling combinations of unusual frequencies that provide little descriptive information about the operating conditions of the motor. Therefore, modern procedures for tracking motor conditions are not reliable or efficient enough. The recent performance of neural networks in dynamically modeled complex systems holds the promise of reducing these issues and achieving better fault detection performance [37]. Neural networks can describe any nonlinear model without knowing the exact form, returning fast results during the recall process. Combined with Short Time Fourier Transform (STFT), an analysis method using vibration spectrum neural network modeling was developed in [38] to extract fault spectrum features for detecting machine faults. For non-stationary processing signals, the wavelet transform (WT) is a useful approach [39], which has excellent time-frequency characteristics in the local area. The internal generation between the studied signal and the intended wavelet basis will provide detailed information in both time and frequency domains. Due to its multi-resolution inspection capabilities, this approach has shown great ability in fault diagnosis of mechanical machinery [40].

The Discrete wavelet transform (DWT) was presented to extract fault features [41]. The advantage was to reduce the computation time. DWT has been widely applied in motor mechanical fault detection [42] [43] since it can only decompose low-frequency sub-bands.

Wavelet packet transform (WPT) was proposed to decompose the high-frequency band and low-frequency band in parallel to improve its frequency resolution. Although these methods have achieved great performance, they were still limited by the segmentation scheme. WPT cannot split the frequency of the signal, which may severely damage the transient vibration characteristics [44].

To overcome the dichotomous subdivision scheme and achieve adaptive representation, the empirical modal decomposition (EMD) approach was suggested [45]. The multi-modulated vibration signal was decomposed into multiple intrinsic mode functions (IMFs) that were regarded as dominant mode components. It can extract both stationary and non-stationary components of a signal with efficiency. Therefore, it has attracted a lot of attention in signal processing and practical industrial applications. However, the lack of a mathematical theory for EMD methods has led researchers to propose improved methods regarding combinations of other methods in recent years [46]. [47] proposed an empirical wavelet transform (EWT), which combined the advantages of wavelet transform and EMD methods. The EWT method can perform the identification of weak faults and compound faults. Meanwhile, the EWT method can efficiently analyze the signal and extract internal features. In addition, EMD was an adaptive signal processing method that can be perfectly applied to nonlinear and non-smooth processes. The main drawback was the pattern mixing problem. In addition, a new method called Variational Mode Decomposition (VMD) was proposed in [48], which assumed that each extracted pattern has a finite bandwidth. Compression is performed around the central frequency of the match. However, VMD cannot support the model in practical applications, and its modulation capability depends heavily on the intrinsic parameter settings [49].

TABLE 2-1 Highlight of Feature Extraction Method

Reference	Theme	Principle	Highlight
[28]	FFT	• Spectrum analysis of	• Time-frequency domain conversion
[29]		envelope signals	• Poor performance for non-stationary signal
[30]		• Frequency	• No time-frequency analysis
[33]		distribution	
[32]	HHT	• Multi-resolution of	• To avoid complex mathematical operations

[34]		frequency scale	• To analyze signals whose frequency varies with time
[35]			• High calculation burden
[36]	STFT	• Long and short time window movement	• Time-frequency characteristics are acquired
[38]			• High-frequency resolution and high time resolution cannot be acquired simultaneously
[39]	WT	• Signal Decomposition and reconstruction	• Time-frequency analysis
[41]	DWT	• Discrete input and output	• To reduce calculation time
[42]			
[43]	WPT	• Fitting the mutation signal	• Effective splitting of fault-induced resonances and high-frequency band features
[45]	EMD	• Irregular frequency waveforming	• Adaptive data processing
[46]			• Suitable for non-linear, non-stationary time series
[48]	VMD	• Sub-signal decomposition at different frequencies	• To avoid pattern mixing
[49]			• Modulation capability dependent on parameter settings
[47]	EWT	• Adaptive wavelet subdivision scheme	• More consistent decomposition
[44]	LCD	• Adaptive decomposition of a complex signal	• Better time-frequency localization characteristics
[50]			• More efficient extraction of localization information from the original signal
[51]			• Faster calculation speed
[53]	PCA	• Multidimensional feature mapping	• Signal dimensionality reduction
[54]			• To reduce model training time
[57]	CCA	• Information Retention mapping	• Better accuracy
[57]		• Self-organizing mapping	• Linear feature extraction
[57]			• Distance preservation
[58]	SC	• Symmetric component acquisition	• Rapid and accurate computation performance
[60]	SVD	• Matrix decomposition	• To use low-rank approximations to simplify systems
[61]			

Intrinsic Time Scale Decomposition (ITD) is a new adaptive time-frequency analysis approach that allows a non-smooth signal to be decomposed into the sum of several intrinsic

rotational components. Although it has better performance over EMD, the approach cannot account for the physical meaning of the intrinsic rotational components. [50] developed a local characteristic scale decomposition (LCD) algorithm based on the ITD method for the physical significance and its intrinsic rotational components. It can decompose any complex signal adaptively into instantaneous physical frequencies [51] [52].

Compared with EMD, the LCD method has better time-frequency localization characteristics and can extract the localization information of the original signal more effectively to obtain the fundamental characteristics of the signal. Since raw feature vectors will reduce the efficiency of the classification system, and incorrect generalization will eliminate useful details, linear methods are usually applied to reduce the number of features.

Both principal component analysis (PCA) and linear discriminant analysis (LDA) can be utilized for dimensionality reduction of data, achieving clear visualization and detection of different or unknown fault modes [53]. Many researchers have investigated PCA approaches, considering their drawbacks in working with massive data sets when it seeks the global structure of data [54]. The function vector is made up of D computed features and has been expressed in D -dimensional space. Most of the data in the D -space has a nonlinear structure. In recent years, several learning methods [55] [56] have been carried out to retain the information in a lower d -dimensional space, where $D > d$, to solve this problem. Other methods such as Curvilinear Component Analysis (CCA) "find" the right form of the sub-tow cable and vice versa automatically. CCA has been applied in the field of fault diagnosis of motor drive systems. A CCA-based neural network FDD was presented in [57], which started with the selection of the most important features from an initial set formed by computing statistical time features from vibration signals.

The novelty of the method lies in its ability to perform complete fault analysis and diagnosis of various faults in bearings, both local and generalized faults. It is applied to the fault classification structure by performing the feature approximation phase of CCA. The classification task can be accomplished by applying a neural network.

Symmetric component (SC) is a promising method in time-domain FDD analysis and has

received much attention, which can provide various information about the motor voltage or current balance, magnitude, and sequence. However, the generality of SC is limited to different fault classes, which may require detailed machine models and may be limited by computer resources. The SC method presented in [58] was based on stator currents and accomplishes signal feature extraction in multiple data processing steps. It is a low-cost computational method without complex computer models. Furthermore, particle filtering is another efficient tool for sequential signal processing that uses point masses and related discrete probability masses to estimate the state probability density function. It is based on the principle of sequential value sampling and Bayesian theory. Particle filtering has recently been extended to the prediction of machines [59]. Since mechanical failures are nonlinear dynamic problems, particle filtration is particularly effective in solving these problems. In addition, some mathematical models have been developed to explain the fault propagation process in most applications. However, the derivation of these models is complex and requires expertise in the degradation process. The typical fault propagation model is the first-order hidden Markov model (HMM), which is characterized by the fact that the current state of the system, which is determined by the previous state. Moreover, due to the increase of feature nodes, the trained system may contain some redundant nodes, which will lead to poor accuracy. Singular value decomposition (SVD) has been proposed to simplify the system. In the singular value decomposition process, the signal is converted into a matrix where the singular values represent the nature of the faulty signal [60] [61]. In addition, to fuse the information from all the utilized classifiers, [62] proposed a fault diagnosis method based on a motor current signal developing deep learning and information fusion (IF). The novel decision-level information fusion (IF) technique applied the raw signals of multi-phase motor currents as direct inputs and extracted features from the motor current signals of each phase to improve classification accuracy. Table 2-1 summarize all mentioned signal process methods for feature extraction.

2.5. Fault Classification

As the crucial step in fault detection and diagnosis, accurate and efficient classification performance is extremely important. As an attractive method, machine learning includes a variety of model types: 1. Supervised learning, which is responsible for analyzing training data and generating inference functions through algorithms. 2. Unsupervised learning to draw conclusions from unlabeled data. The most common unsupervised learning method is cluster analysis, which is mainly used to discover hidden patterns in grouped data. Deep learning is a sub-domain of machine learning (ML), and its related algorithms are inspired by the structure and function of the brain (ie, artificial neural networks). In traditional machine learning method, extraction and selection of features is usually required, which requires the knowledge and experience of domain experts. Feature engineering is a critical step that affects model performance. In deep learning method, by learning end-to-end feature representations, models are able to learn higher-level features from raw data. Deep learning models can automatically learn hierarchical features in data without manual extraction. Fig. 2-5 illustrates the flowchart of traditional ML and DL. The application of classic machine learning and popular deep learning algorithms in motor FDD are introduced in this section.

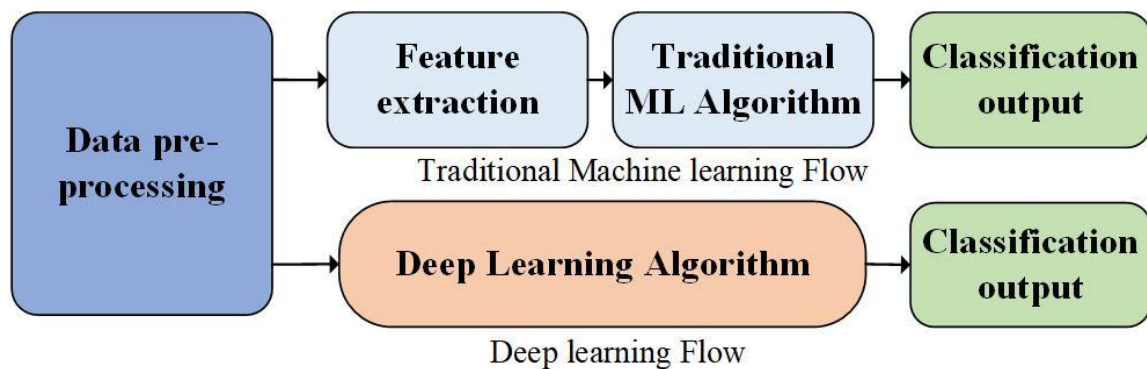


Fig. 2-5. Flowchart of traditional Machine learning and Deep learning.

2.5.1. Support vector machine (SVM) based approach

A support vector machine (SVM) is a binary classification model that attempts to build a

line between two classes of points by mapping the feature vector of an instance to certain points in space. SVM is applied in regression analysis for data classification and system parameter estimation.

SVM has various applications such as handwriting recognition, image recognition, etc. SVM is particularly useful for small samples and database instances. Because of its appealing characteristics and strong analytical results, SVM is becoming increasingly popular in the field of motor drive system fault diagnosis. Fig. 2-6 illustrates the optimal hyperplane for binary classification by SVM.

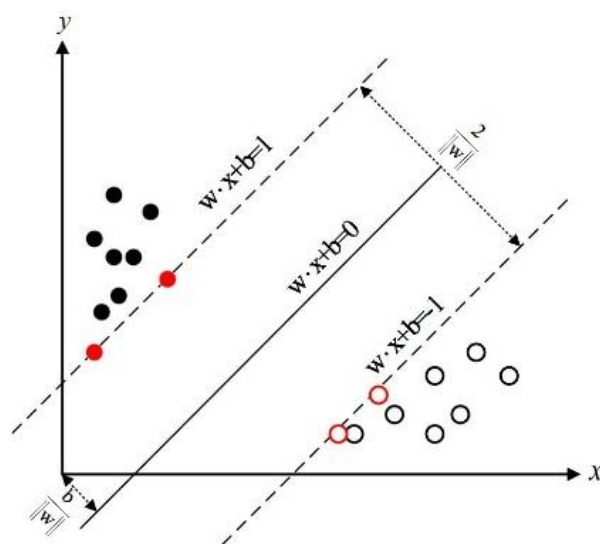


Fig. 2-6. The optimal hyperplane for binary classification by SVM.

$$\min \Phi(w) = \frac{1}{2} \|w\|^2 \quad (2-1)$$

$$\text{subject to, } y_i(w \cdot x_i + b) \geq 1; i = 1, 2, \dots, n \quad (2-2)$$

where w stands for the weight vector, which describes the hyperplane, x_i stands for the input vector, y_i stands for the label associated with x_i , and b stands for a scalar threshold. For the case of nonlinear separation, in high-dimensional spaces, the SVM can construct a hyperplane that allows for linear separation. Only the transformation $\Phi(x)$ from N -dimensional space to Q -dimensional function space of the data is used in SVMs. Since the inner product can be replaced, the mapping translation can be achieved with a kernel operation. By retaining the

influence of high-dimensional transformations, it reduces the computational load. This is the kernel function: $k(x, x_i) = \Phi(x) \cdot \Phi(x_i)$. Many functions can be used as the kernel function. The Gaussian radial basis function (RBF) is a well-known kernel, the equation is:

$$k(x, x_i) = \exp(-\gamma \|x - x_i\|^2); \gamma = \frac{1}{2\sigma_b^2} > 0 \quad (2-3)$$

After optimization, the basic SVM structure can be described as:

$$f(x) = \sum_{i=1}^m \{y_i \alpha_i k(x, x_i)\} + b \quad (2-4)$$

SVM has a nonlinear multi-label classification function. For multiple fault diagnosis, an intelligent fault detection system based on a multivariate integrated incremental support vector machine (MEISVM) is presented in [63] for multi-fault diagnosis. This method can detect a variety of faults, including complex compound faults and faults with different severity thresholds. [64] proposed a grid search support vector machine (GSSVM) approach based on redefined dimensionless indicators (RDI) extracted maximum correlation and minimum redundancy feature selection. Minimum redundancy maximum relevance (mRMR) was used to automatically eliminate redundant and irrelevant features from high-dimensional features to obtain more fault features that indicated the useful information hidden in the vibration signal. The proposed RDI as a new fault feature can effectively solve the shortcomings of the traditional dimensionless index and has a stronger discriminative ability for mechanical faults. Automatically eliminate redundant and irrelevant features in the high-dimensional feature space. The correlation between features and output class labels is maximized, and the redundancy between features is minimized. However, the dimensionless metric is sensitive to faults rather than to operating conditions, whether the classification effect is significant when the operating conditions of the motor change are not given as a validation. A novel intelligent fault detection approach for rolling bearings was proposed based on composite multiscale fuzzy entropy (CMFE) and ensemble support vector machines (ESVMs) to extract the nonlinear features that were embedded in the vibration signal [65]. CMFE was utilized to extract hidden nonlinear fault characteristics from rolling bearing vibration signals, and then ESVM was used to construct a multi-fault classifier to accomplish an automated intelligent diagnosis of rolling

bearings. In [66], Several investigations were carried out to record current conditions during various motor power supply activities, such as internal stator winding short-circuit failures and supply voltage imbalance at different load speeds. A recursive feature elimination algorithm based on the support vector machine (SVM-RFE) was applied to select and maximize the number of appropriate features to be used for classification. It was worth noting that two different feature sets were created. One of them contained load-level details, which were intentionally hidden in the other one. The selected features were used to identify various stator winding fault conditions using a support vector regression (SVR) based classifier. It has been found that the performance of the classifier was better when the load level information was included in the functional layer rather than the load level information was hidden. To make the fault classification algorithm uninterrupted at different load levels, two additional functions were extracted from the Park's vector modulus using detrended fluctuation analysis (DFA). Ultimately, the SVR-based classifier was found to be accurate in detecting and classifying internal motor faults. A satisfactory response was shown in distinguishing between supply voltage imbalance and internal stator faults. Full-spectrum cascade analysis of rotating machine vibrations is an effective method. Abrupt changes in acceleration signals of rotor faults can be detected and the characteristic spectrum of faults is displayed in a full-spectrum cascade diagram. In addition, the fault diagnosis problem becomes more confusing when the current characteristics due to power supply voltage imbalance are significantly similar to those due to internal stator winding faults. It is important to select, rank and optimize the number of valid features used for classification. RFE uses some mathematical or heuristic rules to train the SVM classifier with features that minimize the margins. This feature elimination process is repeated until some stopping criterion is satisfied. Removing features during the iterative process simplifies the computation, but this may lead to sub-optimal solutions. The full spectrum experimental data were used for support vector machine (SVM) training and excellent classification results were obtained [67].

2.5.2. MLP/KNN/RF-based approach

Multi-layer perceptron (MLP) is a simple-structured neural network. The most common MLP includes three layers: the input layer, the hidden layer, and the output layer, with all three layers of the MLP neural network being completely connected, which is widely used in the detection and diagnosis of the motor drive system. Since its capacity to indirectly detect dynamic nonlinear associations between dependent and independent variables, as well as its ability to detect all possible correlations between predictor variables and multiple training algorithms, the MLP feedforward neural network has been adopted [62]. A three-phase asynchronous motor control method based on RBF-MLP cascaded neural network was proposed in [68]. To obtain rich fault knowledge from stator currents, simple statistical features such as standard deviation, kurtosis, energy, entropy, and variance were extracted. PCA was used to pick the most superior functionality to remove obsolete or irrelevant details and reduce the burden of the classification scheme. The classifier is sufficiently robust, i.e., the classification accuracy does not change in the presence of uniform and Gaussian noise in the input and output. The advantage is that good classification performance can be achieved without the requirement for a large amount of accurate measurement data. Furthermore, MLP was utilized to classify inter-turn short-circuit faults in PMSM stator windings at different speeds, loads, and fault severity. These states led to the complexity of the fault features. Depending on the complexity, the nonlinear relationships between the relevant features are identified to detect different severity levels of inter-turn short circuits.

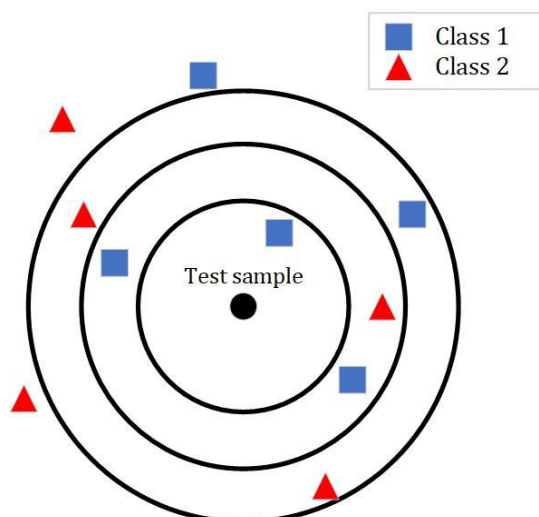


Fig. 2-7. The structure of KNN.

Due to its easy implementation and substantial classification efficiency [69], the k-nearest neighbors (KNN) method is a popular classification method in data mining and statistics. The principle structure of KNN is as shown in Fig. 2-7. [70] presented a system for detecting bearing faults in electric motors and monitoring the bearing loss. The approach used spectral kurtosis (SK) and reciprocal association to extract fault features, which were then combined principal component analysis (PCA) and semi-supervised k-nearest neighbor (KNN) distances to provide health metrics.

TABLE 2-2 Highlight of Classical Machine Learning Method

Reference	Theme	Principle	Highlight
[63]	MEISVM	<ul style="list-style-type: none"> • Sensor information correlation • Pairwise secondary optimization 	<ul style="list-style-type: none"> • Multi-fault diagnosis • Highly rely on input feature data
[64]	mRMR GSSVM	<ul style="list-style-type: none"> • Maximize feature relevance • Minimize redundancy between features 	<ul style="list-style-type: none"> • Fast calculation and high robustness • Random parameter setting
[65]	CMFE ESVM	<ul style="list-style-type: none"> • Obtain vector similarity 	<ul style="list-style-type: none"> • Sensitive to nonlinear feature
[67]	FFT SVM	<ul style="list-style-type: none"> • Structural Risk Minimization 	<ul style="list-style-type: none"> • Acceleration signal analysis application

[68]	RBF MLP	•Competition rules and metric combinations	•Low demand for accurate measurement data •High classification performance
[70]	SK KNN	•Category distance calculation	•To improve speed and space efficiency
[71] [72]	RF	•Random sampling and replacement	•Effective classification ability •Insufficient generalization ability

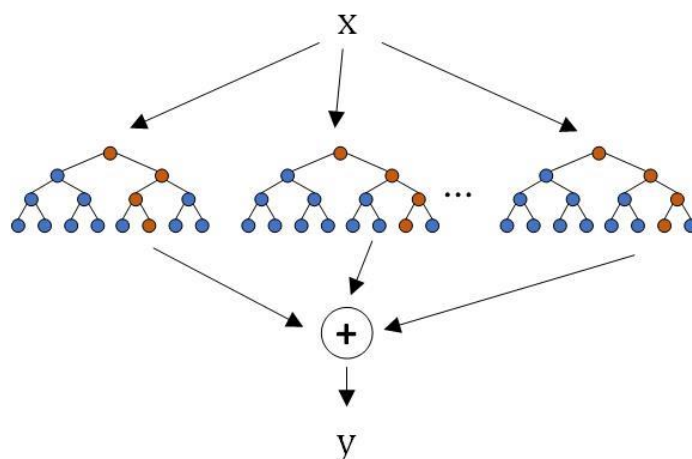


Fig. 2-8. The basic structure of the random forest.

Random forest (RF) models are based on the classification and regression of tree groups (CART) [71]. Random forest is a method that uses integrated learning to combine numerous trees, with the fundamental unit becoming a decision tree, each of which is a classifier. The categorization results for an input sample will then be N trees. The random forest integrates all classification votes and designates the most voted category as the final output, which is a basic bagging idea. Fig. 2-8 illustrates the basic structure of the random forest. A random forest classifier was proposed in [72] for the classification of bearing faults. The statistical features of the bearing vibration signals were computed and fed to the RF and ANN classifiers. [73] developed a hybrid model that combines a fuzzy min max (FMM) neural network with classification and regression tree (CART) for online motion detection and diagnosis tasks. In addition to strong online performance, the FMM-CART produced helpful decision trees to explain the collected functional information.

To sum up, the machine learning methods mentioned above are all shallow models with

simple structures, high computational efficiency, and great classification performance. Table 2-2 summarizes the classical machine learning methods for fault classification.

In contrast to traditional machine learning methods with manual feature labeling, a large amount of research has focused on how to extract representative features from the original signal. On the other hand, the extracted data may contain redundant or insensitive data. To identify sensitive characteristics, certain dimensionality reduction methods were utilized, which may have an impact on diagnostic findings as well as computing performance. Most of the studies on intelligent fault diagnosis have produced valuable results, but there are still two obvious drawbacks. 1). Manual extraction of features requires a priori knowledge, which requires a lot of practical work to determine and may have greater checking popularity. 2). Traditional machine learning techniques cannot effectively distinguish complex information in raw data, and the shallow structure of artificial neural networks limits their ability to understand the complex nonlinear relationships hidden in the measurement data. In terms of a large number of hidden neurons, DNNs can obtain nonlinear representations of data. It has achieved higher performance in the field of motor fault detection and diagnosis.

2.5.3. Convolutional Neural Network (CNN)

Convolutional Neural Network (CNN) is a feed-forward neural network that mainly stimulates the activity of the visual system of the human brain. Local receptive fields, weight sharing, and spatial domain secondary sampling are the three main architectural principles in the structure of CNN. Therefore, CNN is well suited to processing two-dimensional data like images. Convolutional layers (CL), pooling layers (PL), completely connected layers (FL), and SoftMax layers are the four kinds of layers that make up CNN. The following equation can be used to mathematically model the operation of processing input data in the CL:

$$x_j^i = f \left(\sum_{i \in M_j} x_i^{l-1} * k_j^l + b_j^l \right) \quad (2-5)$$

where x_i^{l-1} indicates the input data of layer l , $*$ denotes the convolution operation. The

layer is made up of n kernels, each with its weight matrix and bias vector. Because of its versatility, the rectified linear unit (ReLU) is often used as a CL activation function. The equation for ReLU is:

$$f(y) = \max(0, y) \tag{2-6}$$

The following equation can be used to express PL mathematical operation:

$$x_j^{l+1} = s(x_j^l) \tag{2-7}$$

After the non-linear combination of features extracted by FL, the SoftMax layer acts as a classifier. The SoftMax function converts an N-dimensional real vector into a set of real vectors (0, 1). The SoftMax function has the equation:

$$p_i = \frac{\exp(z_i)}{\sum_{j=1}^N \exp(z_j)} \tag{2-8}$$

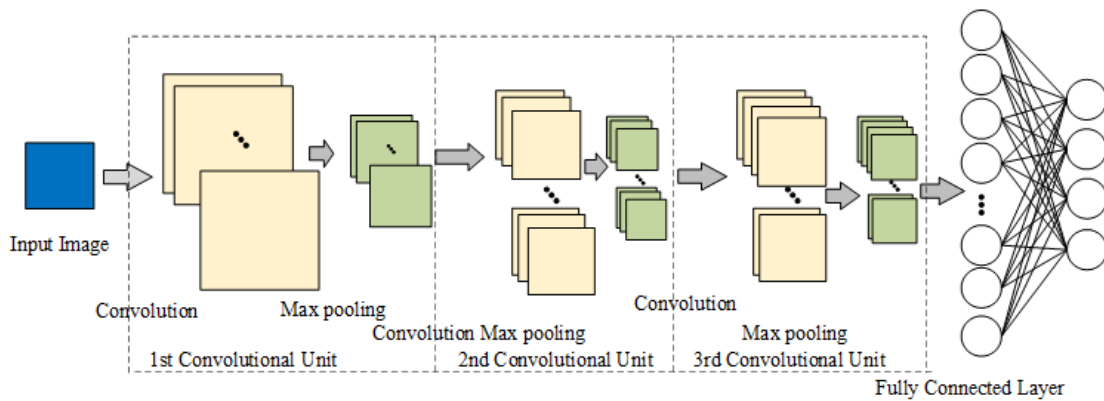


Fig. 2-9. The basic structure diagram of CNN.

Signal processing techniques with different characteristics are combined with CNN for fault signal diagnosis [74] [75]. [74] proposed a novel motion state monitoring framework with an adaptive implementation of 1-D CNN, where the two main modules of traditional fault detection steps included feature extraction and classification were fused into one. The proposed approach extracts the best features through proper training. Therefore, manual parameter adjustment and manual feature extraction are not required, achieving more efficient fault diagnosis capability. [76] proposed an integrated strategy based on data-driven and deep

learning to deal with initial faults. The average moving technique was introduced into the typical correlation analysis (CCA) framework, making the new residual signal more sensitive to initial faults. Moreover, new test statistics that work closely with Kullback-Leibler divergence (KLD) were proposed from a probabilistic perspective and greatly improved fault detection performance. The fault matrix was defined and used as the input of the convolutional neural network (CNN), whose feature extraction capability was greatly improved compared with the conventional method, which helped to diagnose the initial faults accurately. The CNN shown in Fig. 2-9 was used as a construction block multi-signal framework. Randomly initializing the designed model, the deep model was trained using the training dataset, minimizing the error between model output predictions and actual labels by iteratively updating the parameters of the DCNN model [77]. The proposed method has one input and output layer, three hidden convolutional units, each of which was followed by a max-pooling operation, and one fully connected hidden layer following the convolutional and max-pooling layers. ReLu was implemented as an activation function, CWT was used to convert the time-domain signal into gray-scale images as input. The model was trained and verified with experimental data including current and vibration signals. The training time was 201s and 156s, and the accuracy rates of 98.72% and 98.26% were obtained respectively. In addition, CNN combined with other networks has been proposed. A convolutional recurrent neural network (CRNN) was used to diagnose multiple faults of high-speed train (HST) bogies by combining CNN and RNN [78]. The model inherited the functions of both CNN and RNN. A new approach was proposed that combines CNN and extreme learning machine (ELM). CNN demonstrated strong automated feature extraction capabilities, while ELM was proposed as a quick and efficient classification algorithm [79]. To improve the feature learning capabilities, a CNN with a square pool configuration was built and used as an automated feature extractor in the first level. ELM was further used in the second stage to increase classification accuracy and learning speed. In [80] [81], the initial vibration signal was input to a deep convolutional neural network named deep convolutional neural networks with wide first-layer kernels (WDCNN). The. A large first-layer convolutional kernel and a deep network structure with narrow convolutional layers were the

two key features of the WDCNN. The proposed model enhances the accuracy of the current CNN fault diagnosis. Besides, a new model named Convolution Neural Networks with Training Interference (TICNN) was proposed to solve the fault diagnosis problem in [82]. Without the requirements for a time-consuming manual feature extraction process, TICNN processed the raw vibration signal directly. Without any time-consuming denoising pre-processing, the raw time signal was used as data. Meanwhile, the model was independent of any domain adaptation algorithm or target domain information. An online fault diagnosis scheme was proposed in [83]. Conventional ANNs for fault diagnosis classification tasks were trained offline with historical data, and then the trained model was used for online fault diagnosis. Due to the limitations imposed by the time consumption associated with the training process of the model, an online fault diagnosis algorithm including two phases was proposed. In the first stage, an SVM was used to separate the healthy data from the faulty data, and in the second stage, a convolutional neural network (CNN) was trained to learn the features used to isolate the faults. Although the proposed method was an end-to-end self-supervised learning model, the performance of the CNN in the second stage was limited by the number of data sets and the training time consumption. The data was used only in the healthy state through the fault diagnosis function in self-supervised learning. The operating condition or operating condition class of the powertrain was defined in the first stage by using a class of SVMs. The generated health classes were used to train a CNN-based classifier. This approach outperformed current algorithms and approaches that use domain feature extraction. A new LeNet-5-based CNN for fault diagnosis was proposed in [84], three datasets were used to verify CNN models based on LeNet-5 with eight layers, which comprised of three transformed pictures of 64×64 , 64×64 , and 16×16 . On three separate datasets, the presented CNN had prediction accuracies of 99.79%, 99.48%, and 100%. By converting the signal into a two-dimensional (2-D) image, the method extracted the features of the converted 2-D image and eliminates the influence of artificial features. The novel data pre-processing approach presented in the literature transformed raw time-domain signal data into two-dimensional grayscale pictures without the use of any predetermined parameters, removing as much as possible the knowledge of the expert.

However, the limitations of the method in terms of practical applicability included the following aspects. First, the most prevalent fault circumstances must be identified, which may be achieved using a dictionary list type. Otherwise, unknown faults will be categorized incorrectly as known faults. Second, the training procedure took a long time. Transfer learning can be used to minimize training time in the future based on these constraints.

2.5.4. Recurrent neural network (RNN)

Recurrent neural networks (RNN) are presented for sequence learning. RNN establishes the connection between units as a directed loop. Unlike basic neural networks, where multilayer perceptron can only map from input data to target vectors. Fig. 2-10 indicates the structure of RNN. Before the time series are input into the RNN, the data are converted into two-dimensional data according to the size of the time window to maintain their sequential nature. W is a common weight, and W and V are the weight matrices of the input and output layers. In addition, when calculating the state S_t at the current time t , the input value x_i is multiplied by the weight U of the input layer and then the result is obtained by multiplying the common weight W , which is summed to be constant. The equation is shown as below:

$$S_t = f(U * x_t + W * S_{t-1}) \quad (2-9)$$

$$O_t = f(s_{t-1} * V) \quad (2-10)$$

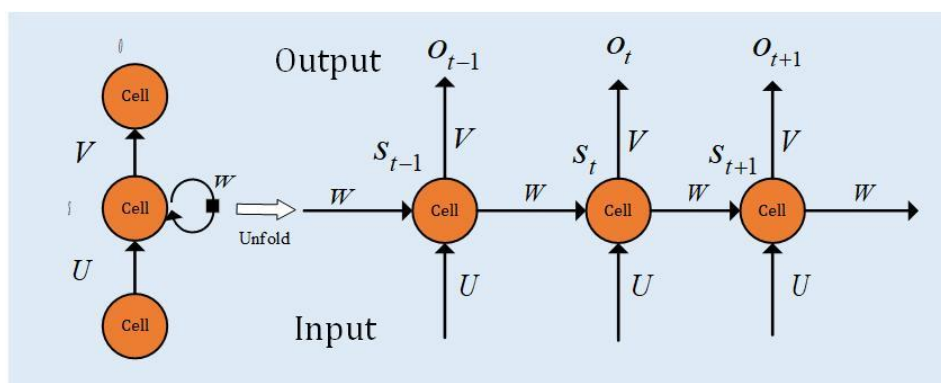


Fig. 2-10. The basic structure diagram of RNN.

Due to the RNN map the target vector from the entire history of previous inputs, the memory

of prior inputs are retained in the internal state of the network. RNN can be trained by backpropagation to accomplish the task of timely supervision. However, the issue of gradient disappearance during the backpropagation of model training hinders the performance of RNN. It means that traditional RNN may not be able to capture long-term dependencies. Therefore, the long short-term memory (LSTM) algorithm is designed to prevent backpropagation errors from disappearing or exploding. To solve the problem of long-term reliance, forgetting gates are incorporated into LSTM. The use of cell state information may be controlled using these applicable forgetting gates. Because it can capture long-term dependencies, LSTM has the advantage over standard RNN for capturing nonlinear dynamics in time-series sensory input and learning an efficient representation of machine states. Considering the ability of LSTM to capture remote dependencies and nonlinear dynamics in time series data, LSTM has been effectively applied to fault diagnosis of motor drive systems [80] [85] [86]. [80] presented the RNN-WDCNN, a new dual-path recurrent neural network with a larger initial kernel and deeper convolutional neural network routes that can operate on raw temporal information. The WDCNN combined the functions of recurrent neural networks (RNN) with convolutional neural networks to capture remote relationships in time-series data and remove input signals in high-frequency noise. Besides, [85] developed a novel approach named convolutional long short-term memory (CLSTM) is developed to handle signal-based FDD in rotating machinery. The developed model improved the efficiency of processing multi-channel input data and learning its Spatio-temporal characteristics. The input channels were subjected to sensitivity analysis, and the results suggest that combining these multi-domain characteristics improves the accuracy of the classifier. However, feature engineering on severely unbalanced data sets while finding the optimal hyperparameters to train the classifier faster without compromising its accuracy is a serious topic. The CLSTM architecture was used to process multi-channel input data and understand its Spatio-temporal characteristics more efficiently. The updated CLSTM supported the FDD approach to properly understand the function of data structures and achieve higher accuracy. [86] proposed a deep neural network architecture for processing raw sensory data, called convolutional bidirectional long-term short-term storage network

(CBLSTM). The proposed method consisted of one layer CNN for feature extraction and the size of the input signal is 100×12 . Then two hidden layer bi-directional LSTMs were implemented to encode the temporal patterns. Two fully connected layers of size 500×600 were used before feeding the representations to the linear regression layer. The activation function was ReLu. One epoch takes 5 seconds to train, and each sample takes 0.027 seconds to test. Compared with RNN, deep RNN, LSTM, etc., the proposed algorithm has better performance. CBLSTM first used CNN to extract stable and information-rich local features from sequential inputs. Then, the temporal information was encoded using a bidirectional LSTM. The long and short-term storage network (LSTM) models linear data and record long-term dependencies, while the bidirectional system captures past and future environments. A stacked fully connected layer and a linear regression layer were constructed on top of the bidirectional LSTM to predict the target values. In addition, two RNN networks were applied as encoder and decoder in place of the general fully connected layer to effectively reduce the dimensionality of the time series data combined with the autoencoder of the RNN [87]. Moreover, [53] was used in combination with a variant autoencoder (VAE), variance and noise are added to make the model generation more realistic. The time-domain vibration signals at 3 different locations were used as inputs, and two RNN networks were developed as encoder and decoder respectively instead of the usual fully connected layer. In addition, the variance and noise were added to make the model generation more realistic, in addition to reconstructing the input data. This method reduced the computational cost. However, when the length of the input sequence was too long, it will cause the information to be diluted during the propagation process thus decreasing the accuracy.

2.5.5. Generative Adversarial Network (GAN)

A Generative Adversarial Network (GAN) is divided into parts: a generator and a discriminator. GAN training aims to achieve a Nash balance between the generator and discriminator based on the binomial zero-sum game principle. The generator and discriminator in the GAN are differential functions that can be optimized by using any gradient-based

approach. The purpose of the generator is to capture the potential distribution hidden in the real sample by using z as input. Therefore, the generator outputs a "fake" sample x_f that is as similar as possible to x_r , thus confusing the discriminator. In addition, the purpose of the discriminator is to distinguish x_f from x_r and to identify the actual sample from the generated sample. Due to the conflicting goals of the generator and discriminator, the two parts of the GAN compete and gradually become more powerful during the training process. Once the GAN is trained correctly, the distribution of the generated samples will match the distribution of the actual samples, which makes it difficult for the discriminator to distinguish the difference between x_f and x_r .

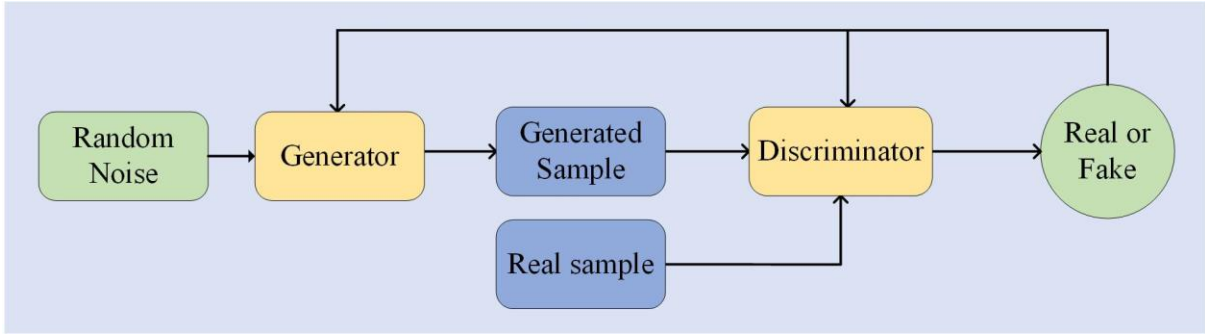


Fig. 2-11. The basic structure diagram of GAN.

Fig. 2-11 indicates the basic principle of GAN. The nonlinear functions of the discriminator and generator approximation are represented as $G(\cdot)$ and $D(\cdot)$, respectively. The distributions of random noise and actual samples are represented as P_{data} and P_n respectively. Due to the different training objectives of the discriminator and generator. The objective function is defined respectively as:

$$\min_G \left\{ L_G(D, G) = E_{Z \sim P_n} \left[\log \left(1 - D(G(z)) \right) \right] \right\} \quad (2-11)$$

$$\max_D \left\{ L_D(D, G) = E_{x \sim P_{data}} [\log D(x)] + E_{Z \sim P_n} [\log(1 - D(G(z)))] \right\} \quad (2-12)$$

where $L_D(D, G)$ and $L_G(D, G)$ represent the objective functions of the discriminator and the generator. Equations (11) and (12) can be combined into a single objective function for the overall training operation of GAN, as seen in equation (13).

$$\min_G \max_D \{L_D(D, G) = E_{x \sim P_{data}} [\log D(x)] + E_{z \sim P_n} [\log(1 - D(G(z)))]\} \quad (2-13)$$

Due to their ability to learn deep representations without deep marking of training results, GANs have received a lot of attention in a wide variety of fields [88] [89]. GAN has also been used in mechanical defect diagnosis in recent years [90] [91]. The data imbalance between different machine health conditions can be addressed [92] [93] and unsupervised fault classification can be achieved by incorporating GAN into certain deep learning algorithms [91]. In general, ML and DL-based FDDs share a universal drawback, which is the models require a substantial quantity of training data to learn the inherent patterns of normal and faulty data in a customized manner. However, for various reasons, it is hard to acquire actual operational data corresponding to different health conditions. 1. low frequency of failures 2. Inserting faults into rotating equipment is expensive and dangerous. 3. labelling data is highly time-consuming even if a large amount of data is available. Therefore, GAN is a method that requires only a small amount of sample data to obtain highly accurate training results. GAN can generate sample ML algorithms in an unsupervised manner. Due to the adversarial generator and discriminator, the GAN will learn samples adaptively for training. When both the generator and discriminator have completed training, the output of the generator will produce samples close to the actual samples even if the input data is random noise. On a variety of image datasets, GAN variants such as DC-GA and AC-GAN have demonstrated strong generative efficiency. [94] applied the GAN method to the FDD of a motor instead of other traditional resampling methods. To increase the imbalance data of the motor, the GAN-based method generated more realistic samples and improved the accuracy of fault diagnosis compared to use other resampling methods. Owing to a complete lack of anomalous samples, single GAN-based fault diagnosis models do not recognize the case of new types of faults. Using stacked noise reduction autoencoders and generative adversarial networks, [95] proposed a fault diagnosis process (SDAE-GAN) that enabled the discriminator to determine the sample fault type and whether the input data is from a real data distribution. However, learning various data distributions simultaneously is a challenge.

Furthermore, the proposed method can eliminate the interaction between the intrinsic distributions of different fault patterns during the training process. Therefore, it has stronger generalization capability compared with a single fault diagnosis method based on GAN. This method is of great significance for solving the problem of difficulty in obtaining fault data in practice. Although FFT requires less expertise than other manual feature extraction methods, it still requires the use of signal processing, and the proposed method cannot be considered as an end-to-end fault diagnosis method. [96] studied multiple GANs to understand the data distribution for each health condition and then developed a semi-supervised approach to improve the feature extraction capability of each GAN with better generalization capability compared to a single GAN-based approach. The generator and discriminator have a symmetrical structure which has one input and output layer and two hidden layers. The size of the input layer of the generator is determined by the size of the random noise vector which is 128×128 . ReLu is applied for the activation function of hidden layers, while sigmoid is used in the output layer. Besides, only 200 samples in each dataset are used for training the model. The performance of testing accuracy is greater than 95% and the standard deviations are below 1.2%.

2.5.6. Deep Belief Network (DBN)

In contrast to traditional neural network discriminative models, deep belief networks (DBN) are probabilistic generative models in which the generative model creates a joint distribution between the observed data and the labels. Layer-by-layer training allows better initial weights to be assigned to the entire network so that the network can be fine-tuned to achieve the best solution. DBNs consist of multiple layers of constrained Boltzmann machines (RBMs), a typical neural network as shown in Fig. 2-12. These networks are "constrained" into visible and hidden layers, with connections between the layers, but there are no connections between the internal units. The hidden layer units are learned to recognize the relevance of the higher-order data displayed in the visible layer. Through the energy function $E(v, h, \theta)$ the relation

weights describe a probability distribution over the joint condition of the visible and hidden cells (v, h) .

$$E(v, h, \theta) = -\sum_{j=1}^m b_j v_j - \sum_{i=1}^n c_i h_i - \sum_{i=1}^n \sum_{j=1}^m v_j w_{i,j} h_i \quad (2-14)$$

The probability distribution of each possible visible and hidden vector pair can be defined by the following energy function similar to that of a general Boltzmann machine.

$$p(v, h; \theta) = \frac{1}{Z(\theta)} \exp(-E(v, h; \theta)) \quad (2-15)$$

Where $Z(\theta) = \sum_{v,h} \exp(-E(v, h))$.

The conditional probabilities of hidden and visible cells are given by:

$$p(h_i = 1|v; \theta) = \frac{1}{[1 + \exp[-c_i - \sum_{j=1}^m v_j w_{i,j}]]} \quad (2-16)$$

$$p(h_i = 1|h; \theta) = \frac{1}{[1 + \exp[-b_i - \sum_{j=1}^n v_j w_{i,j}]]} \quad (2-17)$$

The RBM model with binary cells can be learned by a negative log-likelihood gradient as follows:

$$\Delta w_{i,j} = \eta(\Delta w_{i,j} = \eta(\langle v_j h_i \rangle_{p(h|v)} - \langle v_j h_i \rangle_{recon})) \quad (2-18)$$

$$\Delta b_j = \eta(\langle v_j \rangle_{p(h|v)} - \langle v_j \rangle_{recon}) \quad (2-19)$$

$$\Delta c_i = \eta(\langle h_i \rangle_{p(h|v)} - \langle h_i \rangle_{recon}) \quad (2-20)$$

where η is the learning rate and $\langle \cdot \rangle_{p(h|v)}$ is the expectation value, which is relative to the conditional distribution $p(h|v)$ reconstruction of the distribution of the model. Superposition in the forward direction RBM learning may be used to learn weights in an unsupervised manner, which is referred to as supervised initialization of the learning parameters. It's the same as having a priori knowledge of the supervised learning input data.

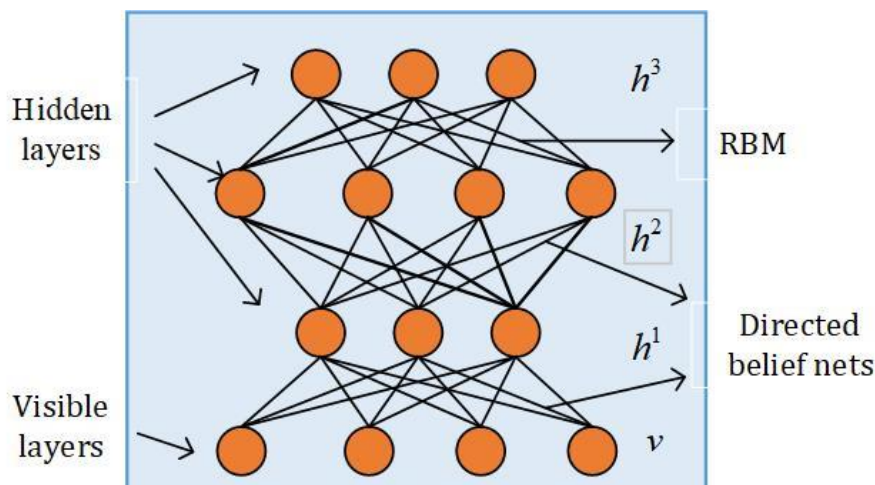


Fig. 2-2. The basic structure diagram of DBN.

Some DBN-based FDD methods are carried out in the motor drive system. A novel hierarchical diagnosis network (HDN) rolling carrying automatic diagnosis method, consisting of two layers of DBN, was proposed in [97]. WPT was used to provide representative features to deal with the non-smoothness of the fault vibration signal. Determination of fault location and its magnitude level can be achieved by HDN and weak points were identified in this way to avoid device performance loss and providing information for the reliability of the designed configuration. [98] proposed an improved convolutional deep confidence network (CDBN) with compressive sensing (CS). The structure of the proposed algorithm was divided into one gaussian input layer, 6 convolutions hidden layers, 6 pooling layers connected with 12 convolutions hidden layers and 12 pooling layers. The output was fed into a softmax classifier for fault classification. The compressed vibration signals as input data and there two cases were considered for verification include single fault and compound faults. The performance of testing accuracy was 94.80% and the standard deviation was 0.53. To improve the analysis efficiency, CS was used to reduce the amount of vibration data. Then, a new CDBN model with Gaussian visible units was developed to enhance the functional learning capability of compressed data. Furthermore, the constructed deep model generalization efficiency was improved using the exponential moving average (EMA) technique. A discriminative deep belief network (ACO-DDBN) based on ant colony optimization was presented in [99]. The proposed method consists of one input layer, two hidden layers and one output layer. The input

signal is a vibration signal with 1024 data points. It takes 1592.5s for training the model. After the training process, the training accuracy and the testing accuracy are 94.7% and 91.2% respectively. The RBM greedy layer-by-layer learning algorithm can effectively pre-train unsupervised models regardless of the amount of available training data. However, the performance of deep belief networks can be affected by their parameters. Since ants find the best choice of parameters throughout the search process, ACO is suitable for selecting parameters. Therefore, the parameters of the model are obtained by using the ACO method. The composition of the DDBN model can be computed automatically without the optimization process and prior knowledge to improve efficiency.

2.5.7. Autoencoder

The autoencoder neural network is an unsupervised learning algorithm that makes the target value equal to the input value by using a backpropagation algorithm. Fig. 2-13 illustrates the basic structure diagram of AE. An autoencoder is a neural network that consists of two components: an encoder function and a decoder that generates reconstructions. Traditionally, autoencoders have been used for dimensionality reduction or functional learning. An improved prototype structure of the autoencoder has resulted in a DAE that first complete the pre-training of the hidden layer using an unsupervised layer-by-layer greedy training algorithm and then uses BP to tune the entire neural network through systematic parameter optimization. This algorithm greatly reduces the performance metrics of the neural network and effectively improves the undesirable situation where the BP algorithm tends to fall into local minima. In short, compared with the original AE, DAE can increase depth, improve learning ability, and help pre-training. SAE only changes one thing: the input data is fed into the model with noise, and then the original image without noise can be restored. Through this method, a better robust representation can be extracted.

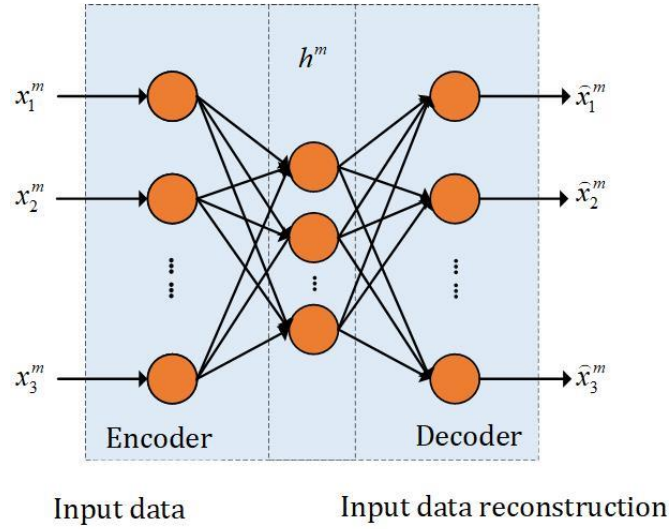


Fig. 2-3. The basic structure diagram of AE.

The dimensionality reduction includes the encoder network. The function reduces the initial high-dimensional data to a low-dimensional representative. The decoder network is the opposite of the encoder network and is part of the restoration process. The function returns the studied low-dimensional features to the high-dimensional data. The equations are shown as below:

$$h_i = f_{\theta_1}(W_1x_i + b_1) \quad (2-21)$$

$$\hat{x}_i = g_{\theta_2}(W_2h_i + b_2) \quad (2-22)$$

where W and b are the weights and biases of the network.

The purpose of the autoencoder model is to learn useful hidden representations by minimizing the reconstruction error. Therefore, the parameter sets θ_1 and θ_2 can be optimized by minimizing the reconstruction error L_{rec} while giving n training samples.

$$L_{rec} = \frac{1}{n} \sum_{i=1}^n \|x_i - \hat{x}_i\|^2 \quad (2-23)$$

$$\hat{\theta}_1, \hat{\theta}_2 = \arg \min L_{rec}(\theta_1, \theta_2) \quad (2-24)$$

where $\hat{\theta}_1$ and $\hat{\theta}_2$ denote the optimal values of θ_1 and θ_2 , respectively. The stochastic gradient descent (SGD) algorithm can be used to solve this optimization problem. The equations are shown as follow:

$$\hat{\theta}_1 \leftarrow \theta_1 - \lambda \frac{\partial L_{rec}}{\partial \theta_1} \quad (2-25)$$

$$\hat{\theta}_2 \leftarrow \theta_2 - \lambda \frac{\partial L_{rec}}{\partial \theta_2} \quad (2-26)$$

where λ is the learning rate.

A monitoring method based on stacked denoising autoencoders was proposed in [100]. The stacked denoising autoencoder-based approach can effectively extract robust features from corrupted data and shows well potential in the field of process monitoring. It is suitable for specific health state identification for signals containing environmental noise and fluctuations in operating conditions [101] [102]. A novel method namely local connection network constructed by normalized sparse autoencoder (NSAE-LCN) was proposed for intelligent fault diagnosis [103]. In this approach, the LCN first learned various meaningful features from the vibration signal using NSAE. Then, the LCN generated displacement-invariant features to classify the health condition of the machine based on the learned features. In [104] [105], a new deep learning algorithm for bearing fault diagnosis was proposed. A combination of discriminative and structural information between different fault conditions in a deep autoencoder model was applied. The method can study the association structure and structural relationship information between multiple fault states, which helped to improve the stability of the deep neural network. To effectively assess the health of a motor, various sensors were installed in different locations to obtain more fault signals. However, due to different sensor arrangements and environmental disturbances, the acquired signals may change, which led to different diagnostic results. To improve the reliability of diagnosis, a signal fusion technique was proposed in [106]. The proposed method combined SAE and DBN. Data features were extracted from sensors and fed into SAE for feature fusion. The SAE has two hidden layers with the same structure and parameters, while DBN has three layers. The training data was vibration signals of under inner-race fault and outer-race fault with 1260 samples. The classification accuracy was up to 97.82%. For feature fusion, time and frequency domain features from various sensor signals are extracted and fed into several two-layer sparse

autoencoder (SAE) neural networks. The fused feature vectors are used to machine health indicators. [107] proposed a simple deep learning clustering method, inspired by [43], which applied manifold learning to off-the-shelf embeddings to find an alternative model for clustering networks and simply combined the manifold learning method. The proposed model included 5 layers and the size of the input layer was equal to the size of

TABLE 2-3 Highlight of Deep Learning

Reference	Theme	Principle	Highlight
[77]	DCNN	<ul style="list-style-type: none"> • Multiple hidden layers • Learn hierarchical representations 	<ul style="list-style-type: none"> • Deep mining signal features • To require large training dataset
[74]	CNN	<ul style="list-style-type: none"> • 1-D Convolutional Neural Network • Scalar multiplication and addition • Raw data input 	<ul style="list-style-type: none"> • To decrease computing cost • High efficiency • Insufficient classification accuracy
[75]	Sparse filtering CNN	<ul style="list-style-type: none"> • Unsupervised two-layer neural network • Softmax regression 	<ul style="list-style-type: none"> • Adaptive learning feature • No manual labeling required
[76]	CCA KLD CNN	<ul style="list-style-type: none"> • Moving Average Technique • Fault matrix input 	<ul style="list-style-type: none"> • Statistics are more sensitive to initial failures • To improve computational efficiency • No prior knowledge required
[78]	CNN RNN	<ul style="list-style-type: none"> • Vibration signal input 	<ul style="list-style-type: none"> • Efficient and time-saving
[79]	CNN ELM	<ul style="list-style-type: none"> • Weighted orthogonality constraint • Randomly generate hidden weights 	<ul style="list-style-type: none"> • To reduce training complexity • To reduce manual intervention • To improve generalization performance
[80]	RNN- WDCNN	<ul style="list-style-type: none"> • Vibration data input • Domain adaptation and noise suppression 	<ul style="list-style-type: none"> • No feature extraction required • High Robustness
[81]	WDCNN	<ul style="list-style-type: none"> • Raw vibration signal input • Adaptive batch normalization 	<ul style="list-style-type: none"> • To improve network accuracy • No pre-processing required
[82]	TICNN	<ul style="list-style-type: none"> • End-to-end learning • 1-D structure input • Direct denoising 	<ul style="list-style-type: none"> • No manual feature extraction process required • High robustness • High accuracy
[83]	SVM-CNN	<ul style="list-style-type: none"> • Unsupervised fault detection • Online multi-fault classification 	<ul style="list-style-type: none"> • High generalization ability • Robustness
[84] [108]	CNN	<ul style="list-style-type: none"> • 2-D image conversion 	<ul style="list-style-type: none"> • Time-consuming training

		<ul style="list-style-type: none"> • Eliminate the impact of manual features • Easier handling of big data 	<ul style="list-style-type: none"> • High hardware conditions • Great training capabilities
[85]	FFT CWT CLSTM	<ul style="list-style-type: none"> • Multi-channel array input • Input length sensitivity analysis 	<ul style="list-style-type: none"> • Efficient learning of spatial-temporal features • To enhance classification performance
[86] [109]	LSTM CBLSTM	<ul style="list-style-type: none"> • Original sensing signal composition revealing fault characteristics 	<ul style="list-style-type: none"> • Abstraction and deep learning ability • No expert knowledge required
[87] [53]	AE-RNN	<ul style="list-style-type: none"> • Time series data dimensionality reduction • Raw vibration signal input 	<ul style="list-style-type: none"> • To reduce dimensionality Effective feature extraction • To improve classification efficiency
[110]	SGU RNN	<ul style="list-style-type: none"> • Single-gate joint recurrent neural network • Wavelet Packet Decomposition 	<ul style="list-style-type: none"> • To reduce network parameters • To reduce computation time
[94] [96] [111]	GAN	<ul style="list-style-type: none"> • Unsupervised sample generation • Adaptively learning samples • Generated sample input 	<ul style="list-style-type: none"> • Strong generalization capability • Non-original feature signal input • Not an end-to-end structure
[95]	SDAE-GAN	<ul style="list-style-type: none"> • Estimating the probability distribution • Extended Diagnostic Sample 	<ul style="list-style-type: none"> • Automatic extraction of effective fault characteristics • Stronger noise immunity • Improved generalization capability
[57]	DAAN	<ul style="list-style-type: none"> • Feature compression and visualization • Vibration signal input 	<ul style="list-style-type: none"> • Effectively learn domain-invariant features. • Diagnosis under different operating conditions
[98]	CDBN CS	<ul style="list-style-type: none"> • Reduce vibration data • Layered generation model 	<ul style="list-style-type: none"> • No manual feature extraction required • Great generalizability
[99]	ACO DDBN	<ul style="list-style-type: none"> • Layer-by-layer unsupervised pre-training • Search for the optimal number of neurons and learning rate of the hidden layer 	<ul style="list-style-type: none"> • Accurate determination of model parameters • To increase the computational burden
[54][106]	SAE DBN	<ul style="list-style-type: none"> • Feature Fusion • Unsupervised learning weights 	<ul style="list-style-type: none"> • Insensitive to training samples • High classification accuracy
[97]	HBN	<ul style="list-style-type: none"> • Two-Layer DBN • Vibration signal input 	<ul style="list-style-type: none"> • High reliability • To overcome overlap problem caused

[52] [101]	SDA	<ul style="list-style-type: none"> •Health status division •Greedy training 	by noise <ul style="list-style-type: none"> •Adaptive mining of salient fault characteristics •High diagnostic accuracy •Strong robustness
[103] [105]	NSAE LCN	<ul style="list-style-type: none"> •Raw vibration signal input •Obtain translation invariant features 	<ul style="list-style-type: none"> •To generate displacement invariant characteristics •Effectively identify the mechanical health condition
[104]	AE	<ul style="list-style-type: none"> •Association Matrix 	<ul style="list-style-type: none"> •To dig complex information •High diagnostic accuracy

input data. The ReLu was applied for the activation function while the Adam optimizer was implemented. Bearing fault data was used for experimental validation. The dataset contained 10 types of bearing health conditions with 10000 samples. The average classification accuracy was up to 98.99%. Instead of complex clustering networks, the shallow clustering algorithm presents a new deep clustering method for E2LMC, which is based on autoencoder embedding local stream shape learning for unsupervised bearing fault diagnosis.

Table 2-3 summarizes the deep learning methods for fault classification. The merits and demerits of deep learning are presented as follows.

Merits:

- 1) High learning ability. Deep learning performs well and has a great learning ability.
- 2) Strong adaptability. Deep learning contains complex neural network layers that can be mapped to any function to solve complicated classification problems.
- 3) Well portability. Many frameworks can be used.

Demerits:

- 1) Computationally intensive.
- 2) Deep learning requires large data and computing power so that the cost is extremely high.
- 3) High hardware requirements.
- 4) Complex Model design.

2.6. Other AI-based approaches

In addition to the traditional machine learning and deep learning introduced above, some other popular artificial intelligence-based methods are also reviewed in this section including hybrid algorithms combining fuzzy logic and artificial neural network methods (ANFIS), transfer learning (TL), compressed sensing (CS), Infrared thermography and temperature estimation strategy, and genetic algorithms, etc. Table 2-4 summarizes the characteristics of each AI-based method.

2.6.1. Adaptive neuro-fuzzy system (ANFIS)

Artificial neural networks (ANN) have proven to be a reliable technique for diagnosing motion conditions with high learning capabilities. However, artificial neural networks are not interpretable and cannot explain specific decisions to the user in a human-understandable form. Another technique used for fault detection and diagnosis is fuzzy logic (FL). It can imitate human knowledge according to clear and understandable linguistic terms and then convert the linguistic and heuristic terms into complex machine computed values through fuzzy rules and auxiliary functions. The initial parameters and auxiliary functions of if-then rules are usually prepared by experts. Therefore, fuzzy logic needs to be fine-tuned to obtain an acceptable rule base and to optimize the parameters for the available data. The integration of these two methods can solve only one problem from fuzzy logic or ANN. This method has been applied to motor fault diagnosis [112]. Adaptive Neuro-Fuzzy Inference System (ANFIS) [113] is a special neuro-fuzzy classifier approach that combines the adaptive capabilities of artificial neural networks with a fuzzy logic qualitative approach. It has been successfully implemented for automatic fault detection and diagnosis of induction motors [114]. In recent years, ANFIS and its variations with other methods have been widely developed as fault classification techniques. In terms of bearing fault diagnosis, ANFIS with genetic algorithm [115] and ANFIS with wavelet transform [116] are two examples of combined algorithms. ANFIS has been used to

classify faults in induction motors with variable drive speeds [117]. If the measurement data is large and includes redundant noise, the accuracy of the output will be greatly reduced when the data is fed directly into the classifier. Feature extraction and selection can minimize the dimensionality of the data by selecting the basic features, which refer to the transition of the current features to the lower-dimensional space. However, when feature extraction is completed, each feature set contains several redundant or unnecessary features, as well as significant features in the feature space. Therefore, a feature selection process is required to select the minimum features that define the system state from the entire feature set. As a feature extraction method, decision trees were employed in [118], which was a process for removing redundant features from data to reduce the quantity of data required for efficient learning, classification accuracy, a compact and simply understood knowledge base, and rapid computation. For fault diagnosis of induction motors, it integrated Classification and Regression Trees (CART) and ANFIS adaptive techniques.

Since insufficient accuracy of the measurement equipment, model errors, or the influence of environmental conditions of the measurement process leads to noise in the signal that usually cannot be avoided, noise filtering mechanisms are important to improve the ability to pre-process the measured data for analysis and extraction of valuable information. Singular spectrum analysis (SSA), and sparse filtering (SSA/SF) are promising tools and the effectiveness of FL depends heavily on the accuracy of the fuzzy set, which involves logical relationships between fuzzy rules and relational functions input and output. [119] proposed an ANFIS based on SSA/SF bearing fault detection method, which was combined with an online detection method. Information was extracted from the measurement data with noise by SSA and SF, and a database with tagged data was created. The ANFIS parameters were optimized by the tagged data and then faults were detected by the ANFIS comparator. In [59], a higher-order particle filter was developed to make predictions based on an m-order HMM that integrates ANFIS and modeling noise. Advanced particle filters were applied to system status modeling. By combining ANFIS and process noise, a high-order HMM was formed that can be used to describe the fault process. Due to the dynamics of the system, an online model

adaptive scheme for fault propagation was required. ANFIS was trained with available conditional data to build ANFIS for laminar imaging trend models. A new classification method based on time-frequency representation (TFR) and criteria-based decision-making was proposed in [128]. The fuzzy Doppler delay plane was used as a feature extraction space to reduce the computational effort. This is an error probability model based on a statistical approach for selecting the optimal number of features to be extracted from the streamwise plane and then using the capability of a neural network to learn a nonlinear functional relationship between the input and output. The model is designed to maximize the separability between different classes.

2.6.2. Compressed sensing

The increasing demand for information about complex mechanical systems in recent years has promoted the use of high-dimensional information. To examine health conditions comprehensively, monitoring systems based on traditional sampling theorems are commonly employed. Multiple sensors acquire a large amount of while data at high sampling rates over a long operating cycle puts a burden not only on the hardware but also on the data storage. In the era of big data driving motor health monitoring, how to extract effective information from a large amount of data is an important topic, and compressed sensing (CS) has attracted widespread attention. This method theoretically obtains all the information contained in the original signal and achieves the reduction of the signal in size. It frees the data from Nyquist theory and enables compressive acquisition by nonlinear projection in the transform space. Thus, the sampled data is greatly reduced and contains all the information. Fault diagnosis is achieved based on the measured data in the compressed domain, which is supported by the depth domain. A new intelligent FDD combining CS and DNN was proposed in [120]. Random projections in the transform domain were used as compressed samples to perform sample compression, and then a stacked autoencoder network based on sparse autoencoder (SAE) was built on mining fault information using a deep network architecture. In addition, the detection

of multiple hybrid faults is an essential topic. [121] presented a diagnostic method for tracking and analyzing the frequency of multiple and combined faults in IM, depending on the measurement and optimization of a high-dimensional hybrid feature set. The proposed method can detect the possibility of multiple and combined faults occurring simultaneously.

2.6.3. Infrared thermography and temperature estimation strategy

When constructing an electric motor or selecting its control approach, the significant thermal stress on possibly defective components of the motor must be taken into consideration. Competitive pressure and high production costs, particularly in the automotive industry, lead engineers to look for new ways to increase the safety of embedded materials. Because overheating can severely damage motors, accurate temperature information must be provided during operation. Among the typically critical components sensitive to overheating, such as stator end windings and bearings, permanent magnets in the rotor are particularly susceptible to damage to the motor. Although sensor-based measurements provide a quick and accurate picture of the machine's thermal state, it is not economically or technically feasible to assess rotor temperature in this way. In particular, direct rotor monitoring techniques, such as infrared thermography [122] [123] or classical thermocouples with slip rings on the shaft [124], have not yet entered industrial mass production. Therefore, based on this model, the study focuses on estimating the rotor and permanent magnet temperatures. In contrast to physically driven estimation methods, machine learning (ML) models will differ from any classical approximation of the underlying thermal theory [125]. Fig. 2-14 shows the idea of fitting the ML model to the collected test bench data and eventually informing any controller. The more accurate the thermal state information obtained by the control system, the better the ability to monitor critical operations and apply derating power. In addition, suppose rich data sets can be recorded on the test bench or in production in the automotive industry. In that case, engineers can rely on them to model simpler temperature estimators than deep neural networks. The use of domain-specific expertise and instrumentation specifications can be avoided. In addition,

certain classical supervised learning algorithms can handle the temperature of essential components in PMSM in real-time, as demonstrated by extensive benchmark analysis of many different benchmarks. Alternatively, infrared thermography (IRT) can be used to detect bearing failures in rotating machinery in a non-destructive, non-contact manner. However, performance is limited by the minuscule amount of information and string noise in IR thermal images. To address this problem, [126] developed a two-dimensional discrete wavelet transform (2D-DWT) based IRT technique for identifying different bearing faults in IM, such as inner and outer ring cracks and insufficient lubrication, using a two-dimensional discrete wavelet transform (2D-DWT) based IRT method. Principal component analysis (PCA) was used to decrease the dimensionality of the recovered features to obtain the best feature selection. and then a mar distance (MD) procedure was used to rank the selected features in order of importance. For fault classification and performance evaluation, these chosen characteristics were input into complex decision trees (CDT), linear discriminant analysis (LDA), and support vector machines (SVM).

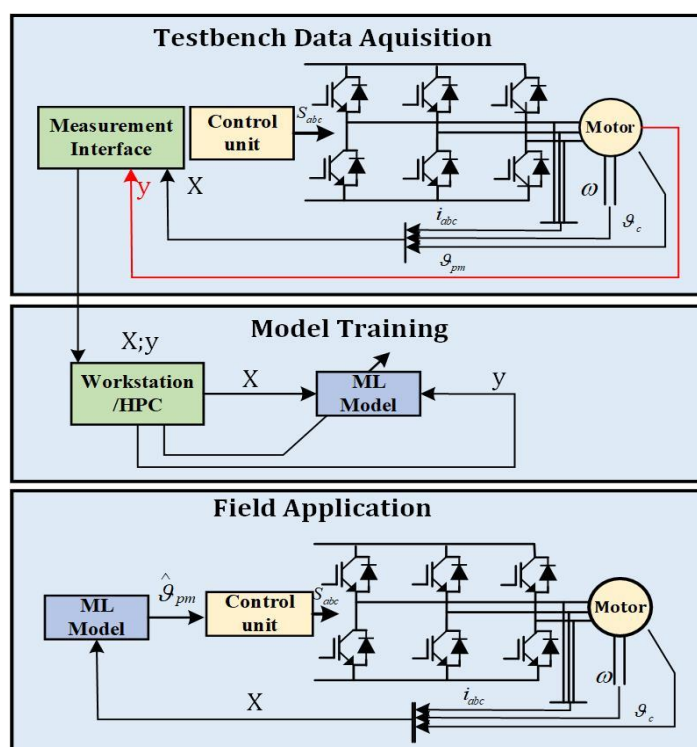


Fig. 2-14. The entire process test bench.

2.6.4. Transfer learning

Fault signal processing includes the separation and extraction of fault features for later use in predictive models. Fault discrimination identifies fault types by testing the fault features obtained through signal processing using a complete training model. Typically, the number of fault samples is usually smaller than the number of regular samples, and the problem of data class imbalance will lead to the overfitting of many data-sensitive classification models. The data imbalance problem can be solved by weighting cost, but for practical motor fault diagnosis, it is difficult to determine the weighting parameters. Therefore, obtaining as much fault data as possible from data sources is a major issue. Simulation of fault scenarios is the easiest way to obtain fault characterization results. However, it is impractical for mechanical parts of motor equipment to intentionally damage them to achieve fault characteristics. Therefore, it is a challenge to make full use of historical data and ensure the accuracy of the new task model. [127] proposed a method to solve the problem of degradation of classification accuracy due to different fault data caused by feature transfer. In feature learning, transfer component analysis (TCA) is a classical approach to solve adaptive problems. Data in both source and target domains are mapped to a high-dimensional replica kernel Hilbert space (RKHS). The data distance between sources is minimized while interior features are preserved. The TCA data feature extraction method is used to discover standard features in both the source and target domains. Through feature learning, a fault diagnosis model under historical operating conditions can be built to address the problem of insufficient data effectively.

2.6.5. GA-based approach

Genetic algorithms are search algorithms based on natural selection and genetic principles, characterized by parallel computation and global optimality, as their derivation process is a method of approaching the optimal solution. Moreover, compared with general optimization methods, genetic algorithms require less information to achieve optimal control. Therefore,

genetic algorithms are often used to optimize the parameters and structure of neural networks or fuzzy logic systems. [28] presented a diagnostic method based on the envelope, FFT, and backpropagation GA-ANN algorithm for rolling bearing faults to determine the NN structure accurately. The proposed GA-ANN combination strategy can be used to assist experts in designing appropriate, fast, and accurate ANN structures for specific diagnostic problems. Besides, to improve feature separability, several feature selection methods include GA and particle swarm-based optimization have different drawbacks consist of the tendency to fall into local optima and computational inefficiency [130]. The presence of redundant and insignificant features in the high-dimensional feature set can minimize fault identification accuracy. Moreover, unlike traditional classifiers, the artificial immune system (AIS) is a commonly used technique for anomaly detection, independent of the a priori knowledge of the model failure modes. For motor bearing faults, traditional fault detection methods are based on solving specific problems and their design depends on various aspects of the bearing. [129] proposed a GA optimization algorithm that combined unique multi-domain feature extraction with a supervised artificial intelligence technique (GA-AIS) to train the detector using the minimum amount of information. The proposed method can be used to detect fault types under a wide range of operating conditions. Generally, there is no universal approach that can be used for all practical fault situations. Negative selection algorithms (NSA) are used for detectors to distinguish standard data from faulty data. NSA and its variants analyze the vibration and current signals of the motor. Different detector generation strategies form NSA with different variants, including GA optimization, clone selection optimization, and stochastic native [131] [132]. However, the increase of data leads to a decrease in the speed of detector generation and detection.

2.6.6. Artificial Ant System (AAS) and dictionary learning

A uniform sampling window samples the signal, while the more petite frame width and smaller size are insufficient to accommodate the input signal [133]. Simultaneously, the high-

dimensional signal increases the computational burden. [134] proposed a new optimization technique based on the Artificial Ant System (AAS). It was successfully validated for motor faults. Besides, dictionary learning is a powerful method for extracting feature conditions. The multiscale dictionary learning method with transformed coefficients performs well in extracting fault signals and requires less learning time compared to ordinary dictionary learning. [135] proposed a faster adaptive parametric multiscale dictionary learning method that adaptively selected the learning scale and simultaneously estimated the sparse coding parameters in dictionary learning. The technique has a relatively short running time and great fault detection performance. [136] developed an effective and responsive motor fault diagnosis method that combined feature extraction, feature incremental generalized learning after collecting the starting sample data and processing it. These processed data were imported into broad learning to train the network. The network was continuously trained by feature incremental broad learning until the test accuracy was satisfactory.

TABLE 2-4 Highlight of Other AI-Based Method

Reference	Theme	Principle	Highlight
[117]	ANFIS	<ul style="list-style-type: none"> • If-then rule • Membership functions input 	<ul style="list-style-type: none"> • Nonlinear Approximation Capability • High adaptability
[118]	DT ANFIS	<ul style="list-style-type: none"> • Rule conversion • Vibration and current signal input 	<ul style="list-style-type: none"> • To reduce data volume • To enhance classification performance • Less accurate classification of the current signal
[119]	ASSBDIM	<ul style="list-style-type: none"> • Sparse filtering • Singular spectrum analysis • Time series data input 	<ul style="list-style-type: none"> • High accuracy • Low calculation cost • Suitable for online applications
[59]	HMM-ANFIS	<ul style="list-style-type: none"> • Markov model prediction • Probability density function 	<ul style="list-style-type: none"> • Nonlinear mapping • Real-time state estimation
[120]	Compress data Deep learning	<ul style="list-style-type: none"> • Nonlinear projection for compression capture • Unsupervised learning 	<ul style="list-style-type: none"> • Do not rely on a priori knowledge • To dig hidden data

[136]	Feature Incremental Broad Learning	<ul style="list-style-type: none"> • Reconfiguration system • Simplify the model 	<ul style="list-style-type: none"> • Suitable for handling large amounts of data • High diagnostic accuracy • Less training time • The feature extraction method is not optimal
[126]	Infrared Thermography ML	<ul style="list-style-type: none"> • 2-D thermal image input • Optimal eigenvector matrix transfer 	<ul style="list-style-type: none"> • Non-destructive • Non-contact detection • Performance affected by redundant information noise
[127]	Transfer learning	<ul style="list-style-type: none"> • Feature transfer • High-dimensional mapping of data 	<ul style="list-style-type: none"> • To reduce feature data requirement • Cannot be applied to multi-target working condition
[128]	TFR	<ul style="list-style-type: none"> • Smooth blurred plane feature extraction 	<ul style="list-style-type: none"> • To reduce computational burden • To improve feature separability
[121]	GA-PCA LDA ANN	<ul style="list-style-type: none"> • Estimating high-dimensional hybrid feature sets 	<ul style="list-style-type: none"> • Simultaneous monitoring multiple faults
[28]	GA-ANN	<ul style="list-style-type: none"> • Weighting and threshold optimization 	<ul style="list-style-type: none"> • Fast structure determination • High classification performance
[134]	AAS	<ul style="list-style-type: none"> • Unsupervised classification • Data Clustering 	<ul style="list-style-type: none"> • To improve monitoring effectiveness • Removal of redundant or irrelevant information
[129]	GA-AIS	<ul style="list-style-type: none"> • Spatial transformation 	<ul style="list-style-type: none"> • To reduce computational complexity
[133]			
[135]	Faster AP-MSDL	<ul style="list-style-type: none"> • Adaptive parameter estimation • Multi-scale learning 	<ul style="list-style-type: none"> • Short running time • Great fault detection performance

2.7. Discussion And Future Development

AI-based techniques have been proven to be highly effective for fault detection and diagnosis

in motor drive systems. Deep neural network-based methods have gradually become attractive in industrial applications due to the continuous upgrading of computer hardware. As the layers of neural networks deepen leading to the disappearance of locally optimal solutions and gradients. Pre-training methods alleviate the local optimal solution problem, and deep learning gradually becomes popular including DBN, CNN, RNN, LSTM, etc. To overcome gradient disappearance, transfer functions such as ReLU and max out replace sigmoid and form the basic form of DNN. DBN simply converts an image matrix into a one-dimensional vector as input without considering the two-dimensional structure information of the image. It can represent the distribution of data from a statistical point of view and can reflect the similarity of similar data itself. However, the generative model cannot obtain the optimal classification surface between different categories, resulting in the classification accuracy may not be as high as the discriminative model. In the area of image recognition, the convolutional neural network is a popular study topic. Its weight-sharing network topology resembles biological brain networks, minimizing the complexity of the model and the number of weights. Traditional recognition methods require extensive feature extraction and data reconstruction, so the image may be utilized directly as the input of the model. The signal of each layer of neuron in CNN can only propagate up one layer, and the processing of samples is independent at each moment, called forward neural network. In RNN, the output of a neuron can act directly on itself at the next timestamp. In addition to solving the temporal gradient disappearance, long and short time memory units (LSTM) are proposed to prevent gradient disappearance by implementing temporal memory function through gate switching. GAN is a generative learning algorithm that can efficiently mine the intrinsic distribution of a dataset using a small number of samples. In addition, the discriminative power of GAN discriminators makes it possible to build integrated fault diagnosis models. Besides, autoencoders can perform unsupervised learning from data samples, achieve great performance on different data sets without any new feature engineering.

The different signal pattern of the motor state is usually uncertain with changing operating conditions, and how to effectively detect motor state under varying operating conditions is also

a major challenge for future research. Traditional static neural networks can be optimized by adjusting the model parameters and structure to obtain higher performance control effects and monitoring performance. In addition, the concept of dynamic neural networks is proposed as a novel research topic in deep learning. Compared to static models with fixed parameters, dynamic neural networks can adapt to different input signals by changing the parameter structure, which offers excellent advantages in accuracy and self-adaptability. Therefore, dynamic neural networks with different state characteristics due to variable load states have great potential in electric vehicle powertrain condition monitoring. Moreover, deep reinforcement learning, a recently popular deep learning algorithm, also offers promising and feasible solutions for control drives of electric motors due to its more efficient learning capability. In conclusion, the adaptive adjustment of neural network parameters and model structure has a wide application space in electric vehicle powertrain system to obtain reliable and efficient motor drive performance to meet the high requirements of safe driving of electric vehicles. Furthermore, data-driven AI-based algorithms can effectively utilize big data, which are motivated by end-to-end frameworks that provide satisfactory performance with low requirements for domain knowledge. The improvement of robustness and generality of AI-based techniques aims further to enhance the AI-based capability of techniques in fault detection and diagnosis applications. They should apply to different tasks, including detection, diagnosis and prediction in various domains. Therefore, the development of interpretable AI-based technologies has attracted increasing attention in intelligent monitoring. In addition to fault detection and diagnosis of motor, they are further used for decision support. Eventually, autonomous condition monitoring and fault warning of the entire electric vehicle powertrain system can be achieved.

In summary, this chapter reviews the application of artificial intelligence techniques in motor fault diagnosis. Comprehensive studies of motor faults and their severity are still rare and have so far been limited to diagnosing faults in motors under specific operating conditions. It is difficult to detect faults in motors under light loads. In addition, the accuracy of fault diagnosis may be reduced due to fluctuations in rotor speed during data acquisition at different loads.

Therefore, it remains an open challenge to consider the impact of motor operating conditions on AI-based fault diagnosis. Artificial intelligence for pattern recognition or fault diagnosis includes a large number of different types of mathematical tools, i.e. pre-processing, extraction and selection of appropriate statistical features, and selection of model parameters. It is a challenge to choose which tool is best suited for a particular problem and machine in different situations. Moreover, there is a lot of scope for research in this area since condition monitoring techniques for fault detection and diagnosis of rotating machinery have been improved from traditional methods to artificial intelligence methods. Artificial intelligence-based diagnostic systems still have some challenging tasks to accomplish in terms of their efficiency, reliability, computation time, adequate database and robustness.

Overall, in this chapter, common electric motor and fault types are presented. The different fault detection and diagnosis methods have been also analysed. The mainstream methods of feature extraction are reviewed, the application of artificial intelligence techniques in motor fault diagnosis is stated in a large space and reviewed in three parts through theoretical background: traditional machine learning, deep learning algorithms and hybrid algorithms. In the deep learning part, almost all algorithms are based on ANNs, developed and changed to achieve different purposes. Finally, the latest developments, research gaps and future challenges in fault monitoring and diagnosis of motor faults are discussed.

Chapter 3 Hybrid Model for Inverter Fault Diagnosis of EV Powertrain

The data-driven approach plays a critical role in the reliability of permanent magnet synchronous motor (PMSM) drive for electric vehicles (EVs). Generally, data limitations and the ability of algorithms to extract fault features significantly affect the performance of the fault diagnosis. It is challenging to obtain the desired number and quality of samples due to the huge

cost of obtaining fault data for motor drive systems under complex operating conditions. Considering the drawbacks of data-driven methods for fault diagnosis including hardware costs and data uncertainty, a combined model and data-driven few-shot learning network was proposed to detect voltage source inverter (VSI) open-circuit faults in PMSM in this chapter. The proposed method utilized the residuals obtained from the observer data and the actual measurement data being used as raw samples to get rid of the effects of harmonics and thus improve the quality of the input data to reduce diagnostic uncertainty. Then, an attention-based vision transformer (ViT) model is applied to explore the association of global features of the input samples rather than local features for the input sample by signal dimension conversion, which in combination with the Siamese network framework. Finally, the experimental results verify that the proposed method is successful in extracting the fault characteristics from the restricted data and achieves stable diagnostic accuracy under varying faulty load conditions.

3.1. Introduction

The electric vehicle (EV) industry has grown rapidly in recent years due to the benefits of being environmentally friendly and energy efficient. A typical powertrain mainly consists of a battery unit, DC/DC converter, voltage source inverter (VSI), motor and gearbox [137]. As a power electronic device that drives a motor by DC/AC conversion, maintaining the reliability of the voltage source inverter (VSI) is critical in the whole EV powertrain system. The percentage of faults occurring in each part of the inverter varies as DC link capacitors 60%, power electronics devices 40%, diodes 3%, and inductive components 6% [138]. In addition, VSI also faces challenges such as electromagnetic interference (EMI) issues [139] [140]. Insulated Gate Bipolar Transistors (IGBTs) are commonly used as power electronics devices to synthesize the AC voltage at the output of converters. In variable speed drives, power semiconductor devices are the most fragile components, especially in high-power applications [141]. Faults in VSI can cause catastrophic consequences by faults propagating or fault propagation. Therefore, accurate and fast detection and diagnosis of faults in VSI are highly

important. Failure modes in inverter power devices are mainly divided into short-circuit faults and open-circuit faults. Failure is usually caused by high voltage, high thermal stress leading to failure of the bonding wires connecting the device terminals and breaking of the silicon chip. Switching short-circuit faults can bring abnormal overcurrent for a short period, which results in a short period, which results in irreversible damage to the inverter.

The short-circuit fault is detected and isolated by the protection circuit [142]. On the other hand, an open-circuit fault will not only damage the drive system but also decreases system performance with current distortion and electromagnetic torque fluctuations [143].

In the state-of-the-art studies, the approaches to open-circuit fault diagnosis of VSI have mainly focused on signal-based, model-based, and data-driven methods [144] [145]. Typically, voltage and current signal-based methods are used to achieve fault diagnosis by analyzing fault features extracted from the signal. Among the methods for current-based fault diagnosis, the average current method [146] and current ramp analysis [147] have attracted the attention of scholars due to the advantage of being independent of machine or inverter models and load transients. In [148], a method based on a reasonable estimate of the current amplitude can be used to deal with single or double signal loss faults. The asymmetric analysis between phase currents proposed in [149] can identify faults by detecting whether the field and torque components of the stator currents are orthogonally aligned, the Park vector method [150], and the normalized DC [151] [152], are also applied for the diagnosis of open-circuit and phase-breaking faults. Furthermore, in the proposed voltage-based approach [153] [154], fast fault detection and localization are achieved by adding additional voltage sensors or circuits with the drawbacks of the increased hardware cost and uncertainty.

Model-based methods have been significantly developed. [155] proposed fault diagnosis method based on zero-sequence current component (ZSCC) and stator current. The parity space method proposed in [156] is robust to parameter variations and suitable for sudden signal transients. Moreover, methods based on different types of observers have been proven to be highly efficient, [157] reported a fault detection method for open-circuit faults in modular multilevel converters based on sliding mode observers. The proposed Luenberger state

observer, nonlinear observer, and proportional-integral observer [158] [159] bring a great diagnosis performance with a relatively short detection time. Since these methods are based on residual values for diagnosis, they are highly sensitive to changes in motor parameters. Furthermore, a suitable threshold selector remains a key issue in ensuring an effective and robust diagnosis performance [160] [161] [162]. In addition, the method of relying on the motor model as a fault detector by computing the error between the estimated signal and the actual signal has been continuously investigated [163] [164] [165].

The data-driven approach examines the distributional characteristics of the training set to make the most of the diagnostic information in the sample. To identify open-circuit defects in three-phase inverters, a PCA-BN-based diagnosis technique was presented in [166]. In [167], a long-time and short-time memory technique was proposed to detect open-circuit and short-circuit faults in a five-level nested neutral pilot converter, and wavelet packet transform was applied to fault characteristics extraction. [32] investigated a fault diagnostic technique for open-circuit failures in multilevel inverter systems based on principal component analysis (PCA) and multiclass correlation vector machine (PCA-mCVM). Recently, fault diagnosis of power electronics using a hybrid approach combining model and data-driven approaches has become an attractive research hotspot. In previous studies, explicit analytical models based on converters and the learning capability of artificial neural networks (ANNs) have been used to achieve a fast diagnosis of various operating conditions with the help of model information and data-based learning capability. However, the proposed methods fail to consider the uncertainties contained in the signal that can affect the robustness and accuracy of the diagnosis for the extraction of fault variables.

Irrelevant features in the sample of diagnostic variables introduce additional uncertainty in the diagnostic performance. It is impractical to acquire large amounts of motor system fault data under changing operating conditions. It has been a challenge to achieve the desired diagnostic results using restricted fault diagnostic signals. This work proposed a hybrid diagnostic scheme in which a machine learning model for few-shot learning is introduced to comprehensively evaluate and utilize the fault information contained in high-frequency

components. In addition, a state observer is introduced to the analytical model to obtain current residuals as diagnostic variables to get rid of the uncertain components introduced by signal harmonics to improve diagnostic robustness and achieve satisfactory diagnostic accuracy with small sample size data. The contributions of this study are summarized below.

- (1) The analytical model incorporating an observer to calculate the sampling side of the residual value of the VSI fault signal can provide informative diagnostic variables to improve the robust performance of the diagnostic model.
- (2) A data-driven diagnostic model based on a Siamese network framework is proposed to model the sample and distance distribution. The experimental burden of obtaining large training datasets is avoided.
- (3) An attention mechanism-based feature extraction module is applied to extract valuable global features to reveal hidden information associated with VSI open circuit faults. Fast and accurate diagnosis is performed for different fault types.

3.2. Open-circuit Fault Analysis in PMSM Drive System

In a PMSM drive system, space vector pulse width modulation (SVPWM) is the classical control method for three-phase permanent magnet motors, where a specific switching pattern consisting of six power switching elements in a three-phase power inverter generates a pulse width modulated waveform that enables the output current waveform to be as close as possible to an ideal sine waveform. The space vector for the three-phase voltage synthesis is as follows:

$$U_{out} = kU_A(t) + kU_B(t)e^{\frac{j2\pi}{3}} + kU_C(t)e^{\frac{j4\pi}{3}} \quad (3-1)$$

To make the projection of the synthesized space vector on the stationary three-phase coordinate axis equal to the partial vector, the k value is considered as $2/3$, and define the switching function $s_x(x = a, b, c)$, $s_x = 1$ where the upper bridge is turned on and $s_x = 0$ where the lower bridge is turned on. The relational equation for the synthetic vector becomes the switching function of the bridge, so the above equation can be written as:

$$U_{out} = \frac{2}{3}U_{dc} \left(s_a + s_b e^{\frac{j2\pi}{3}} + s_c e^{\frac{j4\pi}{3}} \right) \quad (3-2)$$

The control system needs to output the vector voltage signal U_{out} , which rotates counterclockwise in space at a certain angular frequency ω . When it rotates to a certain sixteen-degree sector of the vector diagram, the system calculates the basic voltage space vector required for this interval and drives the power switching device in the state corresponding to this vector. The six switching transistors can form eight voltage space vectors placed in the sector diagram according to the phase relationship of U_{out} . As shown in Fig. 3-1, take T_1 open-circuit fault as an example, when T_1 is disconnected, it means that the switch signal, which changes from the high signal '1' to the low signal '0'. Sectors with a switch signal of '0' are kept unchanged at '0'. The three-phase voltage inverter current circuit will change due to the open circuit fault, therefore, the voltage excitation on the load will be distorted accordingly. In the vector diagram, six non-zero vectors have the same magnitude, and the adjacent vectors are spaced 60 degrees apart. Two vectors have zero amplitude and are located in the center. The switching signals are associated with open-circuit faults and show that the voltage-space vector has different phase voltage amplitudes in healthy and faulty states.

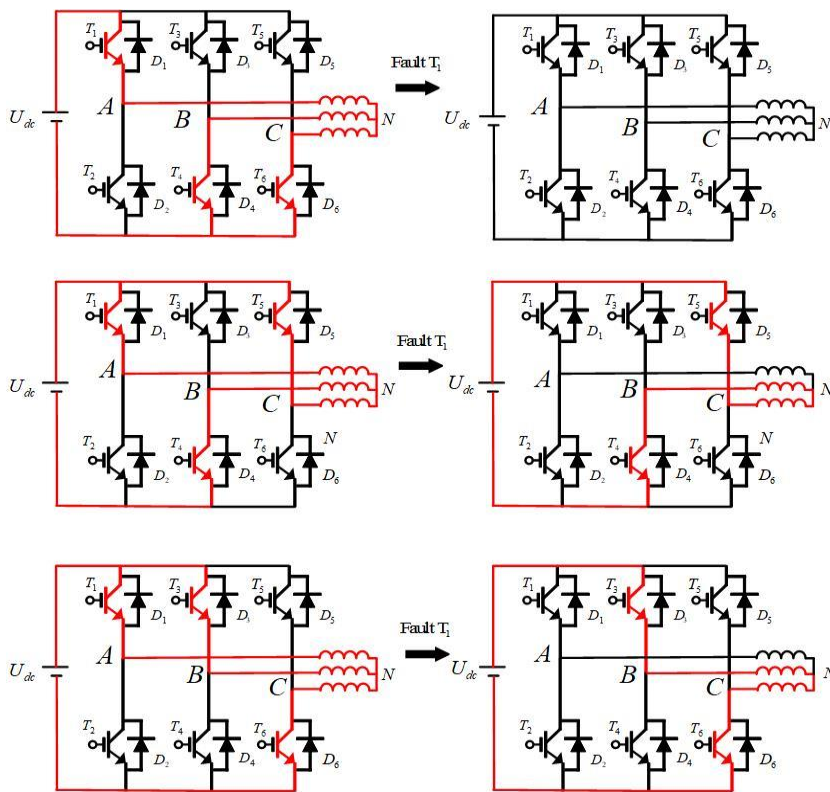


Fig. 3-1. Current loop in healthy and fault conditions.

To explain the mechanism of the T_1 inverter open circuit failure more clearly, the fault system is simulated by MATLAB/ SIMULINK. The PMSM used for simulation has 4 poles, the speed command is 1000 rpm, and the fault is injected at 0.5 seconds. Fig. 3-1. indicates the three-phase stator current waveforms of a PMSM in the switching device open-circuit fault and healthy states. The reasons for the distortion of each phase of the stator current in the fault interval and the normal interval in a complete cycle are analyzed as follows:

Failure interval: From Fig. 3-1, the current distortion occurring in the fault interval is significantly different from the healthy current signal. When the voltage space vector U_{ref} is in the late sector V, sector VI, sector I, and early sector II, the phase voltage V_{AN} obtained from the decomposition of the space vector while the fault state is 0. It means that when U_{ref} goes from the negative half-cycle to the boundary of the space vector while the fault state is 0. It means that when U_{ref} goes from the negative half-cycle to the boundary of the positive half-cycle, the synthetic voltage space vector provided by the system after the fault keeps V_{AN} at zero until U_{ref} enter the negative half-cycle again, V_{AN} is unaffected. Thus, the i_a is observed on the faulty stator current waveform in the negative half-cycle in line with the current waveform in the healthy state and remains at 0 on the positive half-cycle.

Normal interval: In simple terms, the normal interval is when the voltage space vector is in the later sector II, sector III, sector IV and the early part of sector V. The three-phase stator current waveform at this point is the same as the wave.

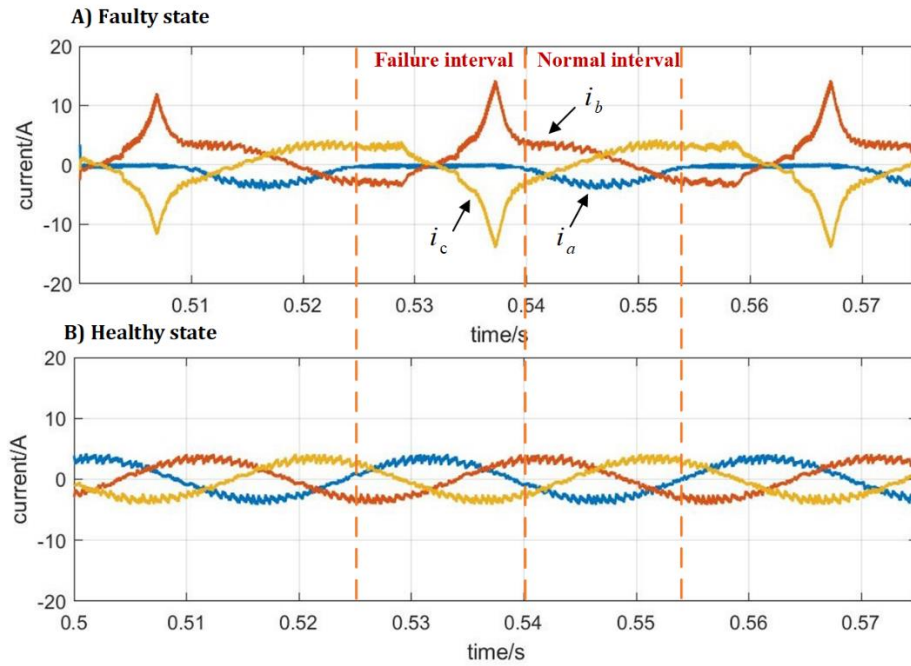


Fig. 3-2. Responses in the faulty half of a fundamental period.

3.3. The Proposed Model-Data-Hybrid-Driven Method

3.3.1. Luenberger Observer for the diagnosis variables

Based on the precise PMSM drive system model, the observer can be constructed at first. The Luenberger observer is created to enable fast current tracking at different speeds and load when the inverter is in a healthy state. Due to the sudden change in current during the open-circuit fault, the feedback gain of the observer does not allow the residuals to converge quickly, so the residuals deviate from zero. The main function of the Luenberger observer is to estimate the three-phase motor currents. The space state model used is based on the PMSM current dynamic model expressed as follows:

$$\begin{pmatrix} \frac{di_d}{dt} \\ \frac{di_q}{dt} \end{pmatrix} = \begin{pmatrix} -\frac{R_s}{L} & \omega_e \\ -\omega_e & -\frac{R_s}{L} \end{pmatrix} \begin{pmatrix} i_d \\ i_q \end{pmatrix} + \begin{pmatrix} \frac{1}{L} & 0 \\ 0 & \frac{1}{L} \end{pmatrix} \begin{pmatrix} u_d \\ u_q \end{pmatrix} + \begin{pmatrix} 0 \\ -\frac{\omega_e \psi_f}{L} \end{pmatrix} \quad (3-3)$$

The general state space model is given by:

$$\begin{cases} \dot{x}(t) = Ax(t) + Bu(t) + D \\ y(t) = Cx(t) \end{cases} \quad (3-4)$$

where $x(t) = \begin{pmatrix} i_d \\ i_q \end{pmatrix}$ represents the state quantity of the system, $u(t) = \begin{pmatrix} u_d \\ u_q \end{pmatrix}$ represents the control quantity, $y(t)$ represents the observed output of the system, and $C = \begin{pmatrix} 1 & 0 \\ 0 & 1 \end{pmatrix}$.

Since the observer is observable, the reconstructed *Luenberger* state observer equation is given by the following equation:

$$\begin{cases} \dot{\hat{x}}(t) = A\hat{x}(t) + Bu(t) + D + K(y(t) - \hat{y}(t)) \\ \hat{y}(t) = C\hat{x}(t) \end{cases} \quad (3-5)$$

where $(y(t) - \hat{y}(t))$ represents the difference between the estimated measured values and K represents the feedback gain. Moreover, the selection of K value affects the dynamic performance of the observer.

$$\text{Assume } \begin{cases} e = x - \hat{x} \\ \dot{e} = \dot{x} - \dot{\hat{x}} \end{cases} \quad (3-6)$$

where e represents the error between the observed value and the feedback. Substituting e into the above equation, giving:

$$\dot{e} = (A - KC)e \quad (3-7)$$

If we need to make e tend to be 0, then all the characteristic roots (i.e., poles) of the matrix $(A - KC)$ should be negative, which is:

$$\text{Re}[eig(A - LC)] < 0 \quad (3-8)$$

Through the pole configuration, the feedback gain K of the observer is obtained.

3.3.2. Transformer-Based Machine Learning Model

After the observer provides stable and informative diagnostic variables, machine learning models act as a data-driven approach to evaluate residuals by extracting sample features rather than threshold comparisons, which can simplify the diagnostic process by simultaneously diagnosing and locating faults. In this paper, a Transformer-based machine learning model is proposed. The proposed algorithm has several steps.

Patch embedding and position encoding

Since the model needs the input signal of the sequence, and the 2-dimension input signal of the image is obtained through the previous step, the flatten operation needs to be performed

after the image is divided into blocks. The input to the standard transformer is a 1-dimensional (1-D) token embedding. By converting the graph into a word structure and partitioning the picture into a small patch, each patch is equivalent to a word in a sentence. Patch embedding is the process of compressing each patch into a vector of a certain dimension through a fully connected network. Then, each converted embedding needs to be injected with location information.

$$PE_{(pos,2i)} = \sin (pos/10000^{2i/d_{model}}) \quad (3-9)$$

$$PE_{(pos,2i+1)} = \cos (pos/10000^{2i/d_{model}}) \quad (3-10)$$

where pos is the position that denotes relationships within each patch, and i represents the dimension. Each dimension of the position code corresponds to a sine wave. The wavelengths form a geometric progression between 2π and $2\pi \cdot 1000$. It allows the model to easily learn to focus on relative positions to convert consecutive images into individual tokens which are similar to NLP tasks, a more intuitive approach is used, which is to cut the images into chunks. However, it is worth noting that training large models while expanding the input does not expand the size of the input block, but rather the number of blocks. In many learning frameworks, to be compatible with various types of NLP tasks, a mark is added to the first position of the entire encoder, and the features from the first position of the encoder are then used as classification features to train the classifier. A similar framework is used in ViT, where a learnable class token is added at the first position of the framework, the features are encoded at the first position, and the classification results are finally obtained using the MLP header. As the network is trained, the token is randomly initialized and continuously updated, and it encodes the statistical properties of the entire dataset. In addition, the token aggregates information from all other tokens (global feature aggregation). As it is not inherently based on image content, it avoids bias toward specific tokens in the sequence.

Self-attention Mechanism

The entire network structure is made up solely of self-attention and feed-forward neural

networks. By stacking the transformer, a trainable neural network based on the transformer can be created. Consider RNN with information loss during sequential computation. The attention mechanism can be used to reduce the distance between any two positions in the sequence to a constant. In addition, it offers better parallelism than the sequential structure of RNN. The Attention function can be considered as a mapping from a query(Q) to a set of (key(K)-value(V) pairs. In the process of computing attention, there are three main steps: To obtain the

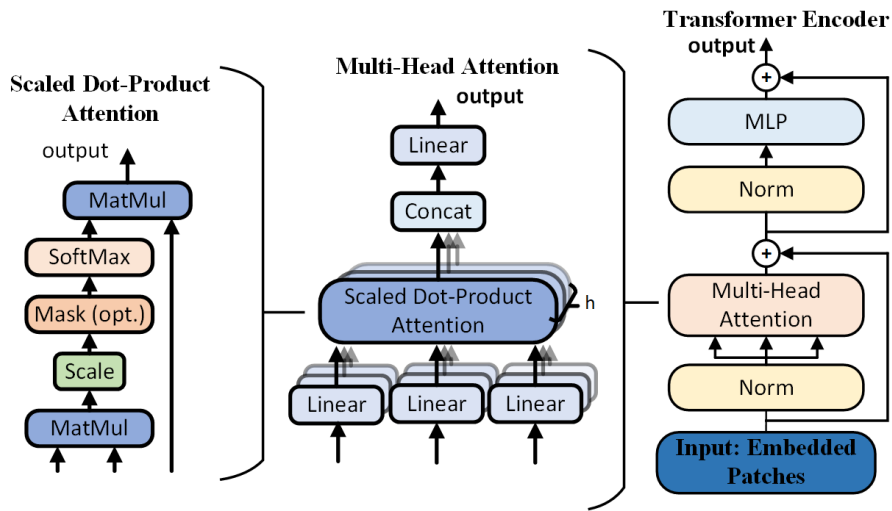


Fig. 3-3. Structure of transformer encoder.

weights, the first step is to calculate the similarity between the query and each key; typical similarity functions include concat, dot, product, and perceptron. In the second step, the weights are normalized using a *softmax* function. To acquire the final attention, the weights and the related key values are weighted and summed.

$$Attention(Q, K, V) = softmax\left(\frac{QK^T}{\sqrt{d_k}}\right)V \quad (3-11)$$

where the dot product of Q and K represents the similarity between Q and K . A larger dot product represents a greater degree of similarity. d_k represents the scaling factor what is introduced to prevent the value becomes too large as input of *softmax* and causing the partial derivatives to converge to zero. The results of Q and K are normalized by *softmax* to give a mask matrix (attention score matrix) with all values from 0 to 1, while V represents the linearly transformed features of the input. The mask matrix is multiplied by V to obtain the filtered features.

The purpose of introducing Multi-Head Attention in Fig. 3-2 above is to divide the model into multiple heads, forming multiple subspaces that allow the model to focus on different aspects of information. multi-Head Attention is the process of doing the Scaled Dot-Product Attention process h times and then combining the outputs.

$$\text{Multihead}(Q, K, V) = \text{Concat}(\text{head}_i, \dots, \text{head}_n)W^O \quad (3-12)$$

$$\text{head}_i = \text{Attention}(QW_i^Q, KW_i^K, VW_i^V) \quad (3-13)$$

Where W represents a different weight matrix.

Distance Metric

The Siamese network maps the input to the target space by a function that uses Euclidean distances in the target space to compare similarities. The training stage minimizes the value of the loss function for a pair of samples from the same category and maximizes the value of the loss function for a bunch of samples from different categories.

$$E_w(x_i, x_j) = \|TE(x_i) - TE(x_j)\| \quad (3-14)$$

where $E_w(x_i, x_j)$ represents the distance of input sample features. $TE(x_i)$ and $TE(x_j)$ represent the extracted features of the input sample after the transformer encoder in this article.

Loss Function

The input to the Siamese network framework is a pair of samples rather than a single sample. Given the label of whether a pair of samples are from the same category. In addition, two identical networks are designed sharing the same weights and a distance measure is applied to the output. A loss function was designed for the input pair of samples to determine whether they were from the same category or not.

$$L(y, w, x_i, x_j) = (1 - y) \frac{2}{Q} E_w^2(x_i, x_j) + 2yQe^{-\frac{2.77}{Q}E_w(x_i, x_j)} \quad (3-15)$$

where $E_w(x_i, x_j)$ is distance and the input is composed of a pair of samples and a label, when they are the same category, $y = 0$, otherwise, $y = 1$. Moreover, Q is the boundary of $E_w(x_i, x_j)$ which is the constant. The main advantage of this framework is that it is light on

labels and has good scalability. It also works well for data sets with a relatively small size of data.

Output

The similarity of the two inputs can be determined by calculating the Euclidean distance of the output with the following formula in terms of whether the output of the model is considered similar or different. The output is mapped to $[0,1]$ where 1 indicates that the two input samples have the highest similarity and 0 indicates the lowest similarity of being identical. $sigm$ is the sigmoid function and FC is the fully connected layer.

$$P(x_i, x_j) = sigm(FC(E_w(x_i, x_j))) \quad (3-16)$$

Training

The training process for fault diagnosis inputs sample pairs with the same or different classes into a ViT based on the dual-channel network framework to extract features, then outputs the similarity distance of the sample pairs, calculates the loss via Equation 15, and optimizes the model.

Testing

The input samples x_i are paired with samples from the support set during testing to create a new sample pair and data set for testing. Here the faults are divided into 4 labels, and the typical number of samples per label when constructing the support set is 5. Thus, 5 calculations are performed under each label on the samples to be tested to obtain the corresponding similarity probabilities and the average is taken as the final output.

Algorithm 1: Proposed algorithm for fault diagnosis

Input: Sample pairs I_{data} is the training data collected from the wavelet transform of residual variables. D is the depth of the network.

Output: Network parameters θ^l ($l=1, 2 \dots D$) obtained after training.

- 1: **Init ViT model** and network parameters θ_1^l , θ_2^l .
 - 2: **for** $episode = 1, \dots, i$ **do**
 - 3: $TE(x_i), TE(x_j) \leftarrow$ **ViT model** (I_{data})
 - 4: Calculate Euclidean distance $E_w(x_i, x_j) = \|TE(x_i) - TE(x_j)\|$
 - 5: Update θ_1^l , θ_2^l to minimize:

$$L(y, w, x_i, x_j) = (1 - y) \frac{2}{Q} E_w^2(x_i, x_j) + 2yQe^{-\frac{2.77}{Q}E_w(x_i, x_j)}.$$
 - 6: When the stopping criterion is satisfied.
 - 7: **End for**
 - 8: **Return** The updated network parameters θ_1^l , θ_2^l .
-

3.3.3. Mechanism of the hybrid method

As shown in Fig. 3-3, the flowchart of the model-data-hybrid-driven diagnosis method is divided into parts. A model-based observer is used to obtain the fault current residuals and then an attention-based few-shot learning model is used to efficiently diagnose VSI open-circuit faults. The current residual values are obtained from the measured motor phase currents and the estimated currents from the observer. The obtained residual values are processed to achieve the input pairs for the machine learning model. After the proposed dual-channel ViT module in Siamese network-based framework, the outputs are compared for similarity to determine the type of samples. The detailed procedures of the proposed ML algorithm are shown in Algorithm 1. Subsequently, the superiority of the algorithm has been verified by experiments.

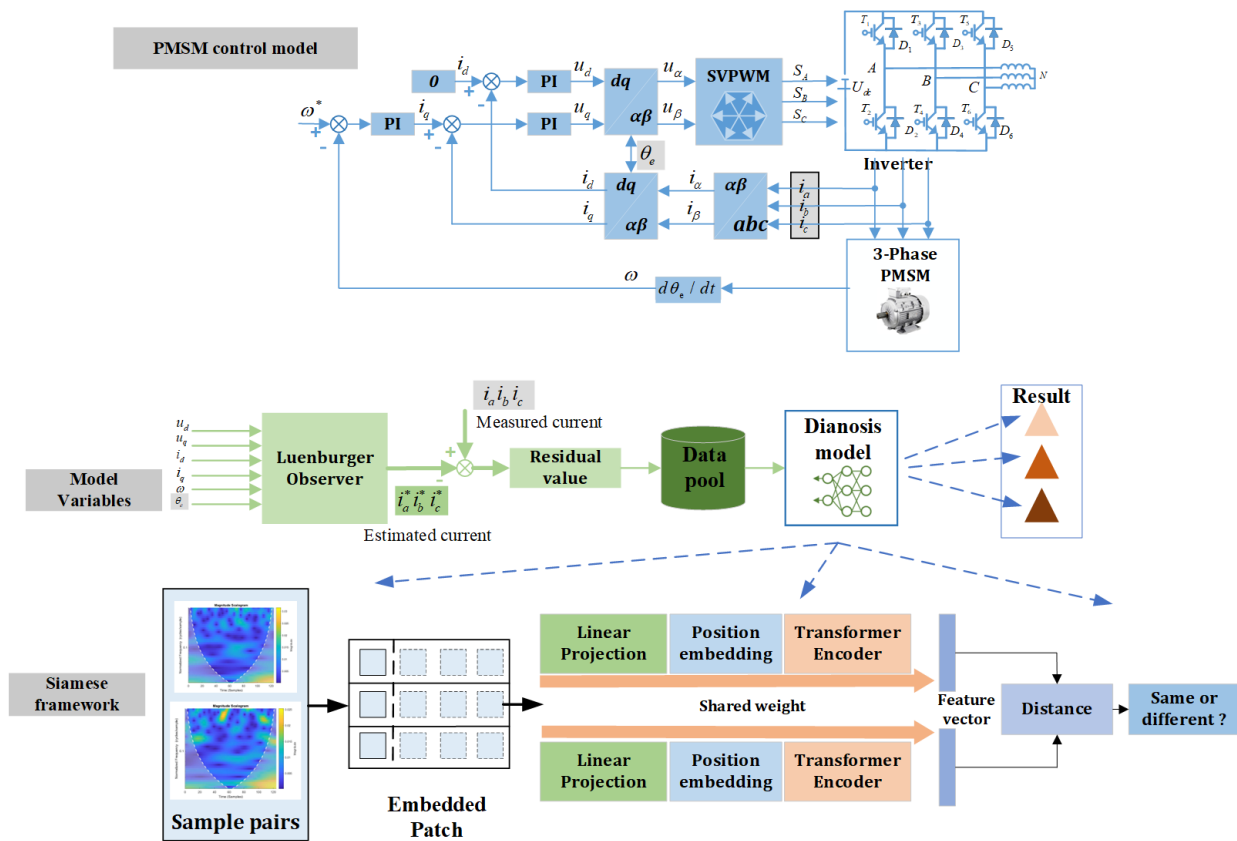


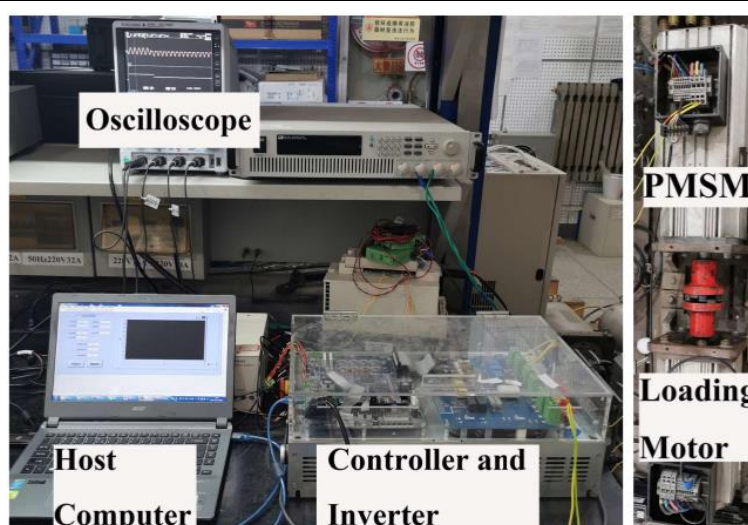
Fig. 3-4. Flowchart of model-data-hybrid-driven diagnosis method.

3.4. Experimental verification

The data used for experimental verification is collected based on the TMS320F28335 PMSM microcontroller, as shown in Fig. 3-4. The ePWM module of the TMS320F28335 includes a Trip-Zone (TZ) sub-module, which allows flexible configuration of the PWM signal for high and low impedance, hence the TZ sub-module was used to inject open-circuit faults in this study. Trip zone are submodules in the ePWM module used to implement overcurrent or other protection mechanisms. In addition, the internal state variables of the controller are transmitted via a D/A converter to an oscilloscope for observation and acquisition. The system sampling frequency is 10 kHz, and the three-phase current residuals are sampled in half an electrical cycle. The controller receives commands from the host computer via RS485. The PMSM parameters used in this experiment are listed in Table 3-1.

TABLE 3-1 The Parameters of The Experimental PMSM

Parameter	Value
number of pole pairs	4
resistance of stator	0.306 Ω
<i>d</i> -axis inductance	2.4 mH
<i>q</i> -axis inductance	2.4 mH
the flux of the rotor	0.281 Wb
DC voltage	60

**Fig. 3-5. The experimental platform.**

Four local experimental units were constructed in the experiment to simulate different inverter open-circuit fault states simultaneously. In the experiment, fault injection is achieved by artificially supplying a switch signal to the inverter module in the controller to simulate a real inverter open-circuit fault. Fault injection is simulated by switching the inverter transistor off, resulting in the current loop in the different phases being changed. During each simulation, the four sets of experiments have the same rating conditions and the number of short-circuit turns. A total of 400 sets of data had to be collected for the experiments. As shown in Table 3-2, the dataset is divided into a total of four sets of samples for four different fault states including the healthy state, Fault T1 state, Fault T1&T3 state, and Fault T1&T4 state. To balance the dataset, their state ratios are expressed as 1:1:1:1. The proposed approach is implemented for training and testing in this experiment using the PyTorch framework which is

a machine learning framework that provides powerful tools and libraries for building and training deep neural networks

TABLE 3-2 FAULTY STATE AND LABEL

Operating Condition	Faulty State	Label
Dynamic	Healthy	01
Dynamic	T1 Faulty	02
Dynamic	T1&T3 Faulty	03
Dynamic	T1 \$T4 Faulty	04

3.4.1. Model-Based Residual Analysis

The qualified diagnostic variables require that the diagnostic variables should remain constant when the system is operating without a fault, regardless of changes in operating conditions. When a fault occurs, these variables will rapidly deviate from the constant point and depending on the cause of the different faulty states shows different features.

Fig. 3-7 shows the three phase residuals under different fault states. Different fault characteristics can be observed from the residual signal in the time domain. Fig. 3-6 shows the variation of the estimated and actual values of the observer in different fault states. It indicates that the feedback gain of the observer when different open circuit faults occur does not allow the residuals to converge quickly causing the residuals to deviate from zero. Otherwise, Fig. 3-8 shows the dynamic response of the A-phase current for different load variations, where the load variation is now sought to increase rapidly for a short period. The dynamic response of the observer fluctuates as the load fluctuates between the different ranges. The residual current varies periodically over a constant range, regardless of whether the load is gradually increasing or suddenly decreasing. It shows that the three-phase residual current can vary periodically within a constant range, regardless of changes in other parameters due to uncertain fluctuations in the load. It demonstrates the robustness of the residual variable as a diagnostic variable. Furthermore, the rapid deviation of the three-phase current residual from the zero value shows

the different characteristics of the fault injection experiment. Therefore, the current residuals obtained using the model-based observer are satisfied with the diagnostic signal as the subsequent data-driven model for fault diagnosis.

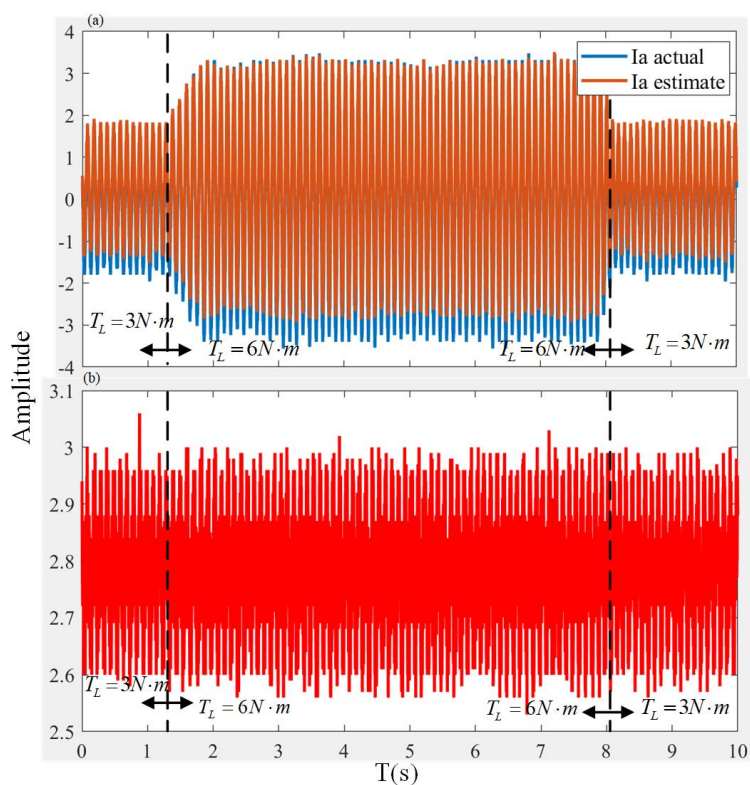


Fig. 3-6. Dynamic responses under load change between 3 N.m and 6 N.m (a) phase A estimate and actual current. (b) phase A residuals.

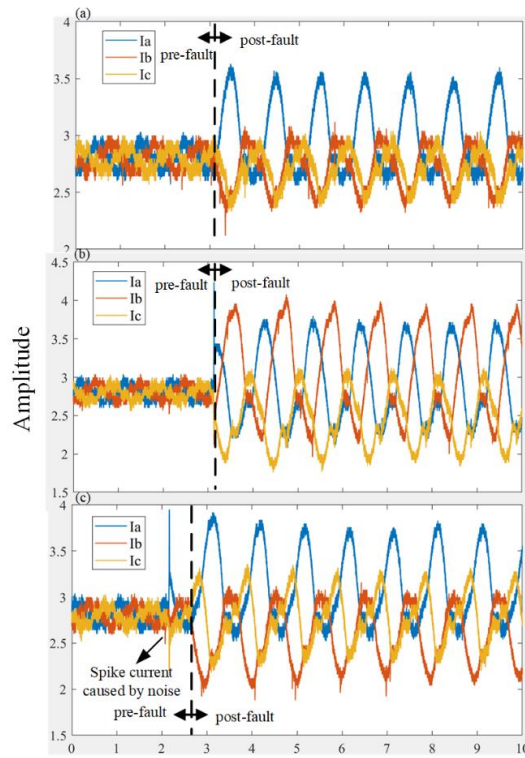


Fig. 3-7. Three phase residuals under different fault states (a) fault T1 state. (b) fault T1&T4 state. (c) fault T1&T3 state.

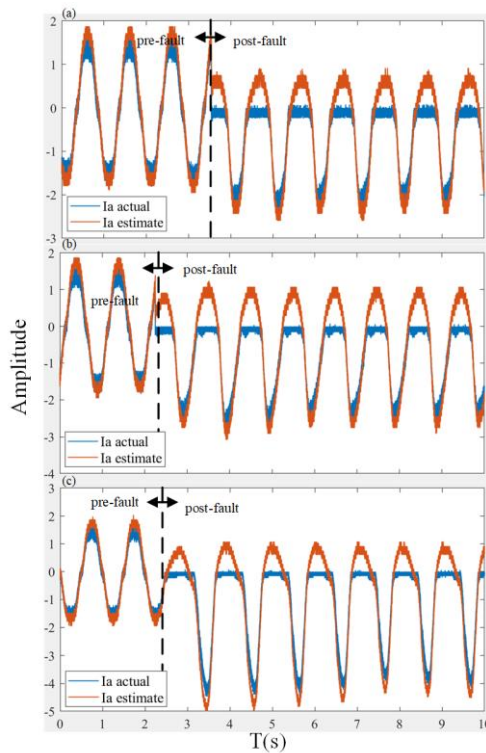


Fig. 3-8. Phase A estimate and actual current under different fault states (a) fault T1 state. (b) fault T1&T4 state. (c) fault T1&T3 state.

3.4.2. Model Optimization of Network Hyperparameters

As can be seen in Table 3-3, the accuracy of the model tends to increase as the depth increases. This indicates that the increase in network depth has a positive effect on the performance of the model in this experimental setup. Batch size has an impact on the performance of the model. Smaller batch sizes may lead to instability in the training process, which affects the accuracy of the model. Whereas larger batch sizes may lead to overfitting phenomena, which can degrade the performance of the model on the test set. Considering various factors, the performance of the model with medium batch size is more stable in this experiment. The learning rate also has an impact on the model performance. A smaller learning rate may cause the training process to converge slowly, while a larger learning rate may cause the training process to oscillate or diverge. In this experiment, the appropriate learning rate performs better. Different optimisation algorithms have an impact on model performance. In this experiment, the adam optimisation algorithm performs better and the model is more accurate on the test set compared to other algorithms. From Table 3-4, different learning rate strategies have an impact on model performance. By using strategies like learning rate decay, learning rate restart, and learning rate warm-up, the accuracy of the model on the test set is improved. With depth and batch size kept constant, for the same learning rate strategy, the accuracy of the model increases as the learning rate decreases. This suggests that using a smaller learning rate helps the model to converge and improve performance. In summary, in this experiment, deeper models and moderate batch sizes combined with a reasonable learning rate strategy result in better model performance. It is worth noting that these conclusions are drawn under specific datasets and hyper-parameter settings, which may need to be adjusted and optimised for specific tasks and data situations in practical applications. Fig. 3-9 indicates the accuracy and loss curve in training and testing process and the computational efficiency and resource utilisation of the model were quantitatively evaluated. Specifically, the training phase of the model required 656.63 seconds of execution time, while the testing phase was

completed in 145.09 seconds. In terms of memory consumption, the training phase used about 970.70 MB of memory while the testing phase consumed about 968.63 MB.

As shown in Table 3-5, the experimental validation introduced other state-of-the-art deep learning models for comparison, including GoogleNet, VGG, AlexNet, as well as ViT (Base, Large, Huge) of different sizes. It can be concluded that the proposed model performs best in terms of precision and recall, showing the ability to accurately identify positive samples and avoid missing negative samples. Meanwhile, GoogleNet and ViT-Huge also show excellent overall performance through multi-scale feature learning and self-focused mechanism with higher F1-Score, VGG and ViT-Large also perform well in terms of recall, with a slightly lower precision but emphasising the focus on global image features. However, AlexNet performs relatively poorly due to its relatively shallow architecture. In terms of the ViT model, we find that ViT-Base performs poorly, which may be due to the challenges of the self-attention mechanism in the image classification task. However, ViT-Large and ViT-Huge perform well, especially ViT-Huge in terms of recall, highlighting the importance of large-scale self-attention mechanisms in capturing image features. Furthermore, a comparison of the different architectures shows that GoogleNet achieves balanced performance using a multi-scale Inception module, while VGG's deep structure and small convolutional kernel help to capture detailed features but can lead to overfitting. As an early deep learning model, AlexNet has relatively weak performance, which may be due to its shallow structure. In conclusion, precision, recall and overall performance should be considered when choosing the best model. This study also highlights the impact of deep learning model architectures and self-concern mechanisms on performance, and future work could focus on further optimising ViT models and exploring combinations of different architectures.

TABLE 3-3 Fault Diagnosis Accuracy Under Different Network Structures and Hyperparameters

Depth	Batch size	Learning rate	Number of head	Optimization algorithm	Accuracy (%)
12	16	0.01	8	adam	76.67
8	16	0.01	8	adam	79.17
4	16	0.01	8	adam	87.50
24	16	0.01	8	adam	90.17
2	16	0.01	8	adam	82.51
24	16	0.05	8	adam	73.34
24	32	0.01	8	adam	91.67
24	32	0.002	8	adam	90.17
24	32	0.003	8	adam	84.17
24	32	0.001	8	adam	83.33
24	64	0.01	2	adam	71.67
24	64	0.01	4	adam	68.33

TABLE 3-4 Fault Diagnosis Accuracy Under Different Network Structures and Hyperparameters

Depth	Batch size	Learning rate	Number of head	Accuracy (%)
24	32	Learning Rate Decay 0.005	8	88.75
24	32	Learning Rate Restart 0.01	8	91.05
32	32	Learning Rate Warm-up 0.01	8	91.72
48	32	Learning Rate Warm-up 0.01	8	92.85

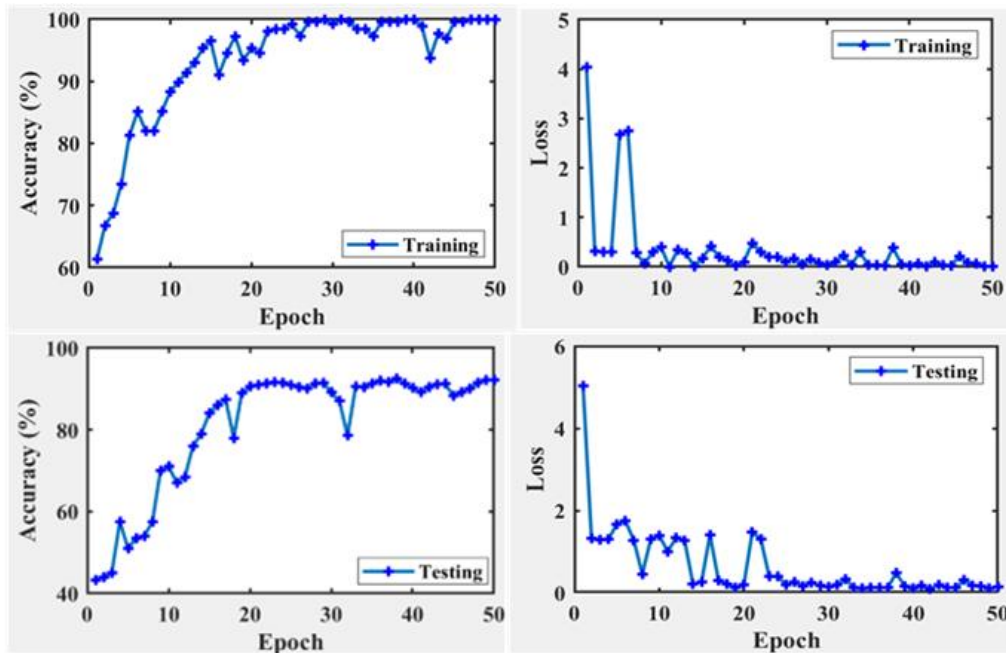


Fig. 3-9. Accuracy and loss curve in training and testing process.

TABLE 3-5 Performance Comparison with Different Models

Model	Precision	Recall	F1-Score
GoogleNet	0.78	0.75	0.76
VGG	0.82	0.85	0.85
AlexNet	0.58	0.56	0.57
ViT-Base	0.63	0.71	0.67
ViT-Large	0.85	0.88	0.86
ViT-Huge	0.86	0.90	0.88
Proposed	0.92	0.91	0.91

3.4.3. Analysis of feature extraction capability under restricted data

To demonstrate the effectiveness of our proposed concatenated network-based approach, we conducted comparative experiments with a small number of other state-of-the-art learning methods, in particular Model Diagnostic Meta-Learning (MAML) and Prototype Networks (PN). In Fig. 3-10, the performance of each method was evaluated under different levels of

adaptation The accuracy of each method was measured for direct comparison. The proposed method consistently outperforms MAML and PN at different adaptation steps. In the 5-step adaptation process, the proposed method achieved an accuracy of 75.45% compared to 54.45% for MAML and 75.34% for PN. In the 30-step adaptation process, the proposed method achieved an accuracy of 92.85%, which was significantly higher than the 84.45% for MAML and slightly higher than the 89.54% for PN. This comparative study validates the effectiveness of the proposed Siamese network approach, especially when the number of adaptations increases.

The ability of the proposed method to deal with restricted samples was evaluated. Thus, a non-parametric strategy can construct the sample distance distribution such that comparable samples are near each other, and different samples are far apart. The proposed approach based on the Siamese Network framework trains the pairwise network for learning in a supervised manner, constructing different pairs of samples in a combinatorial manner and feeding them into the network for training. The top layer determines whether the sample pairs belong to the same class by generating the corresponding probability distributions of distances. In the prediction period, the pairwise network processes each sample pair between the test sample and the support set, with the final prediction being the class with the highest probability on the support set. To verify the superiority of the proposed method. It is experimentally compared based on the same dataset. Fig. 3-11 shows that a single ViT model with a limited number of samples is weak in diagnosing the three faults, and ordinary ViT networks tend to mistake them for differently labeled samples. However, the proposed algorithm overcomes the effect of

restricted sample data and achieves high diagnostic accuracy when processing four samples, with only a few samples being identified as coming from other categories.

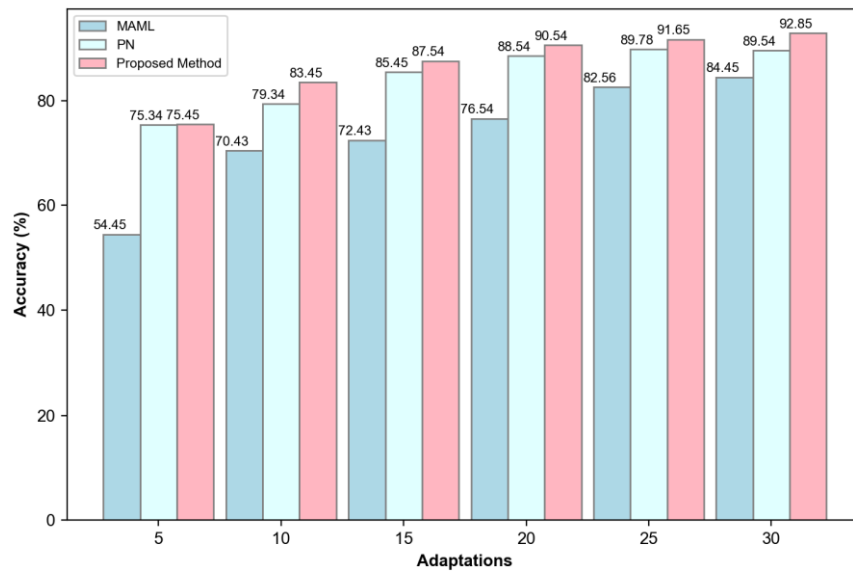


Fig. 3-10. Performance comparison with classical few-shot learning methods with 5 steps adaptations.

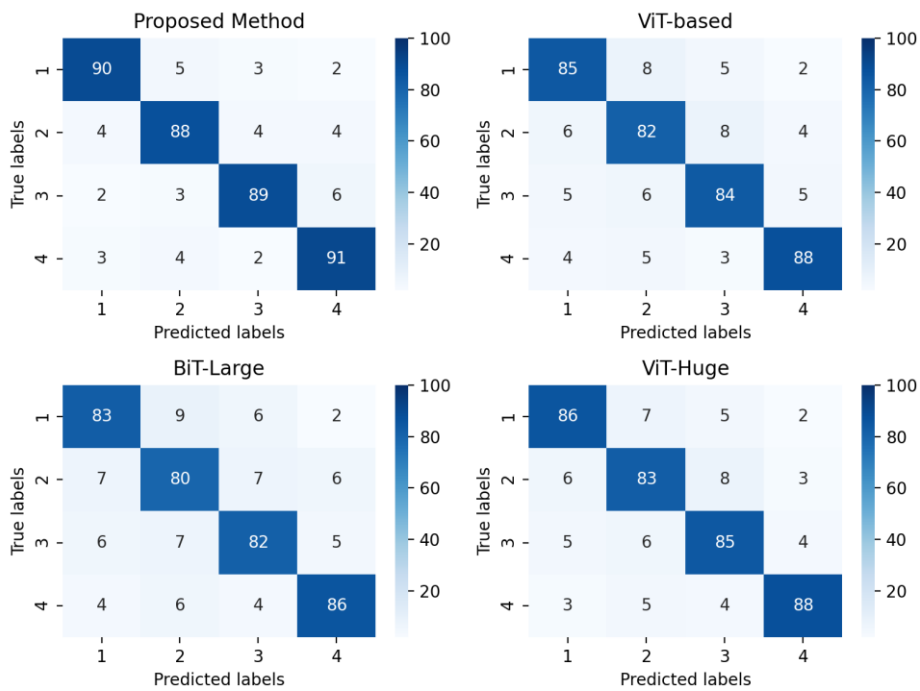


Fig. 3-11. (a) Confusion matrix of ViT for the diagnosis of each category. (b) Confusion matrix of the proposed method for the diagnosis of each category.

Due to the superior performance of the proposed algorithm, it has the potential to be applied to other types of motor systems. However, for internal permanent magnet synchronous motors, the permanent magnets are embedded inside the rotor, which may introduce a series of nonlinear magnetic field behaviors, which need to be detected in the fault Special consideration in diagnostic models. In addition, due to their structural differences, the resulting fault characteristics will be different. This requires future work to further verify the generalization in different data sets.

3.5. Conclusion

This chapter investigates the performance of combining a mode-based data-driven hybrid model for VSI open-circuit fault diagnosis. An observer is used to obtain motor fault current residuals as input samples for fault information. A Siamese network framework based on few-shot learning is constructed for VSI open circuit fault diagnosis. The current signal in the fault condition contains uncertain components due to torque pulsation being used as features to input the diagnostic model can lead to unnecessary redundant diagnoses. By using the residual values as input signals, the uncertain current components are removed, resulting in better diagnostic performance. The problem of sample sparsity due to limited experimental conditions is addressed by constructing few-shot learning based on the Siamese network framework. The adopted attention-based algorithm can extract global features in the signal and obtain higher output classification performance. However, considering that changes in system parameters can affect diagnostic performance, it is required to further investigate the robustness of the hybrid model under varying system parameters.

Chapter 4 Artificial Intelligence Neural Network Based Virtual Vibration Sensor Reconstruction in EV Powertrain

For modern electric powertrain applications (wind, electric vehicles/ships/aircraft,etc), the vibration analysis of the electric motor is one of the most important tasks. Normally, a large number of vibration sensors are placed evenly around the stator of the prototype to sample the acceleration and vibration signals. To decrease the vibration testing cost and time, in this chapter, an attention-based spatial-spectral graph convolutional network (ASSGCN) model is proposed to reduce the number of sensors to reconstruct the vibration signal of the motor. Three spectral features of the vibration signal are modeled separately, and the correlation of the operating condition force (OCF), acceleration and vibro-impedance matrices are investigated and analyzed in the spatial dimension. Via dynamic correlation analysis of spatial configuration and spectral response, the proposed ASSGCN model predicts vibration signals at different sensor sampling points. A 21kW IPMSM testing rig with Brüel & Kjær's vibration sensing equipment is employed to test the proposed ASSGCN model and the proposed method successfully reconstructs the vibration source signal and achieves well performance.

4.1. Introduction

With the popularity of permanent magnet motors (PMSMs) in the electric vehicle, the monitoring and analysis of the vibration characteristics of the PMSMs stator system in electric vehicles can effectively evaluate the operating state of the motor to ensure the reliability and continuity of the powertrain system. In general, the motor vibration signal is used to detect machine faults and noise caused by excessive vibration levels. The main operating condition force sources of excitation for motor vibration and noise include electromagnetic and mechanical forces. Mechanical deformation and vibration of the stator are caused directly by

electromagnetic and mechanical forces. Simultaneously, several electromagnetic sources affect the vibration of the PMSM including cogging torque, radial and tangential forces, torque pulsation, etc. These sources have a specific number of harmonics related to the intrinsic frequency of the PMSM stator [169]-[170]. The effect of radial force harmonics on vibration with low modulus is investigated [171]-[172]. Radial force harmonics with the lowest modal number can produce large low frequency vibration. Optimizing the low-noise design of electrical machines based on the analysis of electromagnetic forces has been proposed [173]-[174]. Therefore, to further meet the low noise requirement, it is significant to evaluate and predict vibration and noise during the quantification stage of motor design [175]-[176].

Methods to calculate vibrational force from air-gap magnetic flux density include the Maxwell stress tensor, virtual work principle, energy method, imaginary magnetic flow, and finite element analysis [177]. Most studies utilize the finite element method (FEM) to analyze the flux density of the air gap to calculate electromagnetic vibrations [178]. By using equations to calculate the waveform of the air gap flux density, vibrations can be predicted. Various approaches have been used to predict the vibrations in the IPMSM during operation. Analytical calculations based on equations for the waveform of the air gap flux density have shown promise in accurately predicting the vibrational behavior of the motor. Furthermore, Finite Element Method (FEM) simulations have been widely utilized to model the motor's electromagnetic and mechanical interactions, providing valuable insights into the structural dynamics. Additionally, combining experimental modal analysis with numerical simulations has proven effective in validating the accuracy of the predicted vibration patterns. By leveraging the analytical and FEM-based techniques together, a comprehensive understanding of the motor's vibrational characteristics can be achieved, enabling better design optimization and reliability in various operating conditions. Expected vibration and noise predictions can be made using FEM [179] [180] based on the proper material attributes and boundary conditions acquired by modal testing. However, the process of using finite element models is time-consuming. The analytical methods are attracting interest in machine design and optimization as an alternative to the noise and vibration prediction [181]. A novel air-gap relative

permeability formula to offset the rotor outer diameter is proposed to predict electromagnetic vibrations in the motor design process [182]. Detailed normal forces based on finite element calculations with phase currents and rotor position look-up tables to predict vibrations have been proposed in [183]. The effect of air gap deformation on the electromagnetic performance and characteristics of radial vibration on integrated permanent magnet synchronous motor (IPMSM) at rated power peak speed is investigated in [184]. The vibration characteristics of a motor are defined by the electromagnetically originated air-gap force and the structural response of the stator assembly, [185] proposed a multiphysics-based sensitivity analysis for vibration prediction that can be freed from analytical derivation for the evaluation of the electromagnetic and structural performance of the motor. [186] proposed a combined model based on the airgap permeance model (APM) and a unique adaptive reluctance network model (ARNM) to qualitatively analyze the air-gap excitation force to evaluate motor vibration.

The Fig. 4-1 shows vibration analysis methods, effective analysis of vibration signals is significant for vibration monitoring. Vibration data contains a wealth of analytical information about the operating state of the machine [187]. The changes in the magnetic flux distribution in the motor lead to changes in the vibration characteristics. Therefore, faulty air gap eccentricity, stator winding or rotor faults, bearing damage and power supply asymmetries can be monitored by vibration signal. The vibration signal is measured by the vibration sensors mounted on the cap of the machine bearing or stator. To monitor the health status of a motor based on vibration, the most suitable vibration sensors and the number of high precision sensors need to be selected to be evenly distributed on the outside of the motor to ensure that faults can be detected, diagnosed and predicted. Due to the high installation and maintenance costs of the sensors and the complex operating conditions of the motors. The high monitoring costs can therefore prevent the effective detection of motor faults and cause more serious hazards.

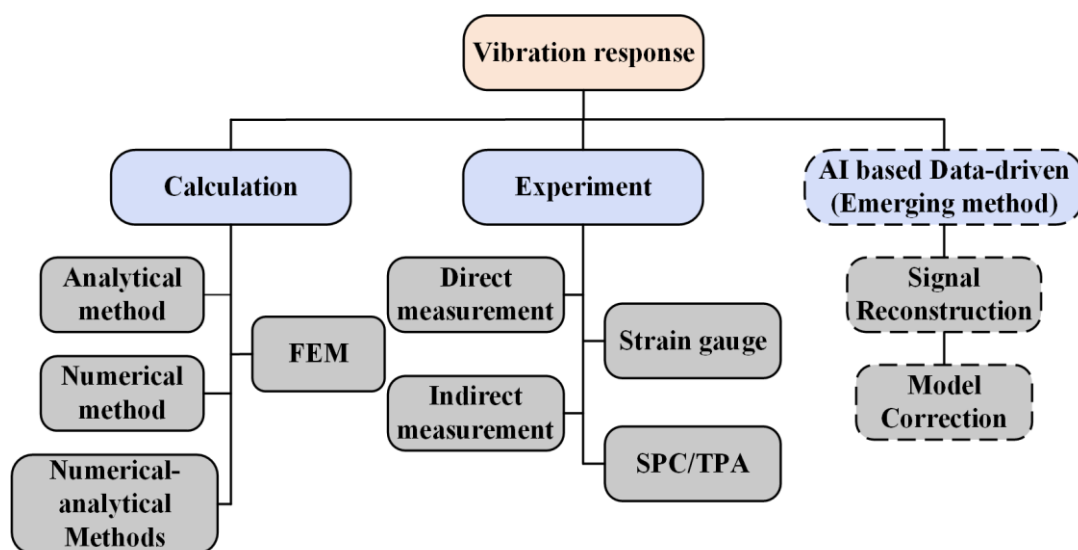


Fig. 4-1. Classification of vibration analysis methods [22].

To decrease the vibration testing cost and time, this paper investigates a data-driven machine learning-based approach to reconstruct vibration signals in combination with the position distribution relationships of vibration sensors to reconstruct the vibration signal to reduce the number of sensors, obtaining an accurate vibration response. In addition, data-driven machine learning methods in prediction and regression tasks have been widely developed in the field of electric vehicle powertrain [188]-[189], [193]-[196]. And graph neural networks (GNN) are suitable for mining graph data for signal features [190]. The effective use of data-driven methods combined with sensor signals to predict vibration signals instead of sensor-dependent solutions is attractive in industrial applications. Unlike the time-domain signal, the proposed model uses the spatial structure relationship of the sensors and the linkage of the vibration spectrum for the extraction of vibration features through an attention mechanism and uses graph convolution for information updating of the target nodes. The contribution of this chapter was summarized as below:

- (1) The paper proposes an innovative solution called the Attention-based Spatial-Spectral Graph Convolutional Network (ASSGCN) model to reduce the number of sensors required for vibration signal reconstruction, thereby decreasing the overall testing cost and time.
- (2) The correlation of the operating condition force (OCF), pulse acceleration signal (PAS), and frequency response function (FRF) are investigated and analyzed in the spatial dimension.

(3) The proposed ASSGCN model leverages dynamic correlation analysis of spatial configuration and spectral response to predict vibration signals at different sensor sampling points.

(4) The experimental verification is performed on a 21kW IPMSM testing rig with Brüel & Kjær's vibration sensing equipment, demonstrating that the proposed method successfully reconstructs the vibration source signal and achieves excellent performance.

4.2. Motor Vibration Analysis

4.2.1. Stator Structure Vibration Model

The inner surfaces of the stator core and windings are subjected to periodic radial electromagnetic forces during the operation of the motor and generate vibrations. The stator of the intercepted micro-element section motor is shown in Fig. 4-2. The number of stator slots is n , and each slot contains a full mass of m_c . The electromagnetic force acting on the inner surface of the stator is $p_m(\theta, t)$. At the same time the stator section surface received respectively from the adjacent micro-element section of the shear force $f_1(\theta, t)_\theta$, shell section surface also received from the adjacent micro-element section of the shear force $f_2(\theta, t)_\theta$ [191].

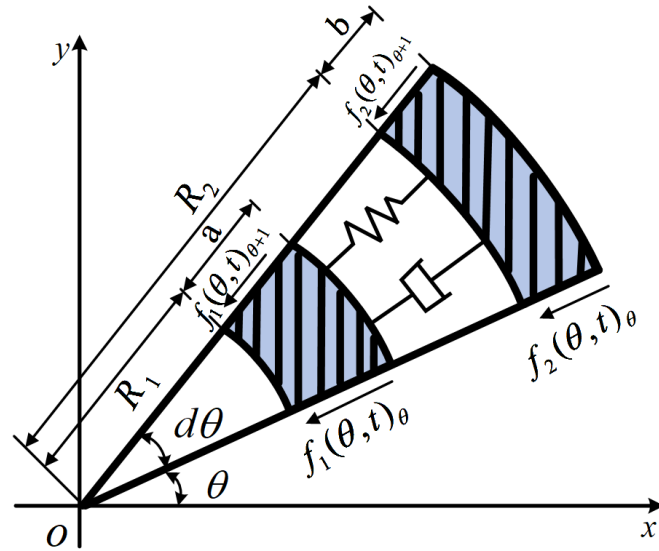


Fig. 4-2. Shell micro-element segment.

The expression for the mass of the shell micro-element segment is shown as follows:

$$dm_1 = (\rho_1 R_1 a + \frac{m_f n}{2\pi} l d\theta) \quad (4-1)$$

The periodic deformation n of the inner surface of the stator caused by electromagnetic forces is used as the base displacement excitation and loaded onto the stator structure to calculate the forced vibration response of the stator housing. Using Lagrange's equation with dissipation, the response is solved as follows:

$$\frac{d}{dt} \left(\frac{\partial L(\theta, t)}{\partial \dot{y}_i(\theta, t)_l} \right) - \frac{\partial L(\theta, t)}{\partial y_i(\theta, t)_l} + \frac{\partial \varphi(\theta, t)}{\partial \dot{y}_i(\theta, t)_l} = F_i \quad (4-2)$$

where $\dot{y}_i(\theta, t)_l$ represents the first-order derivatives of the electromagnetic force and the base displacement concerning time, respectively. Lagrange's equation: $L(\theta, t) = T(\theta, t) - U(\theta, t)$, $T(\theta, t)$ and $U(\theta, t)$ are the kinetic and potential energies. $\varphi(\theta, t)$ is the energy consumed by the damping of the system. The equivalent stiffness $K_i = A_i E_i / l$ of the stator structure, the equivalent damping $C_i = 2\sqrt{m_i K_i} \zeta_i$, where ζ_i is the damping ratio of the system.

$$[M]\{\ddot{y}_l\}d\theta + [C]\{\dot{y}_l\}d\theta + [K]\{y_l\}d\theta = \{F_1\} \quad (4-3)$$

Where M , C , K , F_1 is the mass matrix, the damping matrix, the stiffness matrix and the excitation force, respectively, with the following values:

$$\begin{aligned}
 [M] &= \begin{bmatrix} \rho_1 R_1 a + \frac{m_0 n}{2\pi l} & 0 \\ 0 & \rho_2 R_2 b \end{bmatrix}; & \{y_l\} &= \begin{Bmatrix} y_1(\theta, t) \\ y_2(\theta, t) \end{Bmatrix}; \\
 [C] &= \begin{bmatrix} \sqrt{\rho_1 E_1} R_1 \zeta_1 + \sqrt{\rho_3 3} R_2 \zeta_3 & -\sqrt{\rho_3 3} R_2 \zeta_3 \\ -\sqrt{\rho_3 3} R_2 \zeta_3 & \sqrt{\rho_2 E_2} R_2 \zeta_2 + \sqrt{\rho_3 E_3} R_2 \zeta_3 \end{bmatrix}; \\
 [K] &= \begin{bmatrix} \frac{R_1 E_1}{a} + \frac{R_2 E_3}{R_2 - R_1 - a} & -\frac{R_2 E_3}{R_2 - R_1 - a} \\ -\frac{R_2 E_3}{R_2 - R_1 - a} & \frac{R_2 E_2}{b} + \frac{R_2 E_3}{R_2 - R_1 - a} \end{bmatrix}; \\
 \{F_1\} &= \left\{ R_1 p_n(\theta, t) + 2R_1 a \zeta_1 \sqrt{\frac{\rho_1}{E_1}} \dot{p}_n(\theta, t)_l \right\} + \frac{1}{l} \begin{Bmatrix} -f_1(\theta, t)_\theta - -f_1(\theta, t)_{\theta+1} \\ -f_2(\theta, t)_\theta - -f_2(\theta, t)_{\theta+1} \end{Bmatrix}; \quad (4-4)
 \end{aligned}$$

Equation (3) represents the vibration characteristics of the $d\theta$ segment stator by superimposing all the micro-element segments in the range of $0 \sim \theta$ to give the vibration characteristics in the d-angle range. When superimposed, the internal forces in adjacent segments cancel each other, leaving only the internal forces f and f to the left of the starting segment to cancel. The excitation force is simplified as follows:

$$\{F\} = \begin{Bmatrix} R_1 P_n(\theta, t) + 2R_1 a \zeta_1 \sqrt{\frac{\rho_1}{E_1}} \dot{P}_n(\theta, t)_l \\ 0 \end{Bmatrix} \quad (4-5)$$

Assume $Y(\theta, t) = \int_0^\theta y(\theta, t) d\theta$, $P_n(\theta, t) = \int_0^\theta p_n(\theta, t) d\theta$, then the vibration equation of the stator structure on the whole circumference is equation (11) By solving for 3 then the vibration response characteristics of the stator structure can be obtained.

$$[M]\{\ddot{Y}_l\}d\theta + [C]\{\dot{Y}_l\}d\theta + [K]\{Y_l\} = \{F\} \quad (4-6)$$

4.2.2. Stator vibration modal analysis

To obtain the modal parameters of the stator vibration, experiments are usually carried out using multi-point excitation measurements and modal analysis techniques. The motor stator mode is influenced by the order of the electromagnetic force in the motor. Moreover, to correspond to the order of the electromagnetic force, the modal order of the motor is defined as the same order when the displacement pattern of the vibration coincides with the force pattern of the electromagnetic force. The order of the electromagnetic force represents the spatial characteristics of the force, the n^{th} order radial electromagnetic force produces n force peaks on the motor stator. As the stator vibrates at its intrinsic frequency, electromagnetic forces in the radial, axial, or tangential directions are applied, and the response is generated in each direction when the frequency of the electromagnetic excitation is equal to the intrinsic frequency. Axial vibration is relatively weak due to the high axial stiffness of the stator. The focus in motor vibration analysis is on radial vibration.

The study of vibration characteristics is the key to reducing vibration and noise in electric motors. Experimental modal analysis based on the motor stator is the basic method for obtaining the modal structural parameters. The full modal parameters of the structure can be found by measuring the value of the frequency response function matrix. A single point measurement of the multi-point excitation is made by distributing the excitation points uniformly in a cross section perpendicular to the stator axis and measuring its radial response.

The experimental modal analysis not only provides accurate parameters of the stator system for each order of vibration but also visualizes the shape of the stator system vibration. The obtained modes can be used to build up a vibration calculation model for the stator system and provide the basis for structural optimization.

4.3. Spectral-spatial Graph Model for Vibration Signal Reconstruction

The sensor clusters around the motor stator housing can be considered as different node locations distributed on the motor surface. Each vibration sensor unit is treated as a node and due to the structural features of motor vibration, there are interdependencies between each sensor data. The sensors and their monitoring data are therefore taken as nodes with characteristic properties and the interdependencies between each sensor are treated as edges connecting the nodes. As Fig. 4-3 shows, the resulting data type is the graph structure. By aggregating information from neighbouring nodes of the current node and by analogy to the current node, a representation of the state of the target node under the influence of the surrounding nodes can be obtained. The proposed method is based on the attention-based spatial-temporal graph convolutional network (ATSGCN) model presented in [192] for traffic flow forecasting with an improved application for mining vibration spectrum signals.

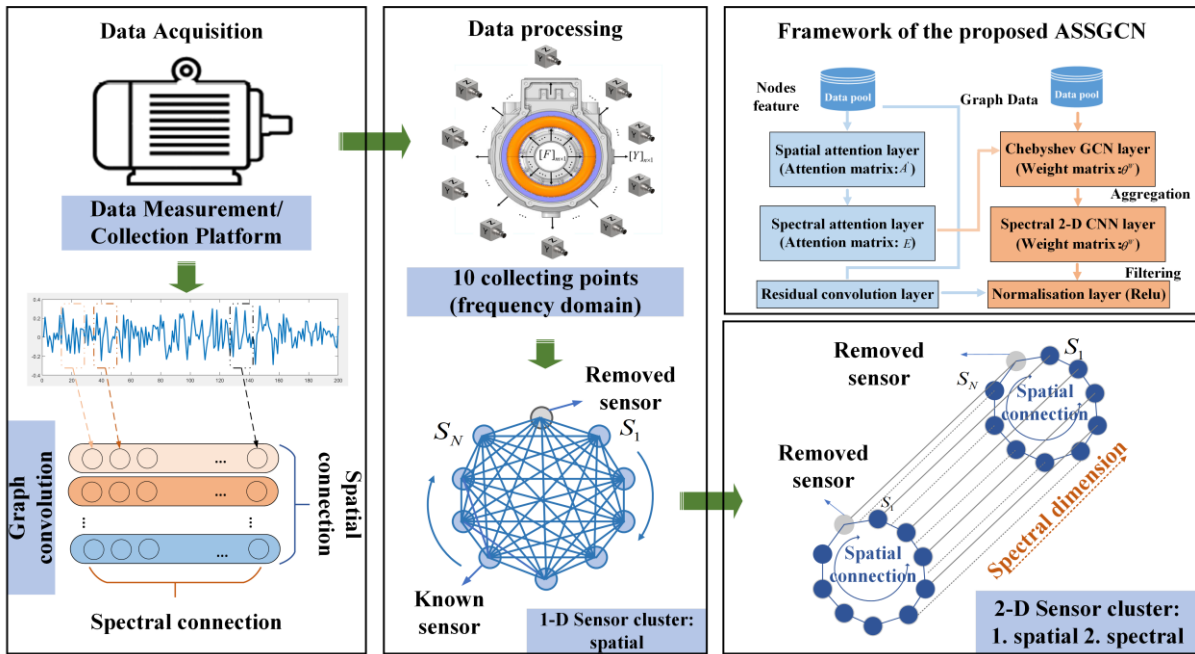


Fig. 4-3. The basic frame of the proposed algorithm.

The processed graph data is noted as $\zeta = \{V, \varepsilon\}$, where $V = \{v_1, \dots, v_N\}$ is the set of nodes with the number $N = |V|$, $\varepsilon = \{e_1, \dots, e_M\}$ is the set of edges with the number M . For a given graph

$\zeta=\{V, \varepsilon\}$, The corresponding adjacency matrix is denoted $A \in \{0,1\}$ with a size of $N \times N$, $A_{i,j}$ denotes the existence of an edge from v_i to v_j , Conversely, it means not present.

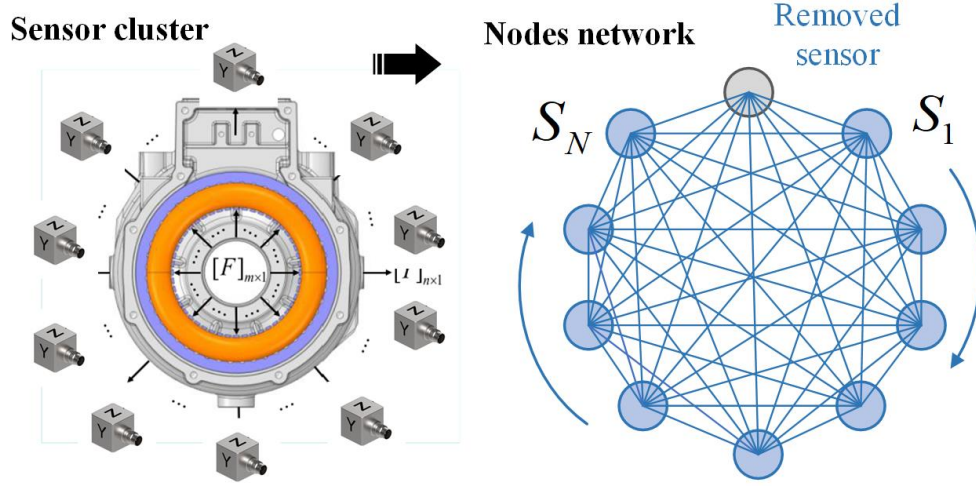


Fig. 4-4. Graph data for sensor cluster distribution.

Laplace matrices are used to study the structural properties of graphs, The symmetrically normalized Laplacian expressions are as follows:

$$L^{sym} = D^{-1/2}L \quad (4-7)$$

where D represents the degree matrix of the nodes. The L is defined as $D - A$. Laplace matrix whose spectrum decomposes as $L^{sym} = U\Lambda U^T$, and $\Lambda = diag(\lambda_1, \lambda_2, \dots, \lambda_n)$ represents the diagonal matrix of eigenvalues. The corresponding graph convolution formula is derived from the ordinary convolution formula:

$$g * x = \mathfrak{I}GF\{\mathcal{GF}\{g\} \cdot \mathcal{GF}\{x\}\} = U(U^T g \cdot U^T x) \quad (4-8)$$

Where $\mathcal{GF}\{\cdot\}$ and $\mathfrak{I}GF\{\cdot\}$ represent the Fourier transform and its inverse transform. g is a Laplacian propagation function $g(L)$ and x denotes the graph input feature. Regard $U^T g$ as the function of the Laplacian eigenvalues $g_\theta(\Lambda) = diag(\theta)$, with the parameters θ . Due to the large number of matrix operations involved, Chebyshev polynomials were used as a basis for approximation.

$$g_\theta * x = U g_\theta U^T x \approx U \sum_{k=0}^K \theta_k T_k(\tilde{\Lambda}) U^T x \quad (4-9)$$

Where k depends on the nearest neighbor node of the central node's order. To prevent overfitting and to simplify calculations, (14) can be expressed as follow:

$$g_{\theta} * x = \theta(I_N + D^{-1/2}AD^{-1/2})x \quad (4-10)$$

Thus, the layer-to-layer propagation expression of the GCN is shown as follows:

$$f(x, A) = \sigma(\tilde{D}^{-1/2}\tilde{A}\tilde{D}^{-1/2}xW) \quad (4-11)$$

Where $\sigma(\cdot)$ represents the activation function and W represents the weighting parameter.

4.3.1. Spectral-Spatial Attention Module

In the spatial dimension of the stator structure, the vibrational states of the different sampled points are interacting with each other, and the influence of different spatial points is highly dynamic. The dynamic correlation between nodes in the spatial dimension is captured adaptively by using an attention mechanism.

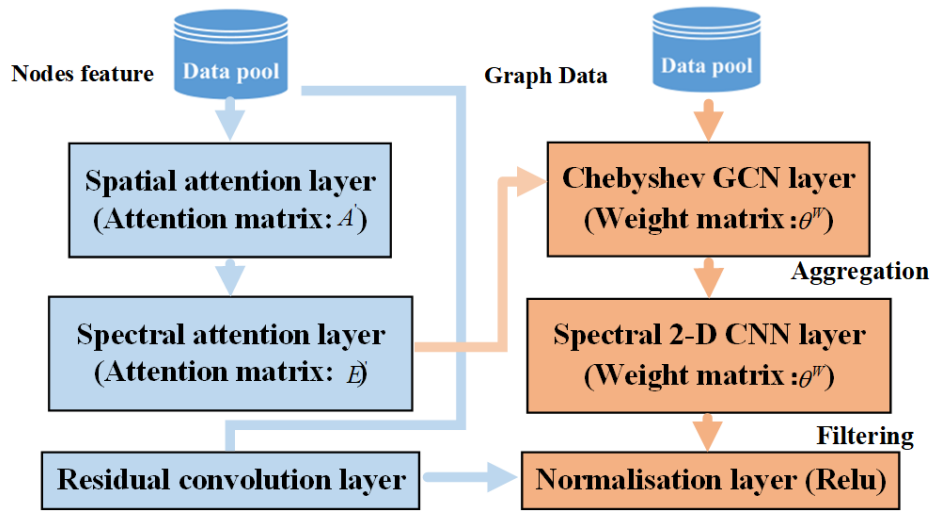


Fig. 4-5. The framework of the proposed ASSGCN.

$$Att_{spa} = h_s \cdot \sigma((\mathcal{X}_f^{(r-1)}W_1)W_2(W_3\mathcal{X}_f^{(r-1)})^T + b_s) \quad (4-12)$$

$$Att'_{spa_{i,j}} = \frac{\exp(Att_{spa_{i,j}})}{\sum_{j=1}^N \exp(Att'_{spa_{i,j}})} \quad (4-13)$$

The sample input signal for the sensor cluster is constructed as $\mathcal{X}_f^{(r-1)} = (X_1, X_2, \dots, X_{r-1})$.

The training parameters including weights and bias are set to W_1, W_2, W_3 and b_s , where $W_1 \in \mathbb{R}^{T_{r-1}}$, $W_2 \in \mathbb{R}^{C_{r-1} \times T_{r-1}}$, $W_3 \in \mathbb{R}^{C_{r-1}}$. C_{r-1} denotes the number of channels of input data on layer r . T is the length of the r^{th} level time dimension. Furthermore, in the frequency domain dimension, the vibration characteristics in different frequency bands are correlated as they are collected by a cluster of sensors distributed in different locations. The correlation of the input data is captured by using an attention mechanism.

$$Att_{spe} = V_e \cdot \sigma((\mathcal{X}_f^{(r-1)})^T U_1) U_2 (U_3 \mathcal{X}_f^{(r-1)})^T + b_e \quad (4-14)$$

$$Att_{spe}'_{i,j} = \frac{\exp(Att_{spe}'_{i,j})}{\sum_{j=1}^N \exp(Att_{spe}'_{i,j})} \quad (4-15)$$

Where the learnable parameters also include $V_e, b_e \in \mathbb{R}^{T_{r-1} \times T_{r-1}}$, $U_1 \in \mathbb{R}^N$, $U_2 \in \mathbb{R}^{C_{r-1} \times N}$, $U_3 \in \mathbb{R}^{C_{r-1}}$.

4.3.2. Spectral-Spatial Convolution Module

To take full advantage of the topological nature of the sensor clusters, graph convolution based on spectral graph theory is used at frequency domain points to directly process the signal in the spatial dimension using the signal correlation on the sensor network. In spectral graph analysis, the graph is represented by its corresponding Laplacian matrix. The nature of the graph structure can be obtained by analyzing the Laplace matrix and its eigenvalues. The full graph signal in the frequency domain dimension is $x = x_t^f \in \mathbb{R}^N$, the graph Fourier transform of the signal is defined as $\hat{x} = U^T x$, and the inverse graph Fourier transform is $x = U \hat{x}$. A graph convolution is a convolution operation implemented by replacing the classical convolution operator with a linear operator diagonalized in the Fourier domain. Therefore, a signal G on a graph x is filtered by a kernel g_θ . $* G$ represents the graph convolution operation. Then use the Chebyshev polynomial approximation:

$$g_\theta * G_x = g_\theta(L)x = \sum_{k=0}^{K-1} \theta_k T_k(\tilde{L})x \quad (4-16)$$

The parameter $\theta \in \mathbb{R}^K$ is the polynomial coefficient vector, $\tilde{L} = \frac{2}{\lambda_{max}}L - I_N$, λ_{max} is the largest eigenvalue of the Laplace matrix, the recursive definition of the Chebyshev polynomial is $T_k(x) = 2T_{k-1}(x) - T_{k-2}(x)$, $T_0(x) = 1$, $T_1(x) = x$. To adjust the correlation between nodes dynamically, for each term of the Chebyshev polynomial, combining $S' \in \mathbb{R}^{N \times N}$ with the spatial attention matrix $T_k(\tilde{L})$ to get $T_k(\tilde{L}) \odot S'$. Therefore, the graph convolution formula above is changed as shown below:

$$g_\theta * G_x = g_\theta(L)x = \sum_{k=0}^{K-1} \theta_k T_k(\tilde{L})x \quad (4-17)$$

Furthermore, the definition can be extended to multi-channel graph signals. Supposing the input is $\mathcal{X}_f^{(r-1)} = (\hat{X}_1, \hat{X}_2, \dots, \hat{X}_{T_{r-1}}) \in \mathbb{R}^{N \times C_{r-1} \times T_{r-1}}$, where each node's feature has C_{r-1} channels. At each frequency point f , perform C_r convolutions on the graph \hat{X}_f to obtain $g_\theta * G_{\hat{X}_f}$ where $\theta = (\theta_1, \theta_2, \dots, \theta_{C_r})$ is the convolution kernel parameter. After the graph convolution operation has captured the adjacency information of each node on the graph in the spatial dimension, the standard convolution layers in the frequency domain dimension are further stacked to signal more unknown nodes by merging the information of known nodes.

$$\mathcal{X}_h^{(r)} = ReLU(\Phi * (ReLU(g_\theta * \mathcal{X}_f^{(r-1)}))) \in \mathbb{R}^{C_r \times N \times T_r} \quad (4-18)$$

Where $*$ is the standard convolution operation and Φ represents the parameters of the time-dimensional convolution kernel. The Spectral-Spatial attention module and the Spectral-Spatial convolution module form a spatial-temporal block. Multiple Spectral-Spatial blocks are stacked to further extract a larger range of dynamic Spectral-Spatial correlations. Finally, a fully connected layer is added to ensure that the output of each component has the same dimension and shape as the predicted target. The final fully connected layer uses *ReLU* as the activation function.

4.3.3. Sensor Cluster Adjacency Matrix Construction

As input to the construction of the proposed module, the adjacency matrix can reflect the structural association between nodes by whether two nodes are connected or not. Similarly, in sensor clusters, the construction of adjacency matrices for sensor clusters is also essential to reflect the correlation of vibration responses at different locations. By setting $A_{i,j}$ to determine whether nodes are connected, 1 means connected and 0 means the opposite.

$$A_{i,j} = \begin{cases} 1, & \text{if } e_{i,j} = \varepsilon \\ 0, & \text{otherwise} \end{cases} \quad i, j = 1, 2, \dots, N \quad (4-19)$$

Where N represents the input nodes number, ε denotes the connection states. The fact that vibrations propagate through the medium and decay in intensity with distance indicates that each node in the graph is constantly changing its state due to the influence of its neighboring nodes and more distant points until the final equilibrium, the closer the neighboring nodes the greater the influence. Information on the nodes containing structural relationships and vibration characteristics will be used as input to the model for parameter training.

4.3.4. Overall structure and training strategy

The detailed steps of the entire algorithm are shown in Fig. 4-5. The data pool is first constructed to include three physical quantities that describe the characteristics of the vibration signal $\{x_i(n), x_j(n), x_h(n)\}, n \in [0, N - 1]$, which N is the number of signals sampled in the time domain. Transformation of vibration signals in the time domain to the frequency domain by applying the Fourier transform calculation as shown below:

$$Y(w) = \sum_{n=0}^{N-1} x(n)e^{-j2\pi wn/N} \quad (4-20)$$

where N is the number of samples of the time domain discrete signal and n is the input of the time domain discrete signal.

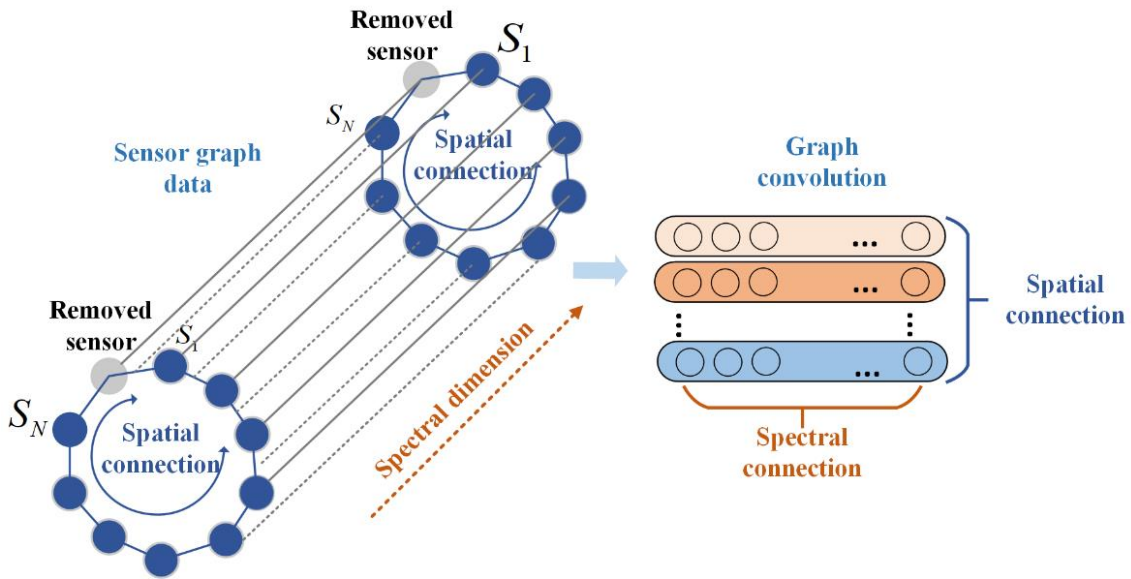


Fig. 4-6. The spectral-spatial correlation diagram of the vibration signal.

To achieve the prediction of the vibration response, the spectral attention matrix $Att_{spe'_{i,j}}$ is calculated by the spectral attention layer after the data pool has been obtained. The spectral attention matrix is then dot-multiplied with the input data and used as input to the spatial attention layer to obtain the spatial attention matrix $Att_{spa'_{i,j}}$. Furthermore, the values obtained by multiplying the resulting attention matrix with the previous layer of dot products are used as input to the graph convolution network. Approximate Laplace matrix eigenvalue decomposition by using Chebyshev polynomials. Position information is obtained by entering the adjacency matrix of the sensor cluster. Further convolution is then performed in the spectral dimension. At the same time, the whole process described above is used as a SS module and then the residual network is used to avoid the issue of gradient disappearance or gradient explosion when the number of layers of the model increases. Finally, through a fully connected layer, the calculated feature space maps the sample marker space and then outputs the predicted frequency response of the vibration signal.

4.4. Experimental setup and validation

A 48-slots, 8-poles IPMSM was chosen as the experimental prototype. The modal experiments of the prototype were carried out by the hammering method. The basic parameters

of the prototype are shown in Table 4-1. In the experiments, the prototype was subjected to static and dynamic experiments using Brüel & Kjær's equipment. The stator system of the prototype was taken out separately and the inertia matrix and natural frequencies of the stator system were tested in the static experiments. In the vibration data acquisition experiment, 10 points are taken as hammer excitation points on the stator tooth surface and 20 points are taken as sensor acquisition points on the outer surface of the frame. The average of the two points in the same group is taken as the final response value. The prototype was installed in the same way for both dynamic and static experiments to ensure that the external physical environment was the same. As the structure and external conditions of the motor remain the same, the inertia matrix of the motor also remains the same. Under dynamic conditions, the prototype was set up with multiple variations of load and speed. Brüel & Kjær's 4520 three-dimension acceleration sensor was used for the experiments. The experimental setup is shown in Fig. 4-7.

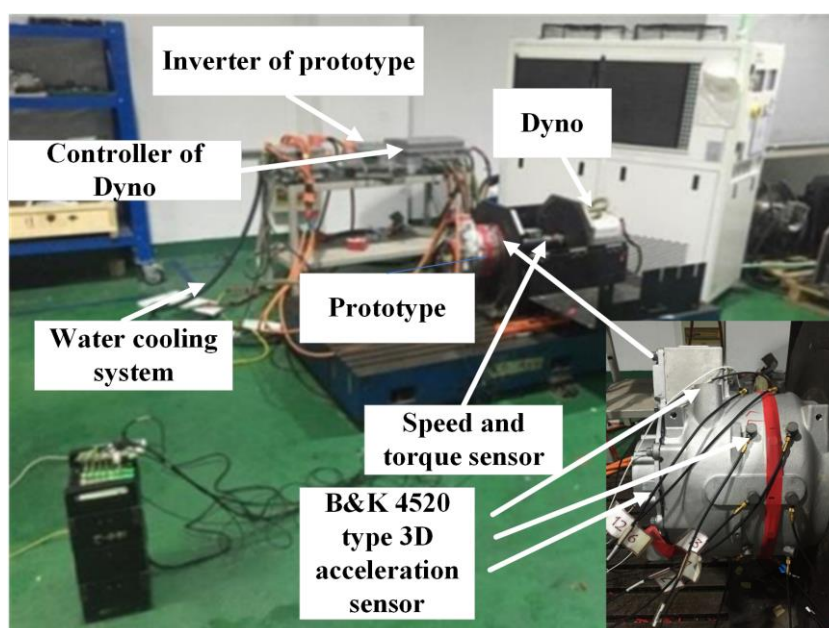


Fig. 4-7. Experimental setup.

TABLE 4-1 Experimental Setup Parameters

Parameters	Value
Number of poles and slots	8/48
Rated power/kW	21

Out radius of stator/mm	200
Out radius of rotor/mm	123.4
Internal radius of rotor/mm	43
Length of core/mm	110

4.4.1. Data Preprocessing and Description

The vibration signals collected in this paper are based on vibration response predictions over a wide motor frequency band (1-6400Hz). Fig. 4-8 indicates the sampling datasets of 10 sensor distribution points in the frequency domain. To verify the robustness of the algorithm, the acquired motor operating conditions include different speeds under on-load and no-load. The purpose of this article on vibration prediction is to investigate the characteristics of the internal operating condition force (OCF) of a motor under a variety of operating conditions. Therefore, the frequency response function (FRF) and pulse acceleration signal (PAS) of the internal OCF under a variety of operating conditions are used as reference indicators.

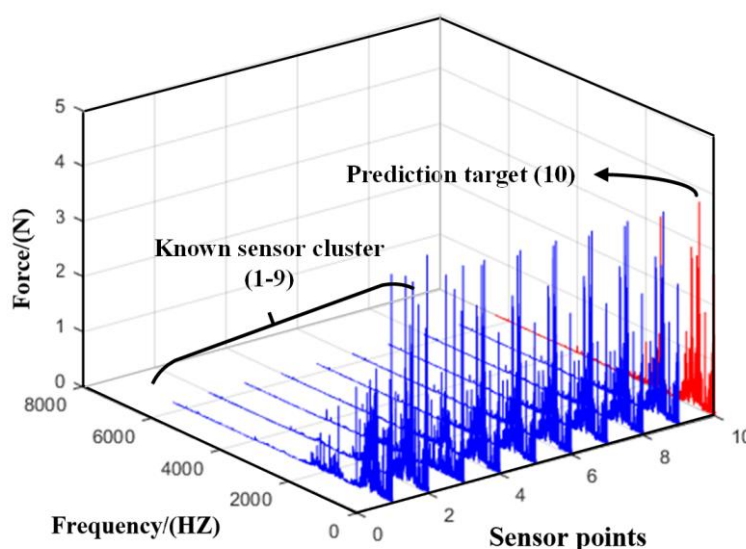


Fig. 4-8. Sampling dataset of 10 sensor distribution points in the frequency domain.

In addition, [25] proposed vibration impedance matrix theory is necessary for the development of a mathematical analysis model of the OCF. The data set used for the experiments was therefore divided into eight groups based on different operating conditions.

Each operating condition includes three indicators for assessing the vibration characteristics. Furthermore, the dataset is divided into a training and a test set in the ratio of 7:3. The proposed algorithm is constructed based on the Pytorch framework. The mean absolute error (MAE) of the loss function used for training in the experiments is a commonly used regression loss function, which is the mean value of the absolute sum of the difference between the target and predicted values and represents the mean magnitude of the error in the predicted values, without regard to the direction of the error. The equations are shown below:

$$MAE = \frac{\sum_{i=1}^n |f(x) - y|}{n} \quad (4-21)$$

compared to MSE, MAE is less sensitive to outliers in the training process. It has a stable gradient regardless of the input value, which does not lead to gradient explosion problems and has a more robust prediction performance.

There are some significant parameters to consider in lifting the ASSGCN model. The step size represents the length of the specified sequence. Longer spectral steps may capture wide spectral-spatial relationships but may also increase the computational burden. Meanwhile, the input feature dimensions depend on the feature dimensions in the specific problem, which in this article include the amount of vibration signal description, operating condition force, acceleration, and vibro-impedance matrices. In addition, the adjacency matrix describes the connectivity between nodes in the graph data and contains information on the spatial location of the sensors. In ASSGCN, a one-dimensional convolution operation is typically used, so the convolution kernel size specifies the size of the convolution window in the time dimension. The number of convolution layers determines the depth of the model, and the graph convolution kernel size specifies the range of local neighbours between nodes when graph convolution operations are performed in space. The learning rate is used to control the update step of the model parameters, and for optimal model stability, the batch size specifies the number of samples used to update the model parameters in each training iteration. The choice of these hyperparameters depends on factors such as the complexity of the input signal, the size of the data and the computational resources. The optimal combination of parameters is usually chosen

through experimentation and tuning.

4.4.2. Prediction performance with multiple operation conditions

To verify the robustness of the prediction model, vibration signals were collected under both no-load and on-load conditions in the multiple operations. In addition to acceleration and force in the frequency domain, the impedance matrix is used as input to the model as the three components describing the vibration characteristics. Table 4-2 and Table 4-3 illustrate the predictive performance of the model at different loads and speeds according to three indicators including mean absolute error (MAE), mean square error (MSE), and root mean square error (RMSE). From Table 4-2, the prediction accuracy of the vibration signal OCF at a low speed of 3000 rpm is higher than that at a higher speed of 6000 rpm under the same load at 66N. However, the prediction performance of the FRF is the opposite of the prediction performance of F. At the same load of 66N, the prediction accuracy is higher in terms of the higher speed of 6000 rpm than at a lower speed.

TABLE 4-2 Comparison of Results

Operating Conditions	MAE	MSE	RMSE
3000-66-OCF	0.1378	0.2608	0.5107
6000-66-OCF	0.3734	1.7489	1.3225
8200-48-OCF	0.37	0.451	0.6716
3000-66-FRF	0.8032	1.1564	1.0753
6000-66-FRF	0.694	0.9218	0.9601
8200-48-FRF	0.8201	1.398	1.1824
3000-66-PAS	0.1973	0.2165	0.4653
6000-66-PAS	0.9156	1.3965	1.1817
8200-48-PAS	0.4032	0.5114	0.7151

With the same predictive performance of OCF, the predictive performance of PAS which high speed for the same load. Furthermore, under the same load and speed conditions, OCF has the best prediction performance among the three vibration parameters. Table 4-3 illustrates the

investigation of the predicted performance of the three vibration signal parameters at different speeds under no-load conditions. The data set was collected at four speeds including 2000 rpm, 3000 rpm, 6000 rpm and 8200 rpm. The prediction accuracy of OCF at 8200 rpm was the highest for the different speed conditions compared to the other speed conditions. And the predicted performance of FRF is best at 6000 rpm. In addition, PAS has the lowest prediction accuracy at 3000 rpm and has the lowest average prediction error compared to the component models with the best learning for PAS signal features. It presents an intuitive indication of the trend in the predictive performance of the proposed model for the vibration signal under changes in torque and speed conditions. For MAE values, the trend in the prediction error rate of the model varies with increasing torque for the three vibration signal components at the same speed. The prediction of OCF performs significantly better than the other two vibration components, and the prediction accuracy is stable within a fixed range. This is because the proposed model is more effective in extracting the Force signal characteristics than the other two signals, which show strong robustness. Among the other three evaluation metrics, the predictions of FRF and PAS fluctuate more radically under variable load and variable speed conditions. For the MSE value, the prediction accuracy of the FRF decreases and then increases as the torque increases from 0nm to 66nm at a speed of 8000 rpm, representing a wide range of errors. Differences in the learning performance of models for different vibration signals indicate that the adaptability of the proposed model for different signals remains to be improved.

TABLE 4-3 Comparison of Results

Operating Conditions	MAE	MSE	RMSE
2000-no-OCF	0.3578	0.2608	0.5107
3000-no-OCF	0.395	0.2686	0.5182
6000-no-OCF	0.3137	1.1709	1.0821
8200-no-OCF	0.2757	0.0764	0.2764
2000-no-FRF	0.659	0.8313	0.9117
3000-no-FRF	0.474	0.4252	0.6521
6000-no-FRF	0.7604	0.9975	0.9988
8200-no-FRF	0.3964	0.2705	0.5201
2000-no-PAS	0.3529	0.3523	0.5935
3000-no-PAS	0.1956	0.0666	0.2581

6000-no-PAS	0.2057	0.0621	0.2492
8200-no-PAS	0.4476	0.9634	0.9764

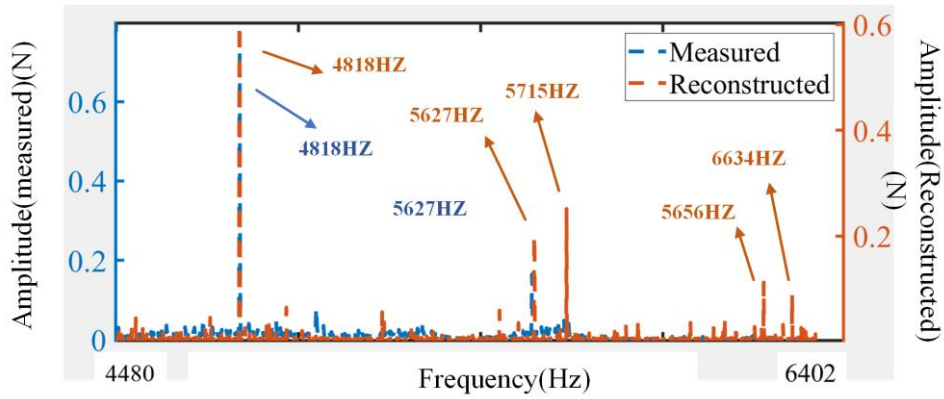


Fig. 4-9. Measured and reconstructed value of OCF under the condition of 6000rpm without load.

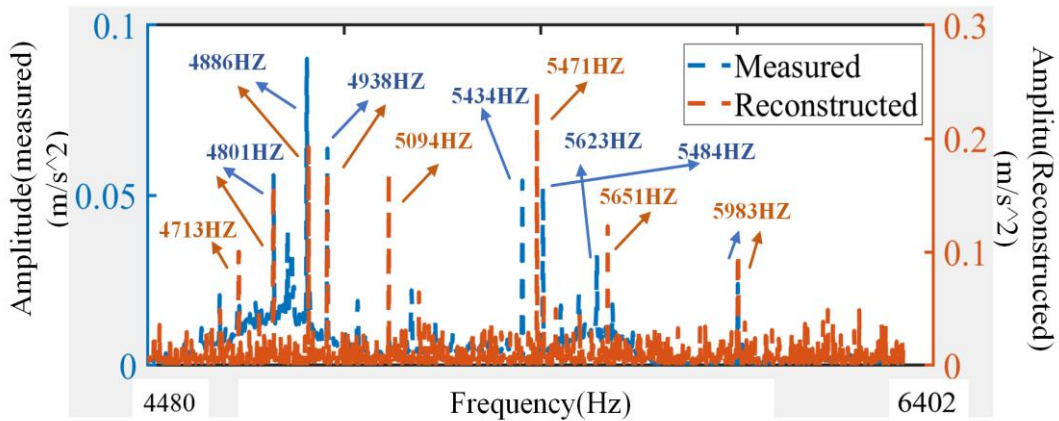


Fig. 4-10. Measured and reconstructed value of acceleration response under the condition of 6000rpm without load.

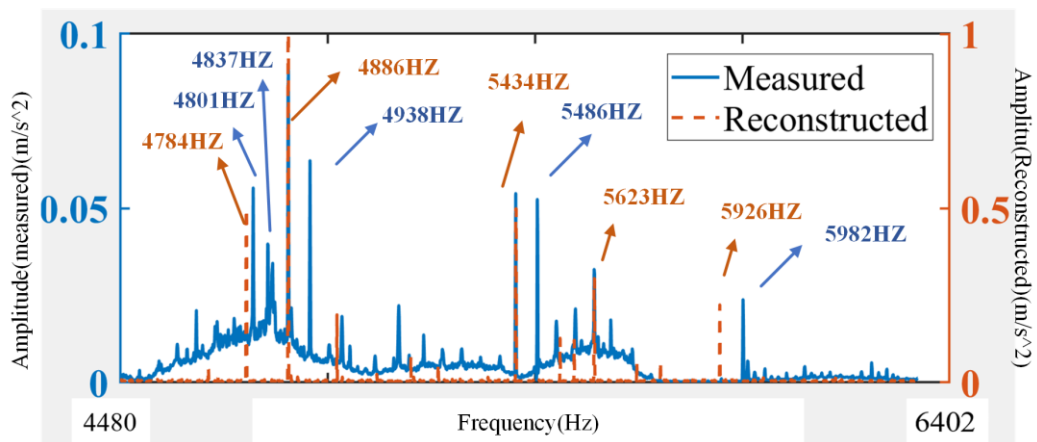


Fig. 4-11. Measured and reconstructed value of acceleration response under the condition of 6000rpm without load.

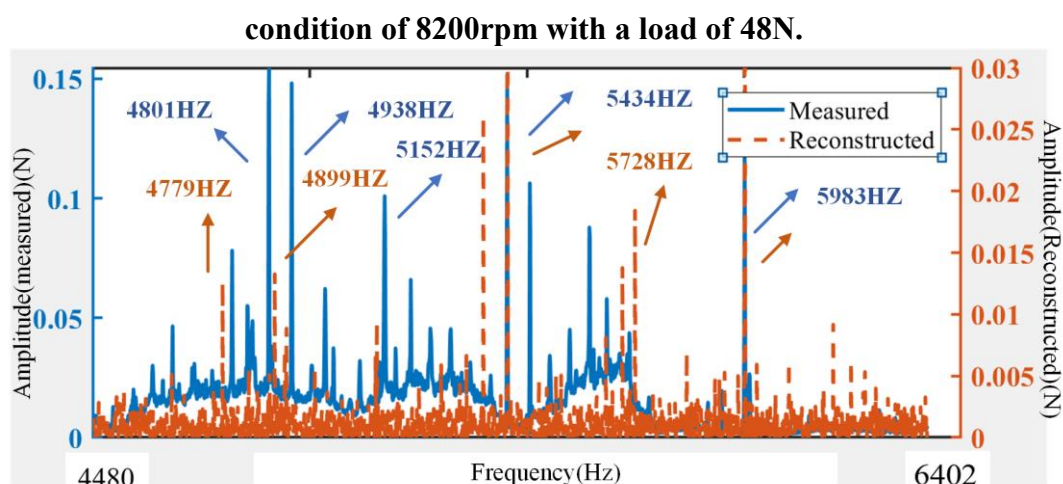


Fig. 4-12. Measured and reconstructed value of OCF under the condition of 8200rpm with a load of 48N.

4.4.3. Error analysis and performance discussion

It is worth noting that the paper focuses on the reconstructed performance of the vibration response in the high-frequency range. The experiment is for the prediction of the frequency response of a high-frequency vibration signal from 4480-6402hz. Fig. 4-9 to Fig. 4-10 show a comparison of the reconstructed signal and the actual response at 6000rpm without load. Fig. 4-11 to Fig. 4-12 indicate the results of the signal reconstruction under the condition of 8200rpm with a load of 48N. Fig. 4-9 illustrates that the frequency response of the OCF at 4818hz and 5627hz is relatively large and that the proposed algorithm can accurately reconstruct the response at this frequency. The reconstruction values of 48186Hz and 5627Hz frequency points are consistent with the experimental values which indicate the effectiveness of the proposed model. The measured acceleration response amplitudes were in the range of 4801-4938 and 5801-4938hz, with relatively large responses. The model predicts the corresponding frequency bands between 5094-5671hz and 5623-5983hz and the corresponding results deviate from the measured results by approximately 3.8%. Due to the underfitting or overfitting of the vibration signal training samples, the generalization error brought by the model is reflected in the frequency of 5094hz, and the reconstructed value has a large error from the real value. It is required to be reduced by increasing the training samples or further

optimizing the model. It suggests that the learning capability of the model decreases as the complexity of the operating characteristics increases due to the change in speed accompanied by multiple changes in vibration amplitude. At the same time, the prediction performance under load conditions is similar to that under no-load conditions. The number of noticeable acceleration responses and high OCF amplitudes was slightly less at the operating condition of 6000 rpm without a load than at 8200 rpm. Fig. 4-13 to Fig. 4-14 show the vibration response of adjacent points to the reconstructed points to investigate their spatial connection under different operating conditions. Point 10 represents the reconstruction point, point 1 and point 9 are two vibration points adjacent to the reconstruction point. The amplitude curves of the reconstructed points are similar to those of the adjacent points as can be seen from the graph. It indicates that the vibration characteristics of the adjacent points of the motor are similar with high response amplitude at several frequency points.

TABLE 4-4 Experimental Accuracy and Computational Burden

Operating Conditions	Experimental Accuracy	Training time (s)	Testing time (s)
OCF without load	0.8542	45.63	31.45
FRF without load	0.9136	54.34	37.54
PAS without load	0.9521	44.54	45.45
OCF with load	0.9124	48.43	46.34
FRF with load	0.9432	47.64	45.65
PAS with load	0.9620	38.54	43.54

The predictive performance of regression models in general is related to the size of the training data, with limited data set causing overfitting problems in regression models. As shown in Fig. 4-15 the MAE training error in the various operation states 25 epochs to a lower range and stabilizes in a certain interval. It means that the proposed model has generalization capability to the input vibration data set. However, after 100 epochs of training, basically decreases from the initial high training loss of around there is some fluctuation in the training loss of the training set for the different operation states, which indicates a slight overfitting of

the model. Therefore, the effect of balancing the training performance of training datasets in different operation states on the ultimate prediction behaviour deserves further investigation in subsequent work.

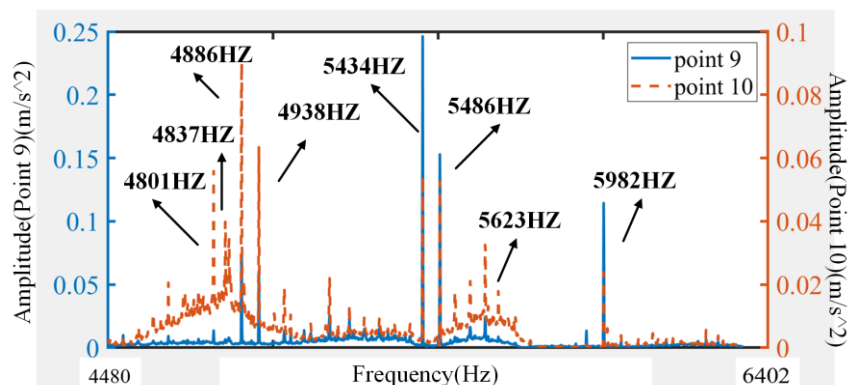


Fig. 4-13. Spectrum of OCF under the condition of 6000rpm without load for sensor point 1 and point 10.

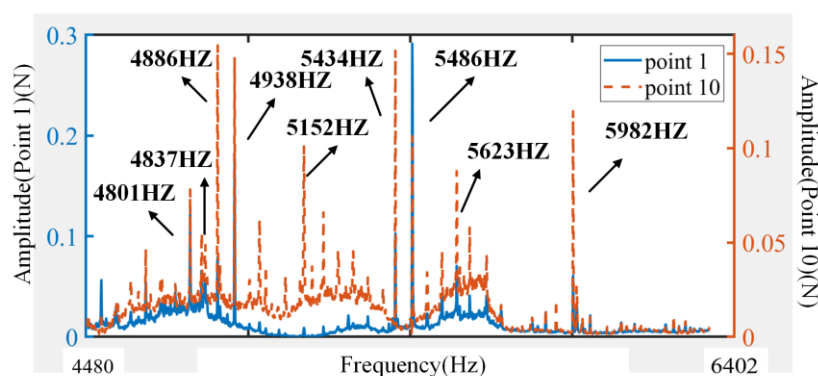


Fig. 4-14. Spectrum of OCF under the condition of 8200rpm without load for sensor point 9 and point 10.

TABLE 4-5 Comparison Results

Methods	Training sample (%)	Condition	Experimental Accuracy
Standard GCN	60	Conditions 1-7	84.32%
Standard CNN	60	Conditions 1-7	79.64%
KCN	60	Conditions 1-7	92.34%
IGNNK	40	Conditions 1-7	95.67%
SVR	40	Conditions 1-7	72.34%
ASSGCN	60	Conditions 1-7	96.20%

Table 4-5 compares a number of advanced reconstruction models, and the ASSGCN method also performs particularly well, with the highest experimental accuracy of 96.20%. This demonstrates the effectiveness of the method in achieving high accuracy. the IGNNK method achieves a good experimental accuracy of 95.67% with a training sample of 40%. the KCN method achieves an accuracy of 92.34%, demonstrating its reliability in conditional prediction. The standard GCN and standard CNN methods achieved accuracies of 84.32% and 79.64% respectively. Although not as high as IGNNK and ASSGCN, they still provided reasonably good performance. On the other hand, the SVR method had the lowest experimental accuracy of 72.34%, suggesting that it may not be as effective as the other methods in predicting conditions.

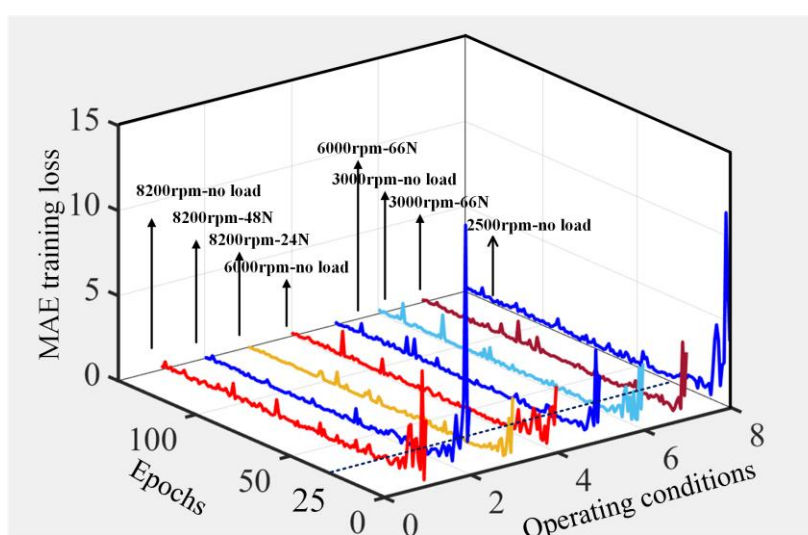


Fig. 4-15. Curve of MAE training loss with different epochs.

As shown in Table 4-4, the Vibration acceleration response had the highest experimental accuracy of 0.9521 without load, followed by FRF and OCF. The accuracy of the FRF and OCF was 0.9432 and 0.9124 respectively. The training and testing times were within reasonable limits for all operating conditions. The training times ranged from 38.54 to 54.34 seconds and the test times ranged from 31.45 to 46.34 seconds. By comparing the experimental accuracies, it can be seen that the proposed algorithm exhibits relatively high prediction accuracies under all operating conditions. This indicates that the

algorithm has good performance in vibration signal prediction. In addition, the algorithm shows good accuracy with and without load, which indicates that it has good generalization capability for different operating conditions. The relatively short training and testing times imply that the algorithm is highly efficient and can complete the training and testing processes in a short period. In summary, the proposed algorithm has high accuracy and high efficiency in vibration signal prediction, which is potentially valuable in practical applications. However, further research and experiments may be required to validate and evaluate the adaptability and robustness of the algorithm more fully.

4.5. Conclusion

The proposed Attention-based Spatial-Spectral Graph Convolutional Network (ASSGCN) model successfully reduces the number of sensors required for vibration signal reconstruction in electric motors. Experimental results on a 21kw IPMSM testing rig with Brüel & Kjær's vibration sensing equipment validate the effectiveness of the proposed method. The following conclusions can be drawn:

1. The ASSGCN model utilizes the correlation analysis of the operating state force, acceleration, and vibration impedance matrices in the spatial dimension. The model predicts the vibration signals of different sensor sampling points by modeling the frequency spectrum features of vibration signals separately and using dynamic correlation analysis.
2. The reconstructed vibration signal is in good agreement with the actual response at a specific frequency point, demonstrating the validity of the proposed model. The lowest MAE is 0.1378 and 0.1956 under no-load and load conditions respectively.
3. The model exhibits high predictive accuracy for OCF at 91.24%, FRF at 94.32% and PAS at 96.2%. And the training loss of 0.67 can be achieved in 25 epochs within a short period indicates the expected performance.

The proposed method offers significant cost and time savings for vibration testing of electric powertrain applications. By reducing the number of sensors required, the overall monitoring cost can be reduced without compromising the effectiveness of fault detection and prediction. the ASSGCN model has the potential to have wider applications beyond specific IPMSM configurations. In summary, the proposed ASSGCN model offers a promising solution for reducing vibration testing costs, increasing efficiency, and improving the overall understanding of motor vibration characteristics. Its adaptability to different motor configurations and wider application in electric powertrain systems make it a valuable tool in the field of vibration analysis and monitoring. The model exhibits robustness in extracting force signal features, making it suitable for applications requiring vibration analysis in electric powertrain systems. In addition, the adaptability of the model to different signals and operating conditions can be further improved.

Chapter 5 The Study of Sensor Distribution Patterns and Random Masking Based on Vibration Sensor Reconstruction

Condition monitoring of motors is critical in a variety of electric powertrain systems, especially in electric transportation, pumping stations of nuclear power plants, etc. Vibration analysis based on sensor data is a popular topic in motor condition testing. As an essential part of condition monitoring, vibration testing can assist in detecting equipment failures, assessing operational status, and providing guidance on preventive maintenance. However, achieving high evaluation accuracy and reliability with fewer vibration sensors and thus reducing the cost of manual operation and maintenance of sensor networks is a challenge. This chapter presents a spatial-spectral based inductive graph neural network for mining vibration sensor-based clusters for spatial connectivity and spectral correlation. The proposed algorithm effectively

aggregates and extracts the features of sensor graph signals in the vicinity of the target location and reconstructs the vibration signals of the virtual sensor by convolutional networks. To verify the effectiveness of the proposed method, experimental verification has been carried out on a 21kw IPMSM testing rig with Brüel & Kjær's vibration sensing equipment.

5.1. Introduction

Permanent magnet synchronous motors (PMSMs) are widely used in various industrial manufacturing fields. Especially in the transportation industries including electric vehicles, ships, and aircraft, etc. As a core industrial facility, effective motor health monitoring is a topic of interest to the industry, such as timely damage detection, optimizing maintenance strategies and reducing resource requirements [197] – [200]. However, motor health monitoring techniques that are based on signal analysis require continuous processing of large amounts of collected sensor signal and the data is inevitably contaminated by random noise, resulting in additional monitoring costs. Health monitoring methods based on vibration signals have received widespread attention as the acquisition of vibration signals can be achieved by mounting velocity or acceleration sensors on the outer surface of the machine. Moreover, the construction of data-driven models based on large amounts of vibration data for predicting and estimating the vibration characteristics of a structure or system can reduce the number of sensors required and the density of arrangements, thereby reducing the demand for actual sensors and the cost of vibration testing.

Fig. 2-1 indicates the three methods for vibration monitoring. Monitoring techniques require non-destructive evaluation techniques to ensure their operability and system integrity. In [201] A new analytical modeling method is developed for modeling transverse vibrations to estimate the inherent frequency of a mechanical component. [202] proposes a method for monitoring the health of a motor at rest through impedance analysis. [203] defined noise characteristics provide a robust small-signal detection method for motor condition monitoring algorithms in harsh industrial environments, using a priori knowledge of harmonics in the motor current

spectrum to maintain performance under non-linear speed variations of the motor. In [204], multiple features with rms-CUMSUM and GRRMD-CUMSUM envelope spectra as two new health monitoring indicators are proposed for the performance degradation conditions of bearings. Extracting additional fault information from vibration signals with high background noise and intrinsic signals to represent the trend and rate of bearing degradation. Considering the susceptibility of sparsity measures (SMs) to impulse noise, [205] proposed an adaptive weighted signal preprocessing technique (AWSPT) to improve the effectiveness of SMs in quantifying the trochoidal aspects of repetitive transients in machine health monitoring. The lack of data, the low sampling frequency, and the interference with the precise control of the system pose a great challenge to the health assessment of high-speed rotating bearings. [206] Using changes in the system energy balance relationship to evaluate component degradation. CNN models are built to describe the energy balance relationship and a transfer learning approach is explored to capture the changes in model parameters as the bearing degrades. For motors under identical conditions, fault monitoring based on spectral analysis is difficult due to the magnetic asymmetry. [207] proposes guidelines for online test results performed under high slip conditions when the motor is stationary or starting to distinguish between magnetic asymmetry and rotor faults. Since bearing shocks are regarded as impulsive resistance torque disturbances, constant rotor flux linkage (CRFL) transient equivalent circuits were developed in [208] to analyze motor in the presence of these high-frequency mechanical disturbances to monitor different types of bearing failures. [209] propose that auxiliary frequency (AF) is injected into the current signal to enhance the characteristic frequency component of the fault. The traditional two-dimensional spectrum was transformed into a massive feature into a single-scale spectral representation to facilitate feature extraction for motor defect detection. [210] proposes a sparse grid-based optimization application for characterizing fault states. An efficient search for the minimum of the objective function on the grid created using hyperbolic cross points (HCP) minimizes the cost and complexity of the system. In general, the condition monitoring techniques for motors in previous research mainly include signal-based feature signature analysis, mathematical model-based diagnostic techniques, and data-driven artificial

intelligence algorithms. The signal collected by the sensors includes voltage and current, vibration and temperature, etc. The acquisition of a precise sensor signal and the construction of an accurate mathematical model are challenging in terms of equipment installation and calculation costs.

The magnetic force and its vibration are reduced by changing the axially varying permanent magnet pole width and copper ring, placing a magnetic slot wedge (MSW) at the slot opening [211]-[213]. Moreover, adding auxiliary winding with the capacitor is an effective way to reduce high frequency vibration [214]. Simplified current contours are used to remove the third harmonic component sum of radial forces [215][216]. Signal reconfiguration is an effective way to reduce monitoring costs. Despite the well variational performance of the time-frequency manifold (TFM) for the analysis of defective bearing vibration signals, the amplitude information is still affected by its non-linear processing. In [217], a signal reconstruction method combining (TFM) and sparse reconstruction are proposed to enhance the fault characteristics of rolling element bearings. Considering the shortcomings of single-scale vibration signal feature collection, [218] proposes a new joint multiple reconstruction autoencoder (JMRAE) with the training objective of jointly optimizing multiple reconstruction losses aimed at automatically capturing complementary and discriminative feature representations of vibration signals from different scales. Furthermore, noise pollution is a pressing issue for vibration signal analysis. In [219], a multi-scale filter reconstruction is proposed to suppress speed-independent components and noise in simulations under variable speed and noise conditions. [220] presents a kriging compressive sensing (KCS) method to reconstruct signals using data collected by the sensing platform. The kriging variance is used to determine the weight coefficients of the kriging-estimated virtual samples to distinguish the fidelity of the real measurements from the virtual samples. The contribution of this chapter was summarized as below:

- (1) Combining the inductive learning model to study the reconstruction efficiency of different sensor distributions.
- (2) Correlation features are extracted from sensor signals at different distances through

multi-scale information fusion.

- (3) Explore the impact of different sensor numbers and distribution locations on reconstruction efficiency.

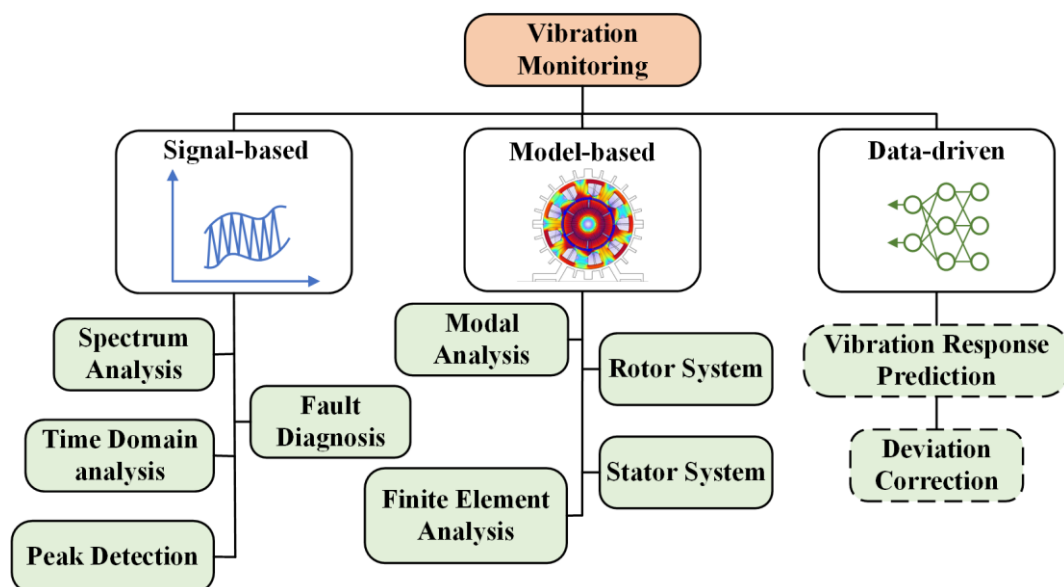


Fig. 5-1. Diagram of vibration monitoring

5.2. Signal Reconfiguration Kriging Problem Migration

This section provides a review of motor structure and vibration testing methods and provides a detailed description of transfer path analysis. Then a brief description of the kriging problem is given. Finally, the migration of signal reconstruction to the field of motor vibration testing is analyzed.

5.2.1. Modal Experiment Analysis

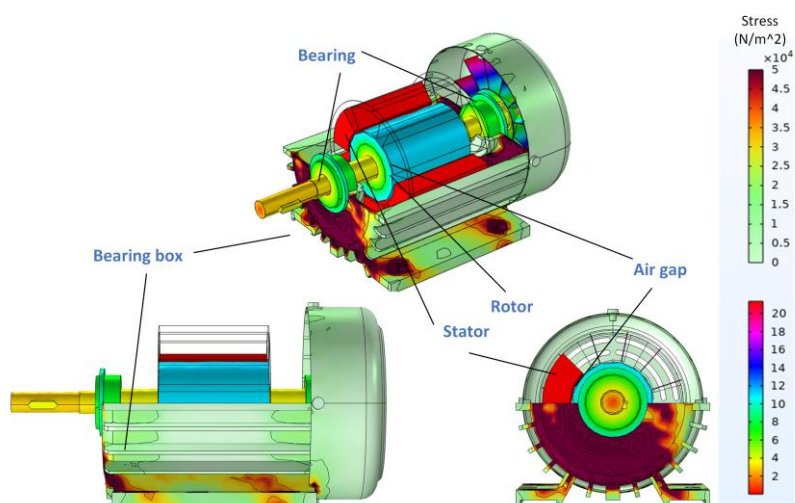


Fig. 5-2. Stator transfer path diagram.

Modal analysis is an experimental method used to determine the vibration characteristics of a structure or system, including natural frequencies, modal patterns, and damping ratios. It involves analysing the propagation path of vibration from the vibration source to the individual parts or elements of the structure. Fig. 5-2 indicates the basic structure of motor and as shown in Table 5-1, in Free vibration experiments, the structure or response of the structure to the vibration is measured using transducers such as accelerometers or displacement transducers. By performing a Fourier transform on the measured vibration signal, the frequency response function of the structure can be obtained, revealing the natural frequencies and vibration modes. In forced vibration experiments, the structure or system is subjected to external excitation at known frequencies and amplitudes. The excitation can be applied using a shaker, an electric motor, or an oscillator. By varying the excitation frequency, the frequency response function of the structure at different frequencies can be determined. This allows for the identification of the inherent frequency, modal shape, and damping ratio of the structure. In addition, Modal analysis plays a crucial role in understanding the dynamic behavior of structures and systems. It helps in design optimization, structural health monitoring, and fault diagnosis. By determining the modal parameters, engineers can assess the structural integrity, improve the performance, and ensure the safety of the analyzed structure or system.

TABLE 5-1 Modal Experimental Analysis

Experimental Method	Description	Measured Parameters
Free Vibration Experiment [222]	The structure is excited and released to undergo free vibration.	Natural frequencies, vibration modes
Forced Vibration Experiment [223]	The structure is subjected to known frequency and amplitude external excitation.	Frequency response function, natural frequencies, damping ratio
Operational Modal Analysis [223]	The vibration response of the structure under actual operating conditions is recorded.	Vibration signals, spectral analysis results, modal parameters

The experimental methods discussed above can be used individually or in combination to obtain accurate modal parameters. During the experiments, suitable transducers and data acquisition equipment are used to record the vibration signals and signal processing and analysis techniques are used to extract the modal parameters. The combined employment of these experimental methods allows for a comprehensive analysis and evaluation of the vibration characteristics of motor structures.

5.2.2. Transfer Path Analysis

The vibration signal collected by the vibration test contains the structural characteristics of the motor. And the occurrence of vibration noise is inevitable in the operation of motor drive systems. Excessive vibrations can impair the stability, reliability, and service life of the motor under different operating conditions. Minimizing and isolating all undesired noise and vibration is the main objective of NVH treatment. Typically, when analyzing vibrations in

complex mechanical systems, the data obtained from the measured target points are superimposed by different excitations passing through multiple transfer paths to the target response location. To better analyze and optimize the overall performance of a product, a comprehensive analysis of the excitation sources and various transmission paths of the mechanical system is required, which reflect the characteristics of the excitation process and appropriate vibration and appropriate vibration and noise reduction measures can be implemented. Therefore, transfer path analysis, as one of the experimental test methods can identify the main transfer paths that contribute most to the target point and solve vibration problems in mechanical systems by controlling or optimizing them.

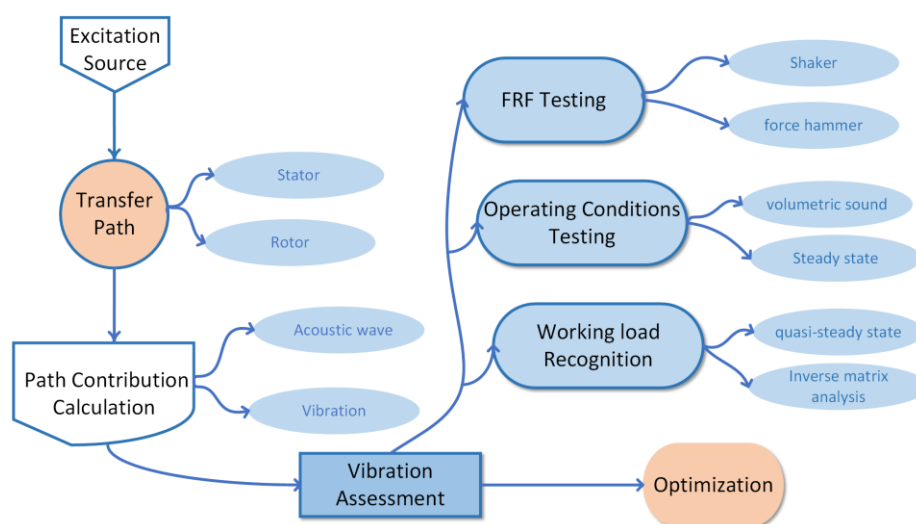


Fig. 5-3. Source-path-contribution flowchart of the motor system.

Depending on the type of data collected at the test point, the transfer path method can be divided into frequency domain analysis and time domain analysis. The former uses the load spectrum of the excitation source and the frequency response function of the path, combined with the excitation characteristics of the excitation source to analyze the key frequencies, which apply to the steady state conditions or quasi-steady state conditions of the mechanical system and can better reflect the overall frequency domain characteristics of the mechanical system, while the latter directly uses the time domain excitation signal of the excitation source and the filter formed by the impulse response function to achieve the transfer path analysis, which can obtain a non-steady state and transient events The latter directly uses a filter formed by the

excitation source and impulse response function to implement the transfer path analysis, allowing detailed information on non-stationary and transient events.

As shown in Fig. 5-3, the whole system is divided into three parts, and the response of the m^{th} reception point can be expressed as:

$$R_m(t) = \sum_{i=1}^n H_{m,i}(t) \cdot f_i(t) \quad (5-1)$$

Where $R_m(t)$ is the response at the m^{th} receiver point and $f_i(t)$ is the excitation force at the i^{th} source point. $H_{m,i}(t)$ is the transfer function between the i^{th} source point and the m^{th} receiver point. The above equation can be rewritten in matrix form as:

$$[R_1 \ R_2 \ \dots \ R_m] = [F_1 \ F_2 \ \dots \ F_n] \begin{bmatrix} H_{11} & H_{12} & \dots & H_{1m} \\ H_{21} & H_{22} & \dots & H_{2m} \\ \vdots & \vdots & \ddots & \vdots \\ H_{n1} & H_{n2} & \dots & H_{nm} \end{bmatrix} \quad (5-2)$$

where R_j ($j \leq m$) denotes the j^{th} the output of the system and F_i ($i \leq n$) denotes the i^{th} input to the system. H_{ij} denotes the transfer function from F_i to R_j which represents the transfer characteristic of the system. The form of the structure plays an important role in the transmission of vibrations. Therefore, when measuring the response, a preliminary subjective assessment is first made based on the form of the structure and a suitable location is found for mounting the transducer. Based on the results of the evaluation, the accelerometers are mounted to form an array under several rules. To obtain the characteristic frequency components of the individual signal points, the sensor signal was required to be preprocessed. The state matrix is obtained by using singular value decomposition (SVD). By obtaining the time-frequency spectrum of the signal at the source point, the components with high energy and more stability can be observed as characteristic components playing a major role in the vibration of the system. As the basis for transfer path analysis, the deployment of vibration sensor arrays and the collection of response signals are crucial. Analysis based on vibration signals is generally subject to interference from external noise.

5.2.3. Kriging Problem Description

The method based on transfer path analysis requires the installation of vibration sensors on the outer surface of the motor vibration test, where the number of sensors and the density of their distribution can have a critical impact on the analysis results. It is therefore attractive to build virtual sensors from known real sensors to reduce the cost of vibration testing. The construction of a virtual vibration sensor on the surface of a motor can be seen as a spatial interpolation problem [224]. Spatial interpolation is the issue of estimating the attribute value of any point (x, y) in the space under the condition of the observed value $Z_i = Z(X_i, Y_i)$ of a certain attribute of several discrete points (X_i, Y_i) in the known space. The formula for kriging interpolation is described as:

$$\widehat{Z}_o = \sum_{i=1}^n \lambda_i Z_i \quad (5-3)$$

Where the \widehat{Z}_o is the estimated value at point (X_o, Y_o) and λ_i is the weight factor, which satisfies a set of optimal coefficients with the smallest difference between the estimated value \widehat{Z}_o at point (X_o, Y_o) and the real value Z_o . Kriging interpolation considers the spatial correlation properties of the described objects in the process of data gridding so that the estimated value is close to the actual value. To optimize the objective function, the kriging error was expressed as follows:

$$\varepsilon_k^2(z_o) := Var(\widehat{z}_o - z_o) \quad (5-4)$$

Where $Var(\widehat{z}_o) = Var(\sum_{i=1}^n \lambda_i Z_i)$, the variance of \widehat{z}_o can be rewritten as follows:

$$Cov(\sum_{i=1}^n \lambda_i Z_i, \sum_{j=1}^n \lambda_j Z_j) = \sum_{i=1}^n \lambda_i \sum_{j=1}^n \lambda_j \cdot Cov(Z_i, Z_j) \quad (5-5)$$

Define semi variance function as below:

$$\mu_{ij} = \gamma^2 - Cov(Z_i, Z_j) \quad (5-6)$$

Where γ^2 represents variance and function can be rewritten as follows:

$$\mu_{ij} = \frac{1}{2}E[(Z_i - Z_j)^2] \quad (5-7)$$

Then, substituting the mentioned formulas, the kriging error was finally expressed as follows:

$$\varepsilon_k^2(z_o) = 2 \sum_{i=1}^n \lambda_i(\mu_{io}) - \sum_{i=1}^n \sum_{j=1}^n \omega_i \omega_j (\mu_{ij}) - \mu_{00} \quad (5-8)$$

To minimize the error of interpolation, the Lagrange multiplier solution is used to find a set of λ_i to obtain the desired variance. Given a target function $z = f(\varepsilon_k^2(z_o))$ and the additional condition to find the extreme point of $z = f(\varepsilon_k^2(z_o))$. Then the Lagrange function $J = F(\omega_1, \omega_2, \omega_n, \lambda_i)$ was created with the parameter λ_i . The first-order partial derivatives of $F = (f(\varepsilon_k^2(z_o)), \lambda_i)$ concerning λ_i be equal to 0.

5.3. The Multiscale-ssgc Model

As shown in Fig. 5-4, the sensor array in a vibration test requires information acquisition and pre-processing, which is then converted into the graph data input required by the algorithm. The sensors distributed on the surface of the motor can be seen as a cluster of nodes. Assume that the sensor cluster represents N spatial data points, $(P, F, n) = (p_i, f_i, n_i)_{i=1}^N$, where p_i , f_i and n_i represent the node position, the node characteristics and the label of data point i . The attributes of each node contain vibration information. The nodes information $F = (a_i, r_i, m_i)_{i=1}^d$ includes acceleration response, displacement, and impedance matrix data which collected by sensors. Generally, the proposed method aims to use the spatial information and attributes of each node to predict the spectral characteristics δ_* of the vibration of the target node n_* .

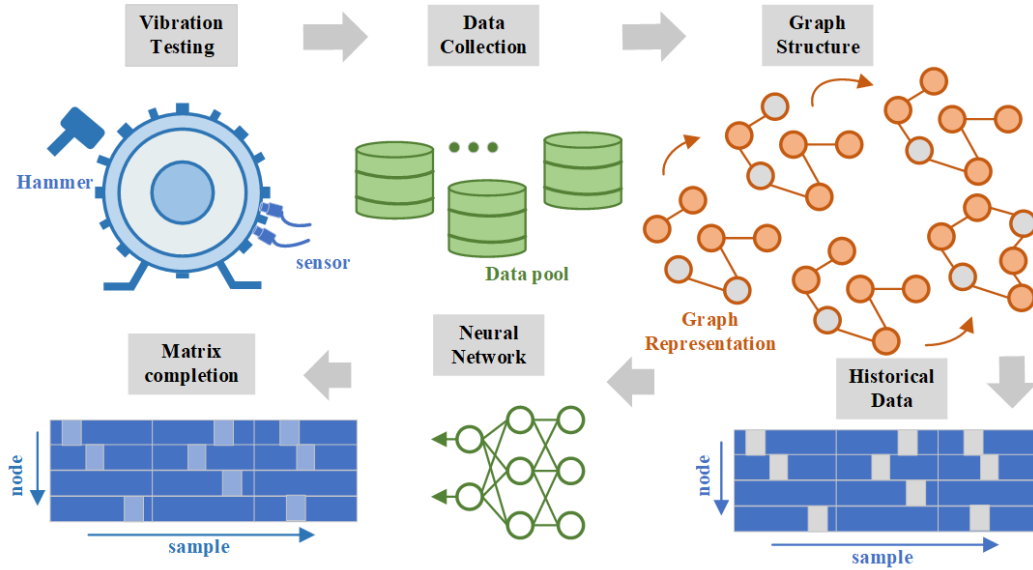


Fig. 5-4. Diagram of data-driven for signal reconstruction in vibration testing.

5.3.1. TPA-based Inertance Adjacency Matrix Construction

In vibration testing, to obtain the elements in the inertia matrix of the motor stator system, it is usually assumed that the mechanical system of the motor stator is divided into m equal parts along its circumference, that the m excitation forces $[F]_{m \times 1}$ are applied to the tooth surface of the motor stator and that the n acceleration responses $[Y]_{n \times 1}$ are measured on the surface of the motor stator frame. The response of the target point is equal to the sum of the responses of the excitation force transmitted by each point through self-inheritance $[H]_{ii}$ and mutual inertances $[H]_{ij}$. Each element of the inertances matrix $[H]$ can be measured by applying an excitation at a single point and collecting the responses at multiple points. The expression can be shown as below:

$$Y_n(\omega) = H_{n1}(\omega)F_1(\omega) + \dots + H_{nm}(\omega)F_m(\omega) = \sum_{j=1}^m H_{nj}(\omega)F_j(\omega) \quad (5-9)$$

where the $Y_n(\omega)$, $H_{nj}(\omega)$ and $F_j(\omega)$ represents the acceleration matrix, the inertance matrix and the excitation matrix in the spectrum dimension respectively. The inertia matrix $H_{nj}(\omega)$ is a convenient indicator to describe the health of industrial machinery systems [211], but it is

necessary to apply appropriate modeling and analysis to the matrix information to assess conditions with highly dynamic characteristics. The goal of the reconstruction is to predict virtual sensor signals at unknown locations based on previously observed vibration signals from the N -associated sensors on the network. Representation of the sensor network as a weighted directed graph $\zeta = (V, E, W)$, which represents nodes, edges, and weighted adjacency matrix $w \in \mathbb{R}^{N \times N}$. Mapping N historical graph signals to unknown T graph signals by learning a function $f(\cdot)$. The mapping relationship can be described as $[X^1, \dots, X^N; \zeta] \xrightarrow{f(\cdot)} [X^{T-1}, \dots, X^T]$. Therefore, a novel spatial-spectral graph model was proposed in this paper. As shown in Fig. 4, the following steps are performed to construct the spatial-spectral graph based on the inertia mentioned above.

- (1) Consider each response point $k = 1, 2, \dots, K$ as a node, connecting each pair of two nodes i and j as an edge \mathfrak{X}_{ij} .
- (2) Construction of heterogeneous subgraphs for training graph networks. The two types of subgraphs ζ^t and ζ^s are determined by the distribution of response points. The response nodes distribution is shown in Fig. 5.
- (3) Finally, the resulting graph includes different subgraphs of the distribution of nodes, i.e., $\zeta = \{\zeta^t, \zeta^s\}$.

Furthermore, the constructed subgraph can be described by its adjacency matrix $\{\zeta^t, \zeta^s\} = \{A_{ij}^t, A_{ij}^s\}$. the adjacency matrix required by the proposed method can be obtained as follows:

$$A_{ij} = \begin{cases} 1, & \text{if } \sigma_{if} \geq \epsilon \\ 0, & \text{otherwise} \end{cases} \quad i, j = 1, 2, \dots, N \quad (5-10)$$

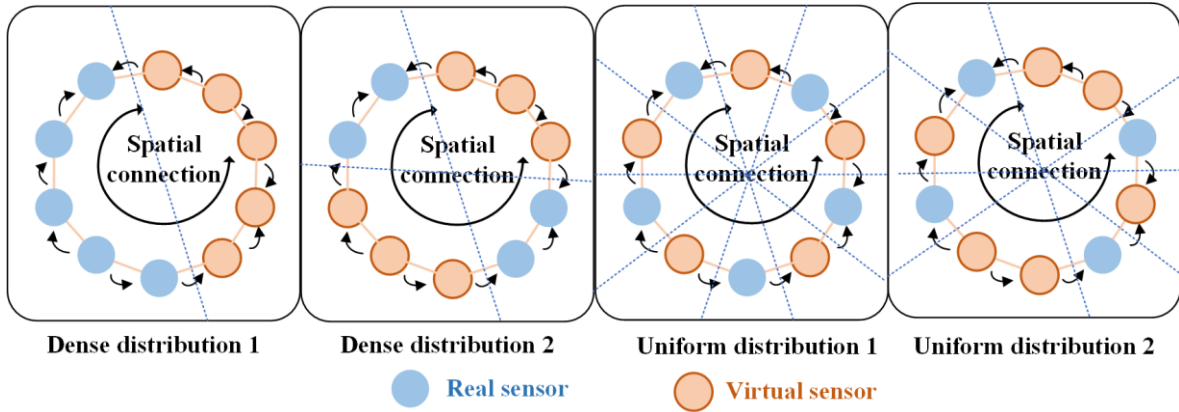


Fig. 5-5. Diagram of different sensor distribution.

where N represents the input nodes number, ϵ represents the threshold denotes the connection states. The article considers the similarity of node data as an indicator of node connectivity status. Employing the cosine similarity calculates the cosine of the angle between two vectors in a vector space as a measure of the magnitude of the difference between the individual nodes. The formula was shown as below:

$$\sigma_{if} = \frac{\sum_{i,j=1}^N x_{ij}^{fea} y_{ij}^{fea}}{\sqrt{\sum_{i,j=1}^n x_{ij}^{fea^2}} \sqrt{\sum_{i,j=1}^n y_{ij}^{fea^2}}} \quad (5-11)$$

where x_{ij}^{fea} and y_{ij}^{fea} represents the sample feature information of the target computing nodes.

The transfer path-based adjacency matrix is constructed to give the model a relationship between each response point, which is measured by the similarity between each node.

5.3.2. Attention-based Feature Fusion Module

The acquisition of measurements of basic parameters is necessary to characterize the vibration signal, measuring the displacement and acceleration response at a point on the vibrating component. By determining the intrinsic frequency of the measured body which is used to identify whether the component is moving properly. The graph convolution operation facilitates nodes to aggregate information from neighboring nodes. The depth at which a node aggregates its neighbors is referred to as p-order perception. Different levels of perception can

capture information at different levels of the original features. Moreover, it is crucial to consider multi-signal fusion and the aggregation of features from different signals in this paper. The purpose of this module is to find the relationship between proximity and global nodes using the attention mechanism and to reconstruct the vibration signal using multi-signal fusion.

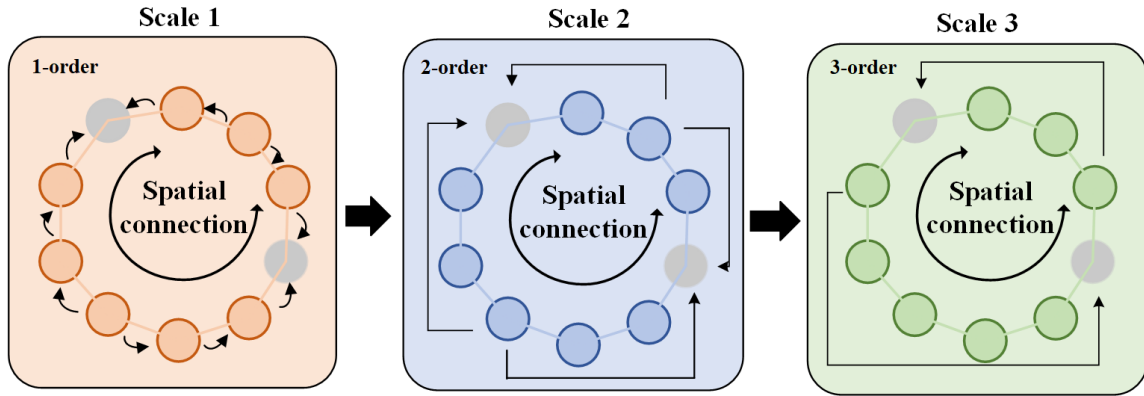


Fig. 5-6. Different adjacency information.

Instead of convolution kernels of different sizes, the scale of the channels is attended to by point-by-point convolution. To make the model as lightweight as possible by employing point-by-point convolution. Mining local and global features using the channel attention module. The channel attention of local features was extracted by point convolution The formula was shown as below:

$$L(X) = B(PWConv_2(\delta(B(PWConv_1(X)))))) \quad (5-12)$$

where the $PWConv$ point convolution reduces the input features channels to $1/r$ of the original number. r and B represent the channel scaling ratio and the batch norm layer, respectively. The number of channels is restored to the original number by point convolution.

The computed weights are used to obtain the output X after the attention operation on the input feature X' , the expression was shown as follows:

$$X' = X \otimes M(X) = X \otimes \sigma(L(X) \oplus g(X)) \quad (5-13)$$

The local channel information is kept at the same size as the input features, so adding the two requires a broadcast operation, \otimes denoting the multiplication of the corresponding elements

of the two feature maps.

5.3.3. Spatial-Spectral (SS) Diffusion Graph Convolution

This section presents the features fusion [225] and extraction of multi-scale node information using the proposed model. Modeling of spatial dependence by relating vibration signals to propagation processes that explicitly capture the structural properties of the vibration. The Diffusion graph convolution (DGCN) in DCRNN as the basic building block of the model. The expression was shown as follows:

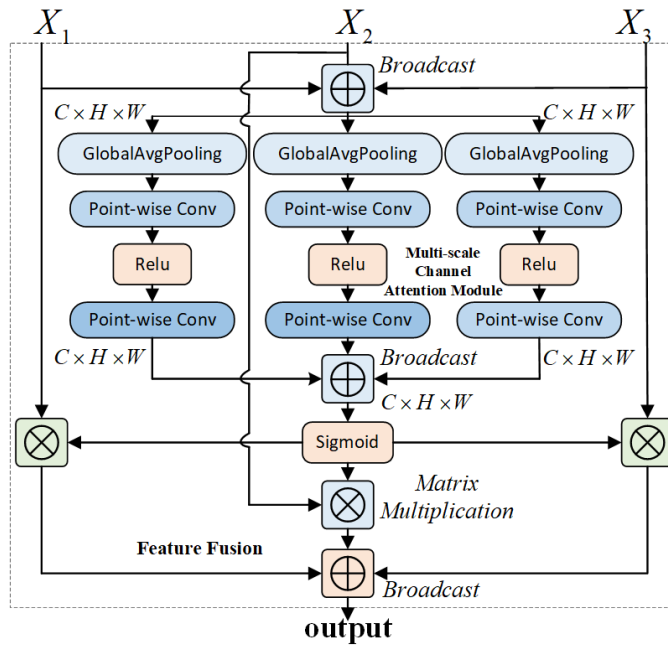


Fig. 5-7. Multiscale feature fusion module.

$$H_{n+1} = \sum_{k=1}^K T_k(\bar{W}_f)H_n\Theta_{b,l}^k + T_k(\bar{W}_b)H_n\Theta_{f,l}^k \quad (5-14)$$

Where K and Θ denote the order of diffusion convolution the learnable parameter, respectively. $\bar{W}_{f,b} = W_{sample}/(W_{sample})_{sum}$ denotes the forward/backward transfer matrices. H_{n+1} is the output of layer n with parameters $\Theta_{b,l}^k \in \mathbb{R}^{h \times z}$ and $\Theta_{f,l}^k \in \mathbb{R}^{h \times z}$. Compared with traditional GNNs that develop a fixed spatial structure, the applied model has a subgraph structure of each sample. Therefore, the neighborhood matrix W_{sample} that

captures the neighborhood information, and the direction of information transfer is also different in each sample. Moreover, the desired structural properties are obtained by adding a deeper network structure to get rid of the effect that the nodes being masked only pass zeros to their neighbors in the first layer. The formula is expressed as follows:

$$H_{n+2} = \sigma\left(\sum_{k=1}^K T_k(\bar{W}_f)H_{n+1}\Theta_{b,n+1}^k + T_k(\bar{W}_b)H_{n+1}\Theta_{f,n+1}^k\right) + H_{n+1} \quad (5-15)$$

Where the $\sigma(\cdot)$ is a nonlinear activation function and $\Theta_{b,n+1}^k \in \mathbb{R}^{h \times z}$ and $\Theta_{f,n+1}^k \in \mathbb{R}^{h \times z}$ are parameters of the next layer. The final different input samples contain information about the sensors with missing data. After obtaining the final graph representation, the reconstruction signal was output using one of the other DGCN. The equation was shown as follows:

$$Y_{out} = \sum_{k=1}^K T_k(\bar{W}_f)H_{n+2}\Theta_{b,n+2}^k + T_k(\bar{W}_b)H_{n+2}\Theta_{f,n+2}^k \quad (5-16)$$

Where Y_{out} represents the output of each branch after propagating the convolution layer based spatial-spectral (SS) diffusion module.

5.3.4. Training Strategy

To reconstruct the vibration signal of PMSM, a multi-signal fusion-based graph propagation neural network model is developed. In addition, to make the learned information transfer mechanism more general for all nodes, applying the total reconstruction error on observed and unknown nodes as our loss function was shown as below:

$$\mathcal{J}(\theta) = \frac{1}{NS} \sum_{i=1}^N \sum_{f=1}^S \|\hat{x}_{i,f} - x_{i,f}\|_F^2 \quad (5-17)$$

where θ denotes all learnable parameters in the proposed model. Then, the trained model will be validated in the test set for reconfiguration performance.

5.4. Experimental Verification

5.4.1. Data Description

To verify the validity of the proposed model, an experimental platform was constructed to collect motor vibration data. For the prototype inertia experiments, the stator tooth surface is chosen to have 10 force hammer excitation points, while the outer surface of the frame has 20 sensor acquisition points. To obtain the final response value, the average of the two points within the same group is taken. Both dynamic and static experiments are conducted with the prototype mounted in the same manner to ensure a consistent external physical environment. Brüel & Kjør's 4520 three-way accelerometers was used for the experiments. The testing rig of the experiments are shown in Fig. 5-8.

TABLE 5-2 Experimental Setup Parameters

Parameters	Value
Number of poles and slots	8/48
Rated power/kW	21
Out radius of stator/mm	200
Out radius of rotor/mm	123.4
Internal radius of rotor/mm	43
Length of core/mm	110

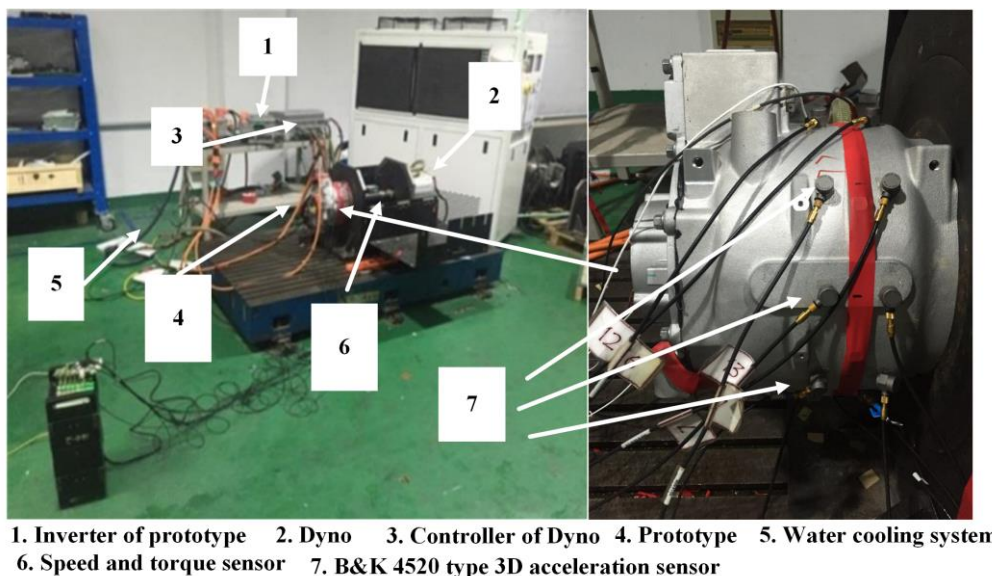


Fig. 5-8. Experiment rig.

TABLE 5-3 Experimental Conditions Description

Conditions	Conditions description
Condition 1	Speed: 2500rpm Load: No
Condition 2	Speed: 3000rpm Load: 66N
Condition 3	Speed: 3000rpm Load: No
Condition 4	Speed: 6000rpm Load: 66N
Condition 5	Speed: 6000rpm Load: No
Condition 6	Speed: 8200rpm Load: 24N
Condition 7	Speed: 8200rpm Load: 48N
Condition 8	Speed: 8200rpm Load: No

The frequency width of the data collected by the experimental test bench is 1-6400HZ as shown in Fig. 5-9. Moreover, to verify the effect of the algorithm on the reconfiguration of the motor under different operating conditions. The data set contains vibration signals at different load and speed conditions. The vibration data collected includes acceleration responses for 8 sets of different operating state, including 4 sets of no-load and load states respectively. The proposed model is constructed in the Pytorch framework. For comparison of accuracy, the root means square error (RMSE), the mean absolute error (MAE) and the mean absolute percentage error (MAPE) were used as metrics to evaluate the prediction performance of all methods. In particular, the MAPE is the preferred indicator for consideration, which can be defined as follow:

$$MAPE = \frac{100\%}{n} \sum_{i=1}^n \left| \frac{\hat{y}_i - y_i}{y_i} \right| \quad (5-18)$$

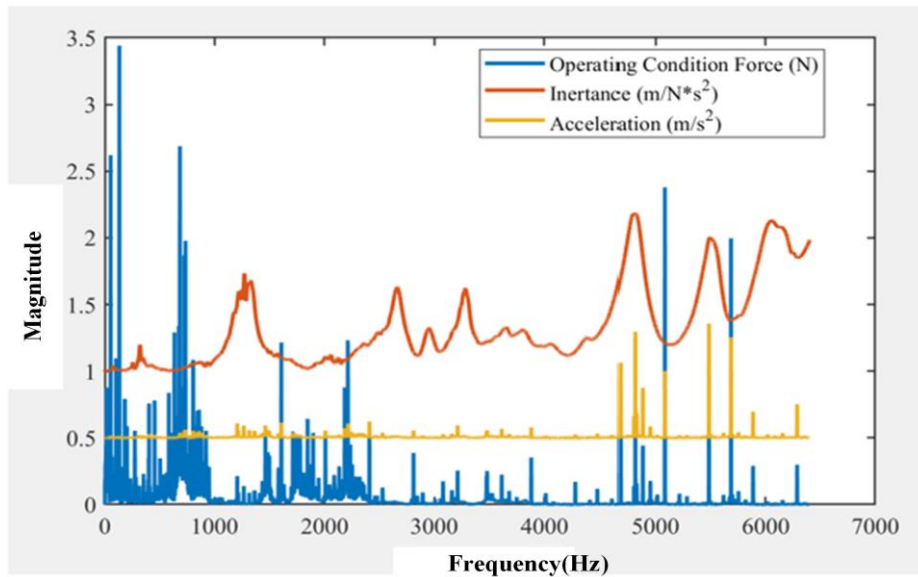


Fig. 5-9. The collecting data.

5.4.2. Accuracy of Reconstruction Performance with Different Operating Conditions

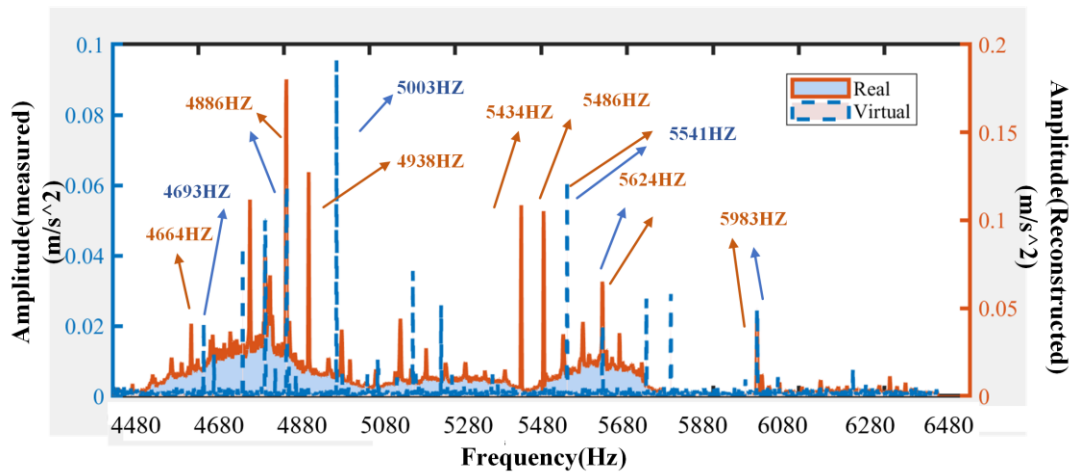


Fig. 5-10. Measured and reconstructed value of acceleration response under the condition of 8200rpm without load.

As shown in Table 5-4, the smallest MAE value of 0.0079 was observed for the operating conditions of 6000-66N in the different scenarios. It indicates that the average difference between the predicted and true values is relatively low, indicating a higher accuracy of

prediction. In contrast, the largest MAE of 0.0117 was observed for the operating conditions of 8200-48N, reflecting a higher average difference between the predicted and true values, indicating a decrease in prediction accuracy. Similarly, the smallest RMSE value of 0.0096 was found for the operating conditions of 3000-66N, which represents a large

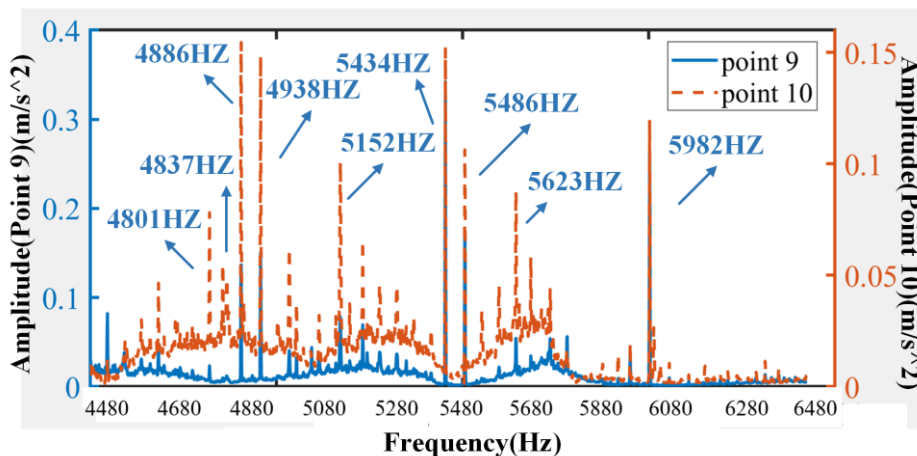


Fig. 5-11. Spectrum of acceleration response under the condition of 8200rpm without load for sensor point 9 and point 10.

average difference between predicted and true values, indicating a decrease in prediction accuracy. On the other hand, a maximum RMSE value of 0.0212 was observed for the 6000 no-load operating condition, reflecting a large mean squared deviation and indicating a decrease in prediction accuracy. Regarding the MAPE, a minimum value of 2.6237% was found for the 6000-66N operating condition, indicating a small mean percentage error between the predicted and true values, indicating high accuracy of the prediction. In contrast, the maximum MAPE of 5.6745% was found at the 6000 no-load operating condition, reflecting a larger mean percentage error and indicating a reduced level of prediction accuracy. Based on this analysis, it can be concluded that the proposed model exhibits variation in prediction accuracy under different operating conditions. It is worth noting that the 6000 no-load operating conditions show higher MAE, RMSE and MAPE, indicating that there are challenges in accurately predicting vibration characteristics under these specific conditions. In contrast, the 6000-66N operating conditions show relatively small MAPE, indicating that the proposed model performs better in predicting the vibration characteristics under these conditions. In

summary, the model shows a degree of generality in capturing the vibration characteristics of the motor under different operating conditions. However, the proposed model needs further refinement to address the different characteristics under various operating conditions.

TABLE 5-4 Experimental Results

Conditions	MAE	RMSE	MAPE
1	0.0077	0.0089	3.1038
2	0.011	0.0096	3.3212
3	0.0103	0.0158	3.4947
4	0.0079	0.0112	2.6237
5	0.0085	0.0212	5.6745
6	0.0093	0.0223	3.389
7	0.0117	0.0142	3.8207
8	0.0101	0.016	4.3275

5.4.3. Performance Comparison Under Different Sensor Organization Numbers

Analysis of the data presented reveals a noteworthy pattern in the relationship between the number of high frequency random points and the corresponding prediction errors, as measured by MAE, RMSE and MAPE. A clear observation is a gradual increase in MAE values as the number of high frequency random points increases. The minimum value of MAE is 0.0077 when a single random point is used for prediction, while the maximum value of MAE is 0.134 when nine random points are used. This escalating trend suggests that as the number of random points used for prediction increases, the accuracy of the prediction decreases. Similarly, the RMSE shows a similar pattern of incremental growth as the number of high frequency random points increases. The lowest RMSE of 0.0089 corresponds to a prediction using a single random point, while the highest RMSE of 0.0286 is observed when nine random points are used. The result suggests that the mean squared difference between the predicted and true values increases as the number of random points used for prediction increases. In addition, the MAPE shows a similar trend, gradually increasing with the number of high frequency random points. The

smallest MAPE recorded was 3.1038% when a single random point was used for prediction, while the largest MAPE observed was 20.9335% when nine random points were used, which suggests that the mean absolute percentage error between the predicted and true values increases as the number of predicted random points increases. The analysis highlights the consistent relationship between the number of high frequency random points and the prediction error. As the number of random points increased, the prediction error increased significantly, implying a decrease in prediction accuracy. The result can be attributed to the reduced amount of information obtained from fewer random points, which impedes the accuracy of the predictions.

TABLE 5-5 Experimental Results

Num	MAE	RMSE	MAPE
1	0.145	0.0097	10.984
2	0.134	0.0086	10.9335
3	0.0112	0.0133	20.5859
4	0.00093	0.0109	21.4495
5	0.0087	0.0016	23.83
6	0.0119	0.0166	11.2029
7	0.0105	0.019	21.041
8	0.0106	0.0115	3.6255
9	0.0077	0.0089	3.1038

As shown in Fig. 5-12, the data presented reveal valuable insights into the relationship between the number of sensors and prediction accuracy under different operating conditions. Specifically, it shows the effect of the number of sensors on the prediction error, as measured by MAE. Firstly, there is a clear upward trend in prediction error as the number of sensors decreases. The trend is consistently observed across the various sensor configurations, as evidenced by the increase in MAE as the number of sensors decreases. Furthermore, the analysis reveals variations in prediction error between different sensor locations, even within the same number of sensors. The variation emphasizes the impact of sensor positioning on prediction accuracy.

At a sensor count of 9, the lowest MAE of 0.0077 was achieved for the 2500 unloaded

condition, while the highest MAE of 0.0109 was achieved for the 6000 unloaded conditions. This suggests that certain sensor locations may have more informative data, thereby improving prediction accuracy. Over a wider range, increasing the number of sensors generally reduces prediction errors. It can be observed by the decreasing trend in MAE as the number of sensors increases from 1 to 9. The reduction indicates that the additional information provided by the extra sensors improves the accuracy of the prediction. However, it is important to note that the marginal gain decreases significantly when the number of sensors exceeds 4. Beyond this threshold, each additional sensor contributes less to the improved prediction accuracy, resulting in a lower rate of decrease in the MAE. The phenomenon is consistent with the concept of diminishing marginal returns, suggesting that the incremental benefit of including more sensors diminishes. While increasing the number of sensors can improve the accuracy of predictions, the growth in reconstruction efficiency slows down when the number of sensors exceeds a specific threshold. Careful consideration of the cost-benefit ratio is essential to determine the optimal number of sensors to achieve the required level of predictive accuracy.

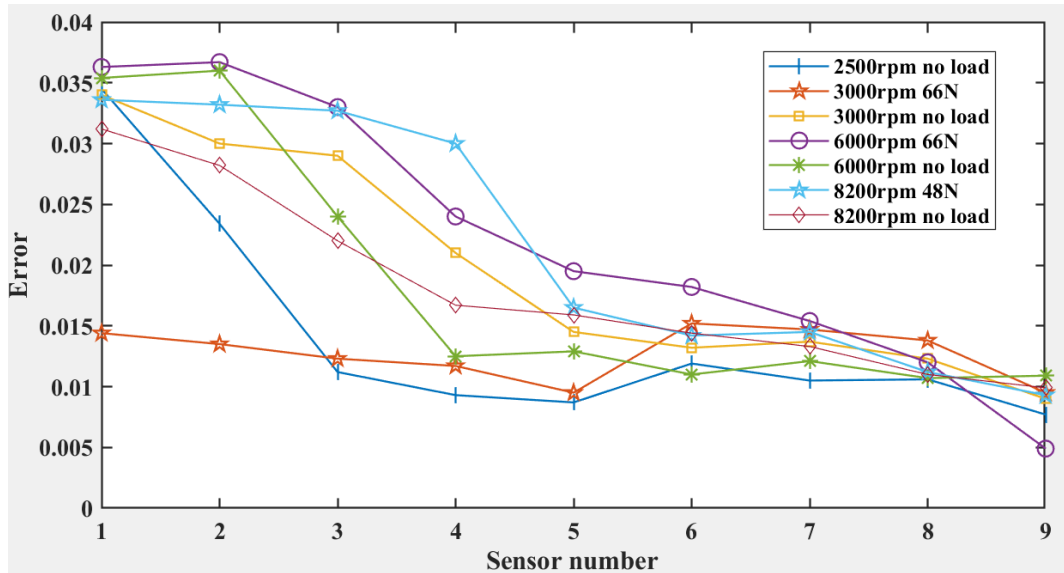


Fig. 5-12. Predicted error in different sensor numbers.

5.4.4. Various Sensor Distribution Discussion

As shown in Fig. 5-12, the reconstruction accuracy exhibited variation concerning the

number and distribution of sensors for a given operating state. Specifically, for the 2500 no-load operating state, the highest reconstruction accuracy was observed when using 5 densely distributed sensors, resulting in a minimum MAE of 0.0047. In contrast, when using 5 uniformly distributed sensors, the reconstruction accuracy was slightly lower, resulting in an MAE of 0.0036, which indicates that the effect of sensor number and distribution on reconstruction accuracy may show variability across different operating conditions. It suggests that the effect of the number and distribution of sensors on the reconstruction accuracy may show variability across different operational states. Furthermore, an increase in the number of sensors may lead to an increase in reconstruction accuracy. Assuming a consistent distribution scheme, the data show a decreasing trend in MAE for most operational states as the number of sensors is increased from 2 to 5. It is worth noting that the MAE continue to decrease as the sensor counts shift from 2 to 5 in a dense distribution of counts. It implies that increasing the number of sensors has the potential to improve the accuracy of the reconstruction. It is worth noting that different operating states may exhibit different levels of sensitivity in response to changes in the number of sensors and distribution. In the 8200-48N and 8200-no-load operating states, the increase in the number of sensors leads to relatively large changes in MAE, while the other operating states have relatively little effect due to the increase in number. Thus, it is important to carefully select the correct number of sensors and distribution strategy, especially for a given operating state. The vibration signal reconstruction data presented provides valuable insight into the effect of sensor number and distribution on reconstruction accuracy. Further analysis and experiments are required to gain a more comprehensive understanding of the reconstruction characteristics for different operational states to optimize the number of sensors and the distribution strategy to improve the reconstruction accuracy.

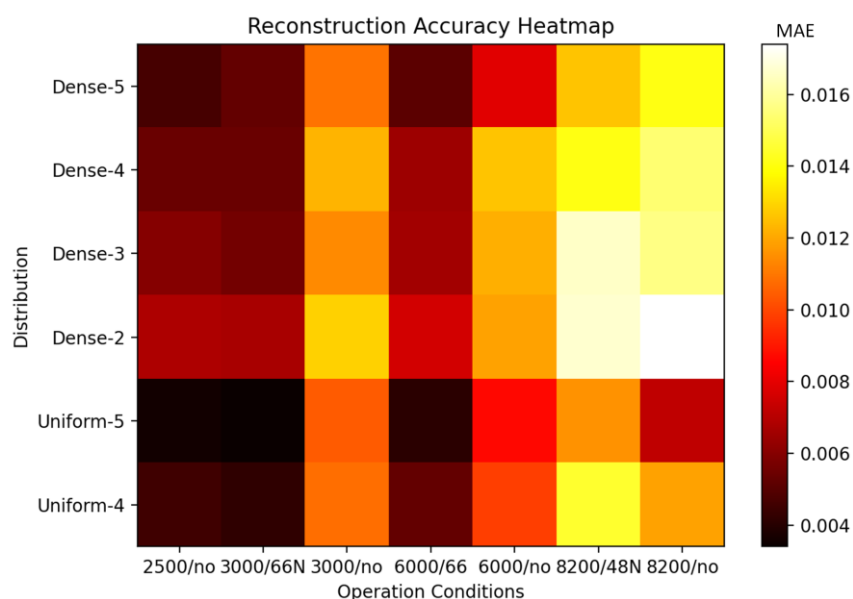


Fig. 5-13. Heatmap for different sensor distribution and operating conditions.

5.5. Conclusion

This chapter presents an algorithm based on a graphical neural network model combined with multi-scale information fusion to reconstruct virtual sensor information at the periphery of the motor stator in vibration testing. The following conclusions can be drawn:

1. The proposed model is capable of mining non-linear patterns and features in motor vibration signals. The reconstruction accuracy is improved by learning the complex interactions between nodes and using the connectivity information between sensors.
2. The experiment verification indicates that the reconstruction performance of uniformly distributed sensors better than densely distributed and the maximum error of 5.67% at 6000 rpm without load and the minimum error obtained using 9 real sensors signal is at 2.62%.
3. The effect of the number and distribution of sensors on the reconstruction accuracy may show variability across different operational states.

Furthermore, the results can be analysed as virtual sensor signals to provide a reference for the evaluation of different motor states, which reduces the cost of installing vibration sensors and increases the efficiency of vibration monitoring. The reconstruction reliability of the

proposed method varies with the number and distribution location of real sensors. In addition, the reconstruction performance improvement requires to be further considered in future work.

Chapter 6 Conclusions and Future Work

6.1. Conclusion

Electric vehicle motor, as the core power source, plays an important role in high efficiency, environmental protection, energy saving and sustainability. However, motors may face various faults and damages during operation, so accurate monitoring of motor status and timely diagnosis of faults become key tasks to ensure the reliability and safety of electric vehicles. Through the research in this paper, using data-driven algorithms, selecting appropriate sensors and reconstructing vibration sensor data signals with virtual positions through different arrangements, accurate and reliable vibration data reflecting the state of the motor can be obtained. Using the hybrid model small-sample learning framework, by processing and analyzing motor current in limited data, extracting key features and performing open-circuit fault diagnosis of the inverter to ensure the safety and reliability of electric vehicles. The main work and contributions of this study can be summarized as follows:

In Chapter 2, application of artificial intelligence techniques in motor fault diagnosis has been reviewed. Comprehensive studies of motor faults and their severity are still rare and have so far been limited to diagnosing faults in motors under specific operating conditions. It is difficult to detect faults in motors under light loads. In addition, the accuracy of fault diagnosis may be reduced due to fluctuations in rotor speed during data acquisition at different loads. Therefore, it remains an open challenge to consider the impact of motor operating conditions on AI-based fault diagnosis. Artificial intelligence for pattern recognition or fault diagnosis includes a large number of different types of mathematical tools, i.e. pre-processing, extraction and selection of appropriate statistical features, and selection of model parameters. It is a challenge to choose which tool is best suited for a particular problem and machine in different situations. Moreover,

there is a lot of scope for research in this area since condition monitoring techniques for fault detection and diagnosis of rotating machinery have been improved from traditional methods to artificial intelligence methods. Artificial intelligence-based diagnostic systems still have some challenging tasks to accomplish in terms of their efficiency, reliability, computation time, adequate database and robustness.

In Chapter 3, the performance of combining a mode-based data-driven hybrid model for VSI open-circuit fault diagnosis was investigated. An observer is used to obtain motor fault current residuals as input samples for fault information. A Siamese network framework based on few-shot learning is constructed for VSI open circuit fault diagnosis. The current signal in the fault condition contains uncertain components due to torque pulsation being used as features to input the diagnostic model can lead to unnecessary redundant diagnoses. By using the residual values as input signals, the uncertain current components are removed, resulting in better diagnostic performance. The problem of sample sparsity due to limited experimental conditions is addressed by constructing few-shot learning based on the Siamese network framework. The adopted attention-based algorithm can extract global features in the signal and obtain higher output classification performance. However, considering that changes in system parameters can affect diagnostic performance, it is required to further investigate the robustness of the hybrid model under varying system parameters.

In Chapter 4, an Attention-based Spatial-Spectral Graph Convolutional Network (ASSGCN) model was proposed to reduce the number of sensors required for vibration signal reconstruction in electric motors. The ASSGCN model utilizes the correlation analysis of the operating state force, acceleration, and vibration impedance matrices in the spatial dimension. The model predicts the vibration signals of different sensor sampling points by modeling the frequency spectrum features of vibration signals separately and using dynamic correlation analysis. The proposed method offers significant cost and time savings for vibration testing of electric powertrain applications. By reducing the number of sensors required, the overall monitoring cost can be reduced without compromising the effectiveness of fault detection and

prediction. the ASSGCN model has the potential to have wider applications beyond specific IPMSM configurations. In summary, the proposed ASSGCN model offers a promising solution for reducing vibration testing costs, increasing efficiency, and improving the overall understanding of motor vibration characteristics. Its adaptability to different motor configurations and wider application in electric powertrain systems make it a valuable tool in the field of vibration analysis and monitoring.

In Chapter 5, an algorithm based on a graphical neural network model combined with multi-scale information fusion was proposed to reconstruct virtual sensor information at the periphery of the motor stator in vibration testing. The proposed model is capable of mining non-linear patterns and features in motor vibration signals. The reconstruction accuracy is improved by learning the complex interactions between nodes and using the connectivity information between sensors. The experiment verification indicates that the reconstruction performance of uniformly distributed sensors better than densely distributed and the maximum error of 5.67% at 6000 rpm without load and the minimum error obtained using 9 real sensors signal is at 2.62%. The effect of the number and distribution of sensors on the reconstruction accuracy may show variability across different operational states. Furthermore, the results can be analyzed as virtual sensor signals to provide a reference for the evaluation of different motor states, which reduces the cost of installing vibration sensors and increases the efficiency of vibration monitoring. The reconstruction reliability of the proposed method varies with the number and distribution location of real sensors.

All in all, as far as the topic of motor condition monitoring based on data-driven algorithms is concerned, this study combines theoretical analysis and simulation/experimental verification, researches and develops data-driven artificial intelligence models to reconstruct motor vibration signals and Accurate diagnosis of open-circuit faults under the sample. This study achieved the following results:

- A comprehensive review of the application of artificial intelligence techniques in the field of motor condition detection

- Developing a Hybrid Drive Model for Motor Inverter Open-Circuit Faults.
- Development of a data-driven graph neural network to reconstruct motor vibration signals.
- Explore the impact of different sensor distributions on reconstruction performance and improve reconstruction efficiency.

6.2. Future Work

Based on the conclusions above and considering the limitations of the existed work, future research could be carried out in the following areas.

Enhancing fault detection and diagnosis: Future research can focus on improving the accuracy and efficiency of fault detection and diagnosis algorithms. This can involve exploring advanced machine learning techniques, such as deep learning or ensemble methods, to better analyze and interpret motor data for more precise fault identification.

Expanding the scope of fault detection: While this study primarily focused on diagnosing inverter open-circuit faults, future research can aim to detect and diagnose a wider range of motor faults. This can include other common faults like rotor misalignment, bearing wear, or stator winding faults. Developing comprehensive fault detection and diagnosis approaches will further enhance the reliability and safety of electric vehicles.

Integrating multiple sensing techniques: To improve the effectiveness of motor condition monitoring, future research can explore the integration of multiple sensing techniques. Combining vibration data with other types of sensor data, such as temperature, current, or acoustic data, can provide a more comprehensive understanding of the motor's condition and enable early detection of potential faults.

Real-time monitoring and predictive maintenance: Investigating real-time monitoring systems that can continuously monitor motor condition during vehicle operation is crucial. Future research can focus on developing real-time monitoring algorithms and techniques that enable proactive maintenance, allowing for timely interventions to prevent failures and optimize the performance and longevity of electric vehicle motors.

Field validation and scalability: Conducting extensive field validation studies using a diverse

range of electric vehicles and motor types will be important for validating the proposed methodologies in real-world scenarios. Additionally, considering the scalability of the proposed approaches to accommodate larger datasets and varying motor configurations will further enhance their practical applicability.

Cost-effective and practical implementation: Future research should also address the cost-effectiveness and practical implementation of motor condition monitoring techniques. Exploring cost-efficient sensor configurations, developing streamlined data acquisition and processing methods, and considering the integration of motor monitoring systems into existing vehicle infrastructure will facilitate the widespread adoption of motor condition monitoring technologies in electric vehicles.

Reference

- [1] H. Heno et al., "Trends in Fault Diagnosis for Electrical Machines: A Review of Diagnostic Techniques," in *IEEE Industrial Electronics Magazine*, vol. 8, no. 2, pp. 31-42, June 2014.
- [2] S. S. S. R. Sarathbabu Duvvuri, "Rotor Inter-turn Short-circuit Fault Diagnostics Relevant Modeling of Slip-Ring Induction Motor," 2018 IEEE 8th Power India International Conference (PIICON), 2018, pp. 1-6,
- [3] R. R. Kumar et al., "Induction Machine Stator Fault Tracking Using the Growing Curvilinear Component Analysis," in *IEEE Access*, vol. 9, pp. 2201-2212, 2021.
- [4] X. Wang, Z. Wang, Z. Xu, M. Cheng, W. Wang and Y. Hu, "Comprehensive Diagnosis and Tolerance Strategies for Electrical Faults and Sensor Faults in Dual Three-Phase PMSM Drives," in *IEEE Transactions on Power Electronics*, vol. 34, no. 7, pp. 6669-6684, July 2019.

Reference

- [5] J. Cai and X. Zhao, "Synthetic Hybrid-Integral-Threshold Logic-Based Position Fault Diagnosis Scheme for SRM Drives," in *IEEE Transactions on Instrumentation and Measurement*, vol. 70, pp. 1-8, 2021, Art no. 1500608.
- [6] M. Z. Ali, M. N. S. K. Shabbir, X. Liang, Y. Zhang and T. Hu, "Machine Learning-Based Fault Diagnosis for Single- and Multi-Faults in Induction Motors Using Measured Stator Currents and Vibration Signals," in *IEEE Transactions on Industry Applications*, vol. 55, no. 3, pp. 2378-2391, May-June 2019.
- [7] X. Wang, S. Lu and S. Zhang, "Rotating Angle Estimation for Hybrid Stepper Motors With Application to Bearing Fault Diagnosis," in *IEEE Transactions on Instrumentation and Measurement*, vol. 69, no. 8, pp. 5556-5568, Aug. 2020.
- [8] A. Soualhi, G. Clerc, and H. Razik, "Detection and diagnosis of faults in induction motor using an improved artificial ant clustering technique," *IEEE Trans. Ind. Electron*, vol. 60, no. 9, pp. 4053–4062, Sep. 2013.
- [9] F. Immovilli, C. Bianchini, M. Cocconcelli, A. Bellini, and R. Rubini, "Bearing fault model for induction motor with externally induced vibration," *IEEE Trans. Ind. Electron*, vol. 60, no. 8, pp. 3408–3418, Aug. 2013.
- [10] Chang, Z. Wang and C. S, "Online fault detection of induction motors using frequency domain-independent components analysis," in *Proc. IEEE Int. Symp. Ind. Electron*, Jun. 2011, pp. 2132–2137.
- [11] Z. Wang, C. S. Chang, and Y. Zhang, "A feature-based frequency domain analysis algorithm for fault detection of induction motors," in *Proc. 6th IEEE Conf. Ind. Electron. Appl*, Jun. 2011, pp. 27–32.
- [12] Motahari-Nezhad, M., & Jafari, S. M. (2021). "Bearing remaining useful life prediction under starved lubricating conditions using time-domain acoustic emission signal processing," *Expert Systems with Applications*, 168(December 2020), 114391.
- [13] Ugras, R. C., Alkan, O. K., Orhan, S., Kutlu, M., & Mugan, A. (2019). "Real-time high cycle fatigue estimation algorithm and load history monitoring for vehicles by

Reference

- the use of frequency-domain methods,” *Mechanical Systems and Signal Processing*, 118, 290–304.
- [14] E. H. El Bouchikhi, V. Choqueuse, and M. Benbouzid, “Induction machine faults detection using stator current parametric spectral estimation,” *Mech. Syst. Signal Process*, vols. 52–53, pp. 447–464, Feb. 2015.
- [15] Kenneth A. Loparo, M. L. Adams and M. Farouk Abdel-Magied, et al, “Fault detection and diagnosis of rotating machinery,” *IEEE Trans. on Industrial Electronics*, pp. 2000, 47(5): 1005- 1014.
- [16] Tan, Tommy W. S. Chow and H. Zhou, “HOS - based non-parametric and parametric methodologies for machine fault detection,” *IEEE Trans. on Industrial Electronics*, 2000, 47(5): 1051- 1059.
- [17] Benbouzid, Mohamed El Hachemi, “A review of induction motors signature analysis as a medium for faults detection,” *IEEE Trans. on Industrial Electronics*, 2000, 47(5): 984- 993.
- [18] P. Priyanga S, K. Krithivasan, P. S and S. Sriram V S, “Detection of Cyberattacks in Industrial Control Systems Using Enhanced Principal Component Analysis and Hypergraph-Based Convolution Neural Network (EPCA-HG-CNN),” *IEEE Transactions on Industry Applications*, vol. 56, no. 4, pp. 4394-4404, July-Aug. 2020.
- [19] M. Kaminski, C. T. Kowalski and T. Orłowska-Kowalska, “Application of radial basis neural networks for the rotor fault detection of the induction motor,” 2011 IEEE EUROCON - International Conference on Computer as a Tool, 2011, pp. 1-4.
- [20] E.M. Tag Eldin, H. R. Emara, E.M. Aboul-Zahab, Sh. S. Refaat, “Monitoring and Diagnosis of External Faults in Three-Phase Induction Motors Using Artificial Neural Network,” *IEEE.trans*, 1- 4244-1298-2007.
- [21] S. Premrudee preechacharn, T. Utthiyuung, K. Kruepengkul, P. Puongkaew, “Induction Motor Fault Detection and Diagnosis Using Supervised and Unsupervised

- Neural Networks,” IEEE ICIT'0Z, Bangkok Bangkok, THAILAND, 0-7803-7657-91021 - 2002.
- [22] R. Natarajan, “Failure Identification of Induction motors by sensing unbalanced stator currents,” IEEE Transactions on Energy Conversion, Vol. 4, No. 4, December 1989.
- [23] S. Aksoy, A. Mühürçü, “Recurrent Neural Network Based Nonlinear State Estimation for Induction Motors,” Journals of International Review of Electrical Engineering, pp. April 2011 (Vol. 6 N. 2) - Papers Part A.
- [24] M. Fernandez-Temprano, P. E. Gardel-Sotomayor, O. Duque-Perez, and D. Morinigo-Sotelo, “Broken bar condition monitoring of an induction motor under different supplies using a linear discriminant analysis,” in Proc. 9th IEEE Int. Symp. Diagnostics Electr. Mach., Power Electron. Drives, Aug. 2013, pp. 162–168.
- [25] J. Seshadrinath, B. Singh, and B. K. Panigrahi, “Investigation of vibration signatures for multiple fault diagnosis in variable frequency drives using complex wavelets,” IEEE Trans. Power Electron, vol. 29, no. 2, pp. 936–945, Feb. 2014.
- [26] W. S. Gongora, H. V. D. Silva, A. Goedtel, W. F. Godoy, and S. A. Q. da Silva, “Neural approach for bearing fault detection in three-phase induction motors,” in Proc. 9th IEEE Int. Symp. Diagnostics Electr. Mach., Power Electron. Drives, Aug. 2013, pp. 566–572.
- [27] O. Duque-Perez, L.-A. Garcia-Escudero, D. Morinigo-Sotelo, P.-E. Gardel, and M. Perez-Alonso, “Analysis of fault signatures for the diagnosis of induction motors fed by voltage source inverters using ANOVA and additive models,” Electr. Power Syst. Res, vol. 121, pp. 1–13, Apr. 2015.
- [28] Unal, M., Onat, M., Demetgul, M., & Kucuk, H, “Fault diagnosis of rolling bearings using a genetic algorithm optimized neural network.,” Measurement: Journal of the International Measurement Confederation, pp. 58(January 2021), 187–196., 2014.

Reference

- [29] D. Yu, J. Cheng, Y. Yang, "Application of EMD method and Hilbert spectrum to the fault diagnosis of roller bearings," *Mech. Syst. Signal Process*, 19 (3) (2005) 259–270.
- [30] Z.K. Peng, P.W. Tse, F.L. Chu, "An improved Hilbert-Huang transform and its application in vibration signal analysis," *J. Sound Vib*, 286 (2005) 187–205.
- [31] Ahmed, G. K. Singh and S. A. K. S, "Vibration signal analysis using wavelet transform for isolation and identification of electrical faults in induction machine," *Electr. Power Syst. Res*, vol. 68, pp. 119–136, 2004.
- [32] V. Iglesias, J. Grajal, M. A. Sánchez and M. López-Vallejo, "Implementation of a Real-Time Spectrum Analyzer on FPGA Platforms," *IEEE Transactions on Instrumentation and Measurement*, vol. 64, no. 2, pp. 338-355, Feb. 2015.
- [33] G. Betta, C. Liguori, A. Paolillo, and A. Pietrosanto, "A DSP-based FFT-analyzer for the fault diagnosis of rotating machine based on vibration analysis," *IEEE Trans. Instrum. Meas*, vol. 51, no. 6, Dec. 2002.
- [34] V.K. Rai, A.R. Mohanty, "Bearing fault diagnosis using FFT of intrinsic mode functions in Hilbert-Huang transform," *Mech. Syst. Signal Process*, 21 (8) (2007) 2607–2615.
- [35] Y. Qin, S. Qin, Y. Mao, "Research on iterated Hilbert transform and its application in mechanical fault diagnosis," *Mech. Syst. Signal Process*, 22 (Nov 2008) 1967–1980.
- [36] N. Mohanti, "Signal Processing Signal Filtering Detection".New York: Van Nostrand, 1987.
- [37] Palos, A. F. Atiya and A. G, "New results on recurrent network training: Unifying the algorithms and accelerating convergence," *IEEE Trans. Neural Netw*, vol. 13, pp. 765–786, May 2000.

Reference

- [38] Su, H., & Chong, K. T, "Induction machine condition monitoring using neural network modeling," *IEEE Transactions on Industrial Electronics*, 54(1), 241–249, 2007.
- [39] R. Jiang, S. Liu, Y. Tang, and Y. Liu, "A novel method of fault diagnosis for rolling element bearings based on the accumulated envelope spectrum of the wavelet packet," *J. Vibrat. Control*, vol. 21, no. 8, pp. 1580–1593, 2015.
- [40] J. Chen et al., "Wavelet transform based on the inner product in fault diagnosis of rotating machinery: A review," *Mech. Syst. Signal Process*, vols. 70–71, pp. 1–35, Mar. 2016.
- [41] Guerreiro, R., Cunha, C., & Teodoro, E, "Machine learning and multiresolution decomposition for embedded applications to detect short-circuit in induction motors," *Computers in Industry*, 129, 2021.
- [42] Hu, Y., Tu, X., Li, F., Li, H., & Meng, G. (2017). "An adaptive and touchless order analysis method based on enhanced empirical wavelet transform for fault detection of bearings with varying speeds," *Journal of Sound and Vibration*, 409(November 2017), 241–255.
- [43] Hu, W., Chang, H., & Gu, X. (2019). "A novel fault diagnosis technique for wind turbine gearbox," *Applied Soft Computing Journal*, 82, 105556.
- [44] Ding, F., Zhang, X., Wu, W., & Wang, Y, "A Fault Feature Extraction Method of Motor Bearing Using Improved LCD," *IEEE Access*, 220973–220979, 2020.
- [45] N. Rehman, M. M. Khan, M. I. Sohaib, M. Jehanzaib, S. Ehsan and K. McDonald-Maier, "Image fusion using multivariate and multidimensional EMD," 2014 IEEE International Conference on Image Processing (ICIP), 2014, pp. 5112-5116.
- [46] J.H. Ahn, D.-H. Kwak, and B.-H. Koh, "Fault detection of a roller-bearing system through the EMD of a wavelet denoised signal," *Sensors*, vol. 14, no. 8, pp. 15022–15038, 2014.

Reference

- [47] M. M. Garcillanosa, A. M. B. Flores, S. M. M. Jala and A. J. P. Toleda, "FPGA Based Powerline and Baseline Interference Removal in Electrocardiogram Using Modified EWT-DWT Filtering," 2019 2nd World Symposium on Communication Engineering (WSCE), 2019, pp. 142-146.
- [48] Zosso, K. Dragomiretskiy and D, "Variational mode decomposition," IEEE Trans. Signal Process, vol. 62, no. 3, pp. 531–544, Feb. 2014.
- [49] X.B. Wang, Z.X. Yang, and X.A. Yan, "Novel particle swarm optimization-based variational mode decomposition method for the fault diagnosis of complex rotating machinery," IEEE/ASMETrans. Mechatronics, vol. 23, no. 1, pp. 68–79, Feb. 2018.
- [50] J. S. Cheng, J. D. Zheng, and Y. Yang, "A nonstationary signal analysis approach—The local characteristic-scale decomposition method," J. Vibrat. Eng, vol. 25, no. 2, pp. 215–220, Feb. 2012.
- [51] Z. Wu, J. Cheng, and Y. Yang, "Autonomous dense local feature scale decomposition method and its application," J. Mech. Eng, vol. 6, no. 11, pp. 1464–1470, Dec. 2015.
- [52] L. Chenjie, W. Bin, and T. Tao, "Blind estimation algorithm of frequency hopping signal parameters using local feature scale decomposition," Signal Process, vol. 5, no. 3, pp. 308–313, Dec. 2015.
- [53] Huang, Y., Chen, C. H., & Huang, C. J, "Motor fault detection and feature extraction using an rnn-based variational autoencoder," IEEE Access, 7, 139086–139096, 2019.
- [54] V. Choqueuse, M. E. H. Benbouzid, Y. Amirat, and S, "Diagnosis of three-phase electrical machines using multidimensional demodulation techniques," IEEE Trans. Ind. Electron, vol. 59, no. 4, pp. 2014–2023, Apr. 2012.
- [55] L. A. O Martins, F. L. C. Pádua, and P. E. M. Almeida, "Automatic detection of surface defects on rolled steel using computer vision and artificial neural networks," Proc. IEEE IECON, Nov. 2010, pp. 1081–1086.

Reference

- [56] G. Duarte, M. I. C. Murguia and S, “An adaptive neural–fuzzy approach for object detection in dynamic backgrounds for surveillance systems,” *IEEE Trans Ind. Electron*, vol. 59, no. 8, pp. 3286–3298, Aug. 2012.
- [57] Prieto, M. D., Cirrincione, G., Espinosa, A. G., Ortega, J. A., & Henao, H, “Bearing fault detection by a novel condition-monitoring scheme based on statistical-time features and neural networks,” *IEEE Transactions on Industrial Electronics*, 60(8), 2013.
- [58] X. F. St-Onge, J. Cameron, S. Saleh and E. J. Scheme, “A Symmetrical Component Feature Extraction Method for Fault Detection in Induction Machines,” in *IEEE Transactions on Industrial Electronics*, vol. 66, no. 9, pp. 7281-7289, Sept. 2019.
- [59] C. Chen, B. Zhang, G. Vachtsevanos and M. Orchard, “Machine Condition Prediction Based on Adaptive Neuro-Fuzzy and High-Order Particle Filtering,” in *IEEE Transactions on Industrial Electronics*, vol. 58, no. 9, pp. 4353-4364, Sept. 2011.
- [60] Zeng, X. An and H, “Fault diagnosis method for spherical roller bearing of wind turbine based on variational mode decomposition and singular value decomposition,” *J. Vibroeng*, vol. 18, no. 6, pp. 3548–3556, Sep. 2016.
- [61] S. W. Fei, “Fault diagnosis of bearing based on wavelet packet transform phase space reconstruction-singular value decomposition and SVM classifier,” *Arabian J. Sci. Eng*, vol. 42, no. 5, pp. 1967–1975, May 2017.
- [62] D. T. Hoang and H. J. Kang, “A Motor Current Signal-Based Bearing Fault Diagnosis Using Deep Learning and Information Fusion,” *IEEE Transactions on Instrumentation and Measurement*, pp. 69(6), 3325–3333, 2020.
- [63] Zhang, X., Wang, B., & Chen, X, “Intelligent fault diagnosis of roller bearings with multivariable ensemble-based incremental support vector machine,” *Knowledge-Based Systems*, 89, 56–85., 2015.

Reference

- [64] Q. Hu, X. Si, A. Qin, Y. Lv and Q. Zhang, "Machinery Fault Diagnosis Scheme Using Redefined Dimensionless Indicators and mRMR Feature Selection," *IEEE Access*, vol. 8, pp. 40313–40326., 2020.
- [65] Zheng, J., Pan, H., & Cheng, J, "Rolling bearing fault detection and diagnosis based on composite multiscale fuzzy entropy and ensemble support vector machines," *Mechanical Systems and Signal Processing*, 85(December 2015), 746–759, 2017.
- [66] S. Das, P. Purkait, C. Koley and S. Chakravorti, "Performance of a load-immune classifier for robust identification of minor faults in induction motor stator winding," *IEEE Transactions on Dielectrics and Electrical Insulation*, pp. 21(1), 33–44, 2014.
- [67] Fengqi, W., & Meng, G, "Compound rub malfunctions feature extraction based on full-spectrum cascade analysis and SVM," *Mechanical Systems and Signal Processing*, 20(8), 2007–2021, 2006.
- [68] V. N. Ghate and S. V. Dudul, "Cascade neural-network-based fault classifier for three-phase induction motor," *IEEE Transactions on Industrial Electronics*, 58(5), 1555–1563, 2011.
- [69] S. Zhang, X. Li, M. Zong, X. Zhu and R. Wang, "Efficient kNN classification with different numbers of nearest neighbors," *IEEE Transactions on Neural Networks and Learning Systems*, 29(5), 1774–1785, 2018.
- [70] Reციoui, A., Benseghier, B., & Khalfallah, H, "Power system fault detection, classification and location using the K-Nearest Neighbors," 2015 4th International Conference on Electrical Engineering, ICEE 2015., 2016.
- [71] Yao, Q., Wang, J., Yang, L., Su, H., & Zhang, G, "A fault diagnosis method of engine rotor based on Random Forests," 2016 IEEE International Conference on Prognostics and Health Management, ICPHM 2016, 0–3. , 2016.
- [72] Patel, R. K., & Giri, V. K, "Feature selection and classification of the mechanical fault of an induction motor using random forest classifier," *Perspectives in Science*, 8, 334–337., 2016.

Reference

- [73] Seera, M., Lim, C. P., & Loo, C. K, “Motor fault detection and diagnosis using a hybrid FMM-CART model with online learning,” *Journal of Intelligent Manufacturing*, 27(6), 1273–1285, 2016.
- [74] T. Ince, S. Kiranyaz, L. Eren, M. Askar and M. Gabbouj, “Real-Time Motor Fault Detection by 1-D Convolutional Neural Networks,” *IEEE Transactions on Industrial Electronics*, 63(11), 7067–7075, 2016.
- [75] Y. Lei, F. Jia, J. Lin, S. Xing and S. X. Ding, “An Intelligent Fault Diagnosis Method Using Unsupervised Feature Learning Towards Mechanical Big Data,” *IEEE Transactions on Industrial Electronics*, 63(5), 3137–3147, 2016.
- [76] Chen, H., Jiang, B., Zhang, T., & Lu, N, “Data-driven and deep learning-based detection and diagnosis of incipient faults with application to electrical traction systems,” *Neurocomputing*, 396, 429–437, 2020.
- [77] S. Shao, R. Yan, Y. Lu, P. Wang and R. X. Gao, “DCNN-Based multi-signal induction motor fault diagnosis,” *IEEE Transactions on Instrumentation and Measurement*, 69(6), 2658–2669, 2020.
- [78] Liang, K., Qin, N., Huang, D., Fu, Y., & Hu, L, “Convolutional Recurrent Neural Network for Fault Diagnosis of High-Speed Train Bogie,” *Complexity*, 2018.
- [79] Chen, Z., Gryllias, K., & Li, W, “Mechanical fault diagnosis using Convolutional Neural Networks and Extreme Learning Machine,” *Mechanical Systems and Signal Processing*, 133, 106272, 2019.
- [80] Shenfield, A., & Howarth, M, “A novel deep learning model for the detection and identification of rolling element bearing faults,” *Sensors (Switzerland)*, 20(18), 1–24, 2020.
- [81] Zhang, W., Peng, G., Li, C., Chen, Y., & Zhang, Z, “A new deep learning model for fault diagnosis with good anti-noise and domain adaptation ability on raw vibration signals,” *Sensors (Switzerland)*, 17(2), 2017.

Reference

- [82] Zhang, W., Li, C., Peng, G., Chen, Y., & Zhang, Z, “A deep convolutional neural network with new training methods for bearing fault diagnosis under noisy environment and different working load,” *Mechanical Systems and Signal Processing*, 100, 439–453. , 2018.
- [83] J. S. L. Senanayaka, H. Van Khang and K. G. Robbersmyr, “Towards Self-Supervised Feature Learning for Online Diagnosis of Multiple Faults in Electric Powertrains,” *IEEE Transactions on Industrial Informatics*, 3203(c), 1–1., 2020.
- [84] L. Wen, X. Li, L. Gao and Y. Zhang, “A New Convolutional Neural Network-Based Data-Driven Fault Diagnosis Method,” *IEEE Transactions on Industrial Electronics*, 65(7), 5990–5998, 2018.
- [85] Jalayer, M., Orsenigo, C., & Vercellis, “Fault detection and diagnosis for rotating machinery: A model based on convolutional LSTM, Fast Fourier and continuous wavelet transforms,” *Computers in Industry*, 125, 103378. , 2021.
- [86] Zhao, R., Yan, R., Wang, J., & Mao, K, “ Learning to monitor machine health with convolutional Bi-directional LSTM networks,” *Sensors (Switzerland)*, 17(2), 2017.
- [87] Luo, T. Wong and Z, “Recurrent auto-encoder model for large-scale industrial sensor signal analysis,” in *Proc. Int. Conf. Eng. Appl. Neural Netw*, Jul. 2018, pp. 203–216.
- [88] Duan, L. D. Xu and L, “Big data for cyber-physical systems in industry 4.0: A survey,” *Enterprise Inf. Syst*, vol. 13, no. 2, pp. 148–169, Feb. 2019.
- [89] Y. Ma, K. Liu, Z. Guan, X. Xu, X. Qian, and H. Bao, “Background augmentation generative adversarial networks (BAGANs): Effective data generation based on GAN-augmented 3D synthesizing,” *Symmetry*, vol. 10, no. 12, p. 734, Dec. 2018.
- [90] L. Deng, “A tutorial survey of architectures, algorithms, and applications for deep learning,” *APSIPA Trans. Signal Inf. Process*, vol. 3, 2014.
- [91] K. Cheng, R. Tahir, L. K. Eric, and M. Li, “An analysis of generative adversarial networks and variants for image synthesis on MNIST dataset,” *Multimedia Tools Appl*, vol. 79, nos. 19–20, pp. 13725–13752, May 2020.

Reference

- [92] H. Apaydin, H. Feizi, M. T. Sattari, M. S. Colak, S. Shamshirband, and K.-W. Chau, “Comparative analysis of recurrent neural network architectures for reservoir inflow forecasting,” *Water*, vol. 12, no. 5, p. 1500, 2020.
- [93] C. Zhang, C. Xiong, and L. Wang, “A research on generative adversarial networks applied to next generation,” in *Proc. 14th Int. Conf. Comput. Sci. Educ. (ICCSE)*, Aug. 2019, pp. 913–917.
- [94] Y. O. Lee, J. Jo, and J. Hwang, “Application of deep neural network and generative adversarial network to industrial maintenance: A case study of induction motor fault detection,” *IEEE Int. Conf.*, Dec. 2017, pp. 3248–3253.
- [95] Z. Wang, J. Wang, and Y. Wang, “An intelligent diagnosis scheme based on generative adversarial learning deep neural networks and its application to planetary gearbox fault pattern recognition,” *Neurocomputing*, vol. 310, pp. 213–222, Oct. 2018.
- [96] L. Wen, X. Li, L. Gao and Y. Zhang, “A generative adversarial network-based intelligent fault diagnosis method for rotating machinery under small sample size conditions,” *IEEE Access*, pp. 7, 149736–149749, 2019.
- [97] Gan, M., Wang, C., & Zhu, C, “Construction of hierarchical diagnosis network based on deep learning and its application in the fault pattern recognition of rolling element bearings,” *Mechanical Systems and Signal Processing*, pp. 72–73, 92–104, 2016.
- [98] Shao, H., Jiang, H., Zhang, H., Duan, W., Liang, T., & Wu, S, “Rolling bearing fault feature learning using improved convolutional deep belief network with compressed sensing,” *Mechanical Systems and Signal Processing*, 100, 743–765, 2018.
- [99] M. Ma, C. Sun and X. Chen, “Discriminative Deep Belief Networks with Ant Colony Optimization for Health Status Assessment of Machine,” *IEEE Transactions on Instrumentation and Measurement*, 66(12), 3115–3125, 2017.

Reference

- [100] Zhang, T., Wang, W., Ye, H., Huang, D., Zhang, H., & Li, M, “Fault detection for ironmaking process based on stacked denoising autoencoders,” *Proceedings of the American Control Conference*, 2016-July, 3261–3267, 2016.
- [101] Lu, C., Wang, Z. Y., Qin, W. L., & Ma, J, “Fault diagnosis of rotary machinery components using a stacked denoising autoencoder-based health state identification,” *Signal Processing*, 130, 377–388, 2017.
- [102] Lee, H., Kim, Y., Kim, C.O, “A deep learning model for robust wafer fault monitoring with sensor measurement noise,” *IEEE Trans. Semicond. Manuf*, 30, 23–31, 2017a.
- [103] Jia, F., Lei, Y., Guo, L., Lin, J., & Xing, S, “A neural network constructed by deep learning technique and its application to intelligent fault diagnosis of machines,” *Neurocomputing*, 272, 619–628, 2018.
- [104] Mao, W., Feng, W., Liu, Y., Zhang, D., & Liang, X, “A new deep auto-encoder method with fusing discriminant information for bearing fault diagnosis,” *Mechanical Systems and Signal Processing*, 150, 107233, 2021.
- [105] Jia, F., Lei, Y., Lin, J., Zhou, X., & Lu, N, “Deep neural networks: A promising tool for fault characteristic mining and intelligent diagnosis of rotating machinery with massive data,” *Mechanical Systems and Signal Processing*, pp. 72–73, 303–315, 2016.
- [106] Z. Chen and W. Li, “Multisensor feature fusion for bearing fault diagnosis using sparse autoencoder and deep belief network,” *IEEE Transactions on Instrumentation and Measurement*, 66(7), 1693–1702., 2017.
- [107] J. An, P. Ai, C. Liu, S. Xu and D. Liu, “Deep Clustering Bearing Fault Diagnosis Method Based on Local Manifold Learning of an Autoencoded Embedding,” *IEEE Access*, pp. 9, 30154–30168., 2021.
- [108] T. Nakazawa and D. V. Kulkarni, “Wafer map defect pattern classification and image retrieval using convolutional neural network,” *IEEE Transactions on Semiconductor Manufacturing*, 31(2), 309–314, 2018.

Reference

- [109] Sabir, R., Rosato, D., Hartmann, S., & Guehmann, C, “LSTM based bearing fault diagnosis of electrical machines using motor current signal,” Proceedings - 18th IEEE International Conference on Machine Learning and Applications, ICMLA 2019, 613–618, 2019.
- [110] Tan, W., Sun, Y., Qiu, D., An, Y., & Ren, P, “Rolling bearing fault diagnosis based on single gated unite recurrent neural networks,” Journal of Physics: Conference Series, 1601(4), 2020.
- [111] Y. Ding, L. Ma, J. Ma, C. Wang and C. Lu, “A generative adversarial network-based intelligent fault diagnosis method for rotating machinery under small sample size conditions,” IEEE Access, pp. 7, 149736–149749, 2019.
- [112] J. Suwatthikul and S. Sornmuang, “Fault detection and diagnosis of a motor bearing shield,” Proceedings of the 6th IEEE International Conference on Intelligent Data Acquisition and Advanced Computing Systems, 2011, pp. 332-335.
- [113] H. Abu-Rub, S. Moin Ahmed, A. Iqbal, M. Rahimian and H. A. Toliyat, “Incipient bearing fault diagnostics for inverter fed induction motor drive using ANFIS,” The XIX International Conference on Electrical Machines - ICEM 2010, 2010, pp. 1-5.
- [114] M. Saeidi, J. Zarei, H. Hassani and A. Zamani, “Bearing fault detection via Park's vector approach based on ANFIS,” 2014 International Conference on Mechatronics and Control (ICMC), 2014, pp. 2436-2441
- [115] J. Zarei, H. Hassani, Z. Wei and H. R. Karimi, “Broken rotor bars detection via Park's vector approach based on ANFIS,” 2014 IEEE 23rd International Symposium on Industrial Electronics (ISIE), 2014, pp. 2422-2426,
- [116] Lei, Y., He, Z., Zi, Y., & Hu, Q, “Fault diagnosis of rotating machinery based on multiple ANFIS combination with GAs,” Mechanical Systems and Signal Processing, pp. 21, 2280–2294, 2007.

Reference

- [117] Lou, X., & Loparo, K. A, “Bearing fault diagnosis based on wavelet transform and fuzzy inference,” *Mechanical Systems and Signal Processing*, pp. 18, 1077–1095, 2004.
- [118] Tran, V. T., Yang, B. S., Oh, M. S., & Tan, A. C. C, “Fault diagnosis of induction motor based on decision trees and adaptive neuro-fuzzy inference,” *Expert Systems with Applications*, 36(2 PART 1), 1840–1849, 2009.
- [119] Q. T. Tran, S. D. Nguyen and T. Seo, “Algorithm for estimating online bearing fault upon the ability to extract meaningful information from big data of intelligent structures,” *IEEE Transactions on Industrial Electronics*, 66(5), 3804–3813, 2019.
- [120] J. Sun, C. Yan and J. Wen, “Intelligent bearing fault diagnosis method combining compressed data acquisition and deep learning,” *IEEE Transactions on Instrumentation and Measurement*, 67(1), 185–195, 2018.
- [121] Aucedo-Dorantes, J. J., Jaen-Cuellar, A. Y., Delgado-Prieto, M., Romero-Troncoso, R. de J., & Osornio-Rios, R. A, “Condition monitoring strategy based on an optimized selection of the high-dimensional set of hybrid features to diagnose and detect multiple and combined faults in an induction motor,” *Measurement*, 178(April), 109404., 2021.
- [122] M. Ganchev, B. Kubicek, and H. Kappeler, “Rotor Temperature Monitoring System,” *The XIX International Conference on Electrical Machines*, pp. 1–5, 2010.
- [123] S. Stipetic, M. Kovacic, Z. Hanic and M. Vrazic, “Measurement of Excitation Winding Temperature on Synchronous Generator in Rotation Using Infrared Thermography,” *IEEE Transactions on Industrial Electronics*, vol. 59, no. 5, pp. 2288–2298, 2012.
- [124] C. Mejuto, M. Mueller, M. Shanel, A. Mebarki, M. Reekie, and D. Staton, “Improved Synchronous Machine Thermal Modelling,” in *8th International Conference on Electrical Machines*, 2008, pp. 1–6.

- [125] Kirchgässner, W., Wallscheid, O., & Böcker, J, “Data-Driven Permanent Magnet Temperature Estimation in Synchronous Motors with Supervised Machine Learning,” ArXiv, 8969(c), 1–9, 2020.
- [126] A. Choudhary, D. Goyal and S. S. Letha, “Infrared Thermography-Based Fault Diagnosis of Induction Motor Bearings Using Machine Learning,” in *IEEE Sensors Journal*, vol. 21, no. 2, pp. 1727-1734, 15 Jan.15, 2021.
- [127] W. Xu, Y. Wan, T. Zuo and X. Sha, “Transfer Learning Based Data Feature Transfer for Fault Diagnosis,” *IEEE Access*, pp. 8, 76120–76129, 2020.
- [128] T. Boukra, A. Lebaroud and G. Clerc, “Statistical and neural-network approaches for the classification of induction machine faults using the ambiguity plane representation,” *IEEE Transactions on Industrial Electronics*, 60(9), 4034–4042, 2013.
- [129] A. Abid, M. T. Khan and M. S. Khan, “Multidomain Features-Based GA Optimized Artificial Immune System for Bearing Fault Detection,” *IEEE Transactions on Systems, Man, and Cybernetics: Systems*, pp. 50(1), 348–359, 2020.
- [130] B. Xue, M. Zhang, and W. N. Browne, “Particle swarm optimization for feature selection in classification: A multi-objective approach,” *IEEE Trans. Cybern*, vol. 43, no. 6, pp. 1656–1671, Dec. 2013.
- [131] X. Z. Gao, S. J. Ovaska, and X. Wang, “Genetic algorithm-based detector generation in negative selection algorithm,” in *Proc.,” IEEE Mountain Workshop Adapt. Learn. Syst.*, Logan, UT, USA, 2006, pp. 133–137.
- [132] X. Z. Gao, S. J. Ovaska, X. Wang, and M.-Y. Chow, “Multi-level optimization of negative selection algorithm detectors with application in motor fault detection,” *Intell. Autom. Soft Comput*, vol. 16, no. 3, pp. 353–375, 2010.
- [133] X. Z. Gao, H. Xu, X. Wang, and K. Zenger, “A study of negative selection algorithm-based motor fault detection and diagnosis,” *Int. J. Innov. Comput. Inf. Control*, vol. 9, no. 2, pp. 875–901, 2013.

- [134] A. Soualhi, G. Clerc and H. Razik, "Detection and diagnosis of faults in induction motor using an improved artificial ant clustering technique," *IEEE Transactions on Industrial Electronics*, 60(9), 4053–4062, 2013.
- [135] Z. Zhang et al., "Faster Multiscale Dictionary Learning Method with Adaptive Parameter Estimation for Fault Diagnosis of Traction Motor Bearings," *IEEE Transactions on Instrumentation and Measurement*, 70, 2021.
- [136] S. B. Jiang, P. K. Wong and Y. C. Liang, "A Fault Diagnostic Method for Induction Motors Based on Feature Incremental Broad Learning and Singular Value Decomposition," *IEEE Access*, 7, 157796–157806, 2019.
- [137] C. Gong et al., "Hybrid DC-Bus Capacitor Discharge Strategy Using Internal Windings and External Bleeder for Surface-Mounted PMSM-Based EV Powertrains in Emergency," *IEEE Transactions on Industrial Electronics*, pp. pp. vol. 68, no. 3, pp. 1905-1915, March 2021.
- [138] A.E.Kalas, "IGBT open gate drive fault diagnosis of a voltage fed three phase PWM inverter drive system," *14th International Middle East Power Systems*, Dec 2010.
- [139] Z. Wang, Y. Xu, P. Liu, Y. Zhang and J. He, "Zero-Voltage-Switching Current Source Inverter Fed PMSM Drives With Reduced EMI," *IEEE Transactions on Power Electronics*, vol. 36, no. 1, pp. 761-771, Jan. 2021.
- [140] X. Huang, K. Zhang, L. Wu, Y. Fang and Q. Lu, "Design of a Dual-Stator Superconducting Permanent Magnet Wind Power Generator With Different Rotor Configuration," *IEEE Transactions on Magnetics*, vol. 53, no. 6, pp. 1-4, June 2017, Art no. 8700204.
- [141] S. Yang, A. Bryant, P. Mawby, D. Xiang, L. Ran and P. Tavner, "An industry-based survey of reliability in power electronic converters," *2009 IEEE Energy Conversion Congress and Exposition*, 2009, pp. 3151-3157.
- [142] B. Gou, Y. Xu, Y. Xia, Q. Deng and X. Ge, "An Online Data-Driven Method for Simultaneous Diagnosis of IGBT and Current Sensor Fault of Three-Phase PWM

- Inverter in Induction Motor Drives," *IEEE Transactions on Power Electronics*, vol. 35, no. 12, pp. 13281-13294, Dec. 2020.
- [143] W. Zhao, S. Zhu, J. Ji, G. Liu and Y. Mao, "Analysis and Reduction of Electromagnetic Vibration in Fractional-Slot Concentrated-Windings PM Machines," *IEEE Transactions on Industrial Electronics*, vol. 69, no. 4, pp. 3357-3367, April 2022.
- [144] I. González-Prieto, M. J. Duran, N. Rios-Garcia, F. Barrero and C. Martín, "Open-Switch Fault Detection in Five-Phase Induction Motor Drives Using Model Predictive Control," *IEEE Transactions on Industrial Electronics*, vol. 65, no. 4, pp. 3045-3055, April 2018.
- [145] J. L. Contreras-Hernandez, D. L. Almanza-Ojeda, S. Ledesma-Orozco, A. Garcia-Perez, R. J. Romero-Troncoso and M. A. Ibarra-Manzano, "Quaternion Signal Analysis Algorithm for Induction Motor Fault Detection," *IEEE Transactions on Industrial Electronics*, vol. 66, no. 11, pp. 8843-8850, Nov. 2019.
- [146] W. Sleszynski, J. Nieznanski and A. Cichowski, "Open-Transistor Fault Diagnostics in Voltage-Source Inverters by Analyzing the Load Currents," *IEEE Transactions on Industrial Electronics*, vol. 56, no. 11, pp. 4681-4688, Nov. 2009.
- [147] C. Cecati, A. O. Di Tommaso, F. Genduso, R. Miceli and G. Ricco Galluzzo, "Comprehensive Modeling and Experimental Testing of Fault Detection and Management of a Nonredundant Fault-Tolerant VSI," *IEEE Transactions on Industrial Electronics*, vol. 62, no. 6, pp. 3945-3954, June 2015.
- [148] C. Wu, C. Guo, Z. Xie, F. Ni and H. Liu, "A Signal-Based Fault Detection and Tolerance Control Method of Current Sensor for PMSM Drive," *IEEE Transactions on Industrial Electronics*, vol. 65, no. 12, pp. 9646-9657, Dec. 2018.
- [149] F. R. Salmasi, "A Self-Healing Induction Motor Drive With Model Free Sensor Tampering and Sensor Fault Detection, Isolation, and Compensation," *IEEE Transactions on Industrial Electronics*, pp. vol. 64, no. 8, pp. 6105-6115, Aug 2017.
- [150] J. O. Estima, N. M. A. Freire and A. J. M. Cardoso, "Recent advances in fault diagnosis

- by Park's vector approach," *2013 IEEE Workshop on Electrical Machines Design, Control and Diagnosis (WEMDCD)*, 2013, pp. 279-288.
- [151] M. J. Duran, I. Gonzalez-Prieto, N. Rios-Garcia and F. Barrero, "A Simple, Fast, and Robust Open-Phase Fault Detection Technique for Six-Phase Induction Motor Drives," *IEEE Transactions on Power Electronics*, vol. 33, no. 1, pp. 547-557, Jan. 2018.
- [152] G. Wang. e. al, "Current Reconstruction Considering Time-Sharing Sampling Errors for Single DC-Link Shunt Motor Drives," in *IEEE Transactions on Power Electronics*, pp. vol. 36, no. 5, pp. 5760-5770, May 2021.
- [153] Q. An, L. Sun, K. Zhao and L. Sun, "Switching Function Model-Based Fast-Diagnostic Method of Open-Switch Faults in Inverters Without Sensors," *IEEE Transactions on Power Electronics*, vol. 26, no. 1, pp. 119-126, Jan. 2011.
- [154] J. Lu, Y. Hu, J. Liu, J. Wang and P. Li, "Fixed-Point Sampling Strategy for Estimation on Current Measurement Errors in IPMSM Drives," *IEEE Transactions on Power Electronics*, vol. 36, no. 5, pp. 5748-5759, May 2021.
- [155] J. Hang, S. Ding, J. Zhang, M. Cheng and Q. Wang, "Open-Phase Fault Detection in Delta-Connected PMSM Drive Systems," *IEEE Transactions on Power Electronics*, vol. 33, no. 8, pp. 6456-6460, Aug. 2018.
- [156] H. Berriri, M. W. Naouar and I. Slama-Belkhodja, "Easy and Fast Sensor Fault Detection and Isolation Algorithm for Electrical Drives," *IEEE Transactions on Power Electronics*, vol. 27, no. 2, pp. 490-499, Feb. 2012.
- [157] S. Shao, P. W. Wheeler, J. C. Clare and A. J. Watson, "Fault Detection for Modular Multilevel Converters Based on Sliding Mode Observer," *IEEE Transactions on Power Electronics*, vol. 28, no. 11, pp. 4867-4872.
- [158] Q. An, L. Sun and L. Sun, "Current Residual Vector-Based Open-Switch Fault Diagnosis of Inverters in PMSM Drive Systems," *IEEE Transactions on Power Electronics*, vol. 30, no. 5, pp. 2814-2827, May 2015.
- [159] D. U. Campos-Delgado and D. R. Espinoza-Trejo, "An Observer-Based Diagnosis

- Scheme for Single and Simultaneous Open-Switch Faults in Induction Motor Drives," *IEEE Transactions on Industrial Electronics*, vol. 58, no. 2, pp. 671-679, Feb. 2011.
- [160] A. Giantomassi, F. Ferracuti, S. Iarlori, G. Ippoliti and S. Longhi, "Electric Motor Fault Detection and Diagnosis by Kernel Density Estimation and Kullback–Leibler Divergence Based on Stator Current Measurements," *IEEE Transactions on Industrial Electronics*, vol. 62, no. 3, pp. 1770-1780, March 2015.
- [161] A. Arafat, S. Choi and J. Baek, "Open-Phase Fault Detection of a Five-Phase Permanent Magnet Assisted Synchronous Reluctance Motor Based on Symmetrical Components Theory," *IEEE Transactions on Industrial Electronics*, vol. 64, no. 8, pp. 6465-6474, Aug. 2017.
- [162] B. Gu, "Study of IPMSM Interturn Faults Part II: Online Fault Parameter Estimation," *IEEE Transactions on Power Electronics*, vol. 31, no. 10, pp. 7214-7223, Oct. 2016.
- [163] B. Wang, J. Wang, A. Griffio and B. Sen, "Stator Turn Fault Detection by Second Harmonic in Instantaneous Power for a Triple-Redundant Fault-Tolerant PM Drive," *IEEE Transactions on Industrial Electronics*, vol. 65, no. 9, pp. 7279-7289, Sept. 2018.
- [164] H. Guo, S. Guo, J. Xu and X. Tian, "Power Switch Open-Circuit Fault Diagnosis of Six-Phase Fault Tolerant Permanent Magnet Synchronous Motor System Under Normal and Fault-Tolerant Operation Conditions Using the Average Current Park's Vector Approach," *IEEE Transactions on Power Electronics*, vol. 36, no. 3, pp. 2641-2660, March 2021.
- [165] J. Park and J. Hur, "Detection of Inter-Turn and Dynamic Eccentricity Faults Using Stator Current Frequency Pattern in IPM-Type BLDC Motors," *IEEE Transactions on Industrial Electronics*, vol. 63, no. 3, pp. 1771-1780, March 2016.
- [166] B. Cai, Y. Zhao, H. Liu and M. Xie, "A Data-Driven Fault Diagnosis Methodology in Three-Phase Inverters for PMSM Drive Systems," *IEEE Transactions on Power Electronics*, vol. 32, no. 7, pp. 5590-5600, July 2017.
- [167] S. Ye, J. Jiang, J. Li, Y. Liu, Z. Zhou and C. Liu, "Fault Diagnosis and Tolerance Control

- of Five-Level Nested NPP Converter Using Wavelet Packet and LSTM," *IEEE Transactions on Power Electronics*, vol. 35, no. 2, pp. 1907-1921, Feb. 2020.
- [168] T. Wang, H. Xu, J. Han, E. Elbouchikhi and M. E. H. Benbouzid, "Cascaded H-Bridge Multilevel Inverter System Fault Diagnosis Using a PCA and Multiclass Relevance Vector Machine Approach," *IEEE Transactions on Power Electronics*, vol. 30, no. 12, pp. 7006-7018, Dec. 2015.
- [169] H. -J. Shin, J. -Y. Choi, H. -I. Park and S. -M. Jang, "Vibration Analysis and Measurements Through Prediction of Electromagnetic Vibration Sources of Permanent Magnet Synchronous Motor Based on Analytical Magnetic Field Calculations," in *IEEE Transactions on Magnetics*, vol. 48, no. 11, pp. 4216-4219, Nov. 2012.
- [170] E. K. Kim et al., "Vibration-Generation Mechanism and Reduction Method in Linear Iron-Cored Permanent-Magnet Synchronous Motors at Stationary State," in *IEEE/ASME Transactions on Mechatronics*, vol. 27, no. 5, pp. 3397-3406, Oct. 2022.
- [171] H. Yang and Y. Chen, "Influence of Radial Force Harmonics With Low Mode Number on Electromagnetic Vibration of PMSM," in *IEEE Transactions on Energy Conversion*, vol. 29, no. 1, pp. 38-45, March 2014.
- [172] J. Du, Y. Li, Z. Yu and Z. Wang, "Research On Radial Electromagnetic Force and Vibration Response Characteristics of Squirrel-Cage Induction Motor Fed By PWM Inverter," in *IEEE Transactions on Applied Superconductivity*, vol. 31, no. 8, pp. 1-4, Nov. 2021.
- [173] J. Le Besnerais, V. Lanfranchi, M. Hecquet and P. Brochet, "Optimal Slot Numbers for Magnetic Noise Reduction in Variable-Speed Induction Motors," in *IEEE Transactions on Magnetics*, vol. 45, no. 8, pp. 3131-3136, Aug. 2009.
- [174] S. -H. Lee, J. -P. Hong, S. -M. Hwang, W. -T. Lee, J. -Y. Lee and Y. -K. Kim, "Optimal Design for Noise Reduction in Interior Permanent-Magnet Motor," in *IEEE Transactions on Industry Applications*, vol. 45, no. 6, pp. 1954-1960, Nov.-dec. 2009.
- [175] Z. Zhao, H. Taghavifar, H. Du, Y. Qin, M. Dong and L. Gu, "In-Wheel Motor Vibration

- Control for Distributed-Driven Electric Vehicles: A Review," in IEEE Transactions on Transportation Electrification, vol. 7, no. 4, pp. 2864-2880, Dec. 2021.
- [176] W. Zhang, Y. Xu, H. Huang and J. Zou, "Vibration Reduction for Dual-Branch Three-Phase Permanent Magnet Synchronous Motor With Carrier Phase-Shift Technique," in IEEE Transactions on Power Electronics, vol. 35, no. 1, pp. 607-618, Jan. 2020.
- [177] R. Pile, E. devillers and J. Le Besnerais, "Comparison of Main Magnetic Force Computation Methods for Noise and Vibration Assessment in Electrical Machines," in IEEE Transactions on Magnetics, vol. 54, no. 7, pp. 1-13, July 2018.
- [178] S. Zuo, F. Lin and X. Wu, "Noise Analysis, Calculation, and Reduction of External Rotor Permanent-Magnet Synchronous Motor," in IEEE Transactions on Industrial Electronics, vol. 62, no. 10, pp. 6204-6212, Oct. 2015.
- [179] Z. Wu, Y. Fan, H. Chen, X. Wang and C. H. T. Lee, "Electromagnetic Force and Vibration Study of Dual-Stator Consequent-Pole Hybrid Excitation Motor for Electric Vehicles," in IEEE Transactions on Vehicular Technology, vol. 70, no. 5, pp. 4377-4388, May 2021.
- [180] J. Hong, S. Wang, Y. Sun and H. Cao, "A High-Precision Analytical Method for Vibration Calculation of Slotted Motor Based on Tooth Modeling," in IEEE Transactions on Industry Applications, vol. 57, no. 4, pp. 3678-3686, July-Aug. 2021.
- [181] J. Le Besnerais, V. Lanfranchi, M. Hecquet, P. Brochet and G. Friedrich, "Prediction of Audible Magnetic Noise Radiated by Adjustable-Speed Drive Induction Machines," in IEEE Transactions on Industry Applications, vol. 46, no. 4, pp. 1367-1373, July-Aug. 2010.
- [182] S. -H. Lee, I. -J. Yang, W. -H. Kim and I. -S. Jang, "Electromagnetic Vibration-Prediction Process in Interior Permanent Magnet Synchronous Motors Using an Air Gap Relative Permeance Formula," in IEEE Access, vol. 9, pp. 29270-29278, 2021.
- [183] Zhangjun Tang, P. Pillay, Yicheng Chen and A. M. Omekanda, "Prediction of electromagnetic forces and vibrations in SRMs operating at steady-state and transient

Reference

- speeds," in *IEEE Transactions on Industry Applications*, vol. 41, no. 4, pp. 927-934, July-Aug. 2005.
- [184] F. Chai, Y. Li, Y. Pei and Y. Yu, "Analysis of Radial Vibration Caused by Magnetic Force and Torque Pulsation in Interior Permanent Magnet Synchronous Motors Considering Air-Gap Deformations," in *IEEE Transactions on Industrial Electronics*, vol. 66, no. 9, pp. 6703-6714, Sept. 2019.
- [185] S. Das et al., "Sensitivity Analysis Based NVH Optimization in Permanent Magnet Synchronous Machines Using Lumped Unit Force Response," in *IEEE Transactions on Industry Applications*, vol. 58, no. 3, pp. 3533-3544, May-June 2022.
- [186] Z. Song, C. Liu, Y. Chen and R. Huang, "Air-Gap Permeance and Reluctance Network Models for Analyzing Vibrational Exciting Force of In-Wheel PMSM," in *IEEE Transactions on Vehicular Technology*, vol. 71, no. 7, pp. 7122-7133, July 2022.
- [187] M. Tsypkin, "The Origin of the Electromagnetic Vibration of Induction Motors Operating in Modern Industry: Practical Experience—Analysis and Diagnostics," in *IEEE Transactions on Industry Applications*, vol. 53, no. 2, pp. 1669-1676, March-April 2017.
- [188] W. Lang, Y. Hu, C. Gong, X. Zhang, H. Xu and J. Deng, "Artificial Intelligence-Based Technique for Fault Detection and Diagnosis of EV Motors: A Review," in *IEEE Transactions on Transportation Electrification*, vol. 8, no. 1, pp. 384-406, March 2022.
- [189] M. S. Rifaq et al., "A Simple Method for Identifying Mass Unbalance Using Vibration Measurement in Permanent Magnet Synchronous Motors," in *IEEE Transactions on Industrial Electronics*, vol. 69, no. 6, pp. 6441-6444, June 2022.
- [190] B. Zhao, X. Zhang, Z. Zhan, Q. Wu and H. Zhang, "Multiscale Graph-Guided Convolutional Network With Node Attention for Intelligent Health State Diagnosis of a 3-PRR Planar Parallel Manipulator," in *IEEE Transactions on Industrial Electronics*, vol. 69, no. 11, pp. 11733-11743, Nov. 2022.
- [191] M. Ni, X. Zhang, Y. Zuo, L. Liao and Z. Yang, "Electromagnetic Vibration Analysis for

Reference

- Permanent Magnet Synchronous Motor," in *Micromotors*, vol. 48, no. 1, Jan. 2015.
- [192] Guo, S., Lin, Y., Feng, N., Song, C., & Wan, H. (2019). Attention Based Spatial-Temporal Graph Convolutional Networks for Traffic Flow Forecasting. *Proceedings of the AAAI Conference on Artificial Intelligence*, 33(01), 922-929.”.
- [193] Q. Li, S. Liu and Y. Hu, "Vibration Characteristics of Permanent Magnet Motor Stator System Based on Vibro-Inertance Matrix Method," in *IEEE Transactions on Energy Conversion*, vol. 37, no. 3, pp. 1777-1788, Sept. 2022.
- [194] D. Chen, Y. Qin, J. Luo and S. Xiang, "Gated Adaptive Hierarchical Attention Unit Neural Networks for the Life Prediction of Servo Motors," in *IEEE Transactions on Industrial Electronics*, vol. 69, no. 9, pp. 9451-9461, Sept. 2022.
- [195] J. Song, F. Dong, J. Zhao, H. Wang, Z. He and L. Wang, "An Efficient Multiobjective Design Optimization Method for a PMSLM Based on an Extreme Learning Machine," in *IEEE Transactions on Industrial Electronics*, vol. 66, no. 2, pp. 1001-1011, Feb. 2019.
- [196] “Z. Zhang et al., "Faster Multiscale Dictionary Learning Method With Adaptive Parameter Estimation for Fault Diagnosis of Traction Motor Bearings," in *IEEE Transactions on Instrumentation and Measurement*, vol. 70, pp. 1-13, 2021”.
- [197] H. V. Dang, H. Tran-Ngoc, T. V. Nguyen, T. Bui-Tien, G. De Roeck and H. X. Nguyen, "Data-Driven Structural Health Monitoring Using Feature Fusion and Hybrid Deep Learning," in *IEEE Transactions on Automation Science and Engineering*, vol. 18, no. 4, pp. 2087-2103, Oct. 2021.
- [198] Y. Mao, S. Zuo and J. Cao, "Effects of Rotor Position Error on Longitudinal Vibration of Electric Wheel System in In-Wheel PMSM Driven Vehicle," in *IEEE/ASME Transactions on Mechatronics*, vol. 23, no. 3, pp. 1314-1325, June 2018.
- [199] W. Deng and S. Zuo, "Axial Force and Vibroacoustic Analysis of External-Rotor Axial-Flux Motors," in *IEEE Transactions on Industrial Electronics*, vol. 65, no. 3, pp. 2018-2030, March 2018.

Reference

- [200] Z. Xing, X. Wang and W. Zhao, "Optimization of Stator Slot Parameters for Electromagnetic Vibration Reduction of Permanent Magnet Synchronous Motors," in *IEEE Transactions on Transportation Electrification*, vol. 8, no. 4, pp. 4337-4347, Dec. 2022.
- [201] M. Zafarani, B. H. Jafari and B. Akin, "Lateral and Torsional Vibration Monitoring of Multistack Rotor Induction Motors," in *IEEE Transactions on Industrial Electronics*, vol. 68, no. 4, pp. 3494-3505, April 2021.
- [202] S. M. Shin, B. H. Choi and H. G. Kang, "Motor Health Monitoring at Standstill Through Impedance Analysis," in *IEEE Transactions on Industrial Electronics*, vol. 63, no. 7, pp. 4422-4431, July 2016.
- [203] S. Choi, E. Pazouki, J. Baek and H. R. Bahrami, "Iterative Condition Monitoring and Fault Diagnosis Scheme of Electric Motor for Harsh Industrial Application," in *IEEE Transactions on Industrial Electronics*, vol. 62, no. 3, pp. 1760-1769, March 2015.
- [204] J. Meng, C. Yan, G. Chen, Y. Liu and L. Wu, "Health Indicator of Bearing Constructed by rms-CUMSUM and GRRMD-CUMSUM With Multifeatures of Envelope Spectrum," in *IEEE Transactions on Instrumentation and Measurement*, vol. 70, pp. 1-16, 2021.
- [05] B. Hou, D. Wang, Y. Wang, T. Yan, Z. Peng and K. -L. Tsui, "Adaptive Weighted Signal Preprocessing Technique for Machine Health Monitoring," in *IEEE Transactions on Instrumentation and Measurement*, vol. 70, pp. 1-11, 2021.
- [206] D. Tang, M. Gong, L. Tian, J. Yu, J. Zhang and Q. Zhang, "Health Indicator Construction of High-Speed Rotating Bearings in Aerospace CMG Based on Physics-Inspired Machine-Learning Approach," in *IEEE Transactions on Instrumentation and Measurement*.
- [207] S. Lee, J. Hong, S. B. Lee, E. J. Wiedenbrug, M. Teska and H. Kim, "Evaluation of the Influence of Rotor Axial Air Ducts on Condition Monitoring of Induction Motors," in *IEEE Transactions on Industry Applications*, vol. 49, no. 5, pp. 2024-2033, Sept.-Oct.

2013.

- [208] F. Dalvand, A. Kalantar and M. S. Safizadeh, "A Novel Bearing Condition Monitoring Method in Induction Motors Based on Instantaneous Frequency of Motor Voltage," in *IEEE Transactions on Industrial Electronics*, vol. 63, no. 1, pp. 364-376, Jan. 2016.
- [209] D. Z. Li, W. Wang and F. Ismail, "An Enhanced Bispectrum Technique With Auxiliary Frequency Injection for Induction Motor Health Condition Monitoring," in *IEEE Transactions on Instrumentation and Measurement*, vol. 64, no. 10, pp. 2679-2687, Oct. 2015.
- [210] F. Duan and R. Živanović, "Condition Monitoring of an Induction Motor Stator Windings Via Global Optimization Based on the Hyperbolic Cross Points," in *IEEE Transactions on Industrial Electronics*, vol. 62, no. 3, pp. 1826-1834, March 2015.
- [211] S. Wang, J. Hong, Y. Sun and H. Cao, "Analysis and Reduction of Electromagnetic Vibration of PM Brush DC Motors," in *IEEE Transactions on Industry Applications*, vol. 55, no. 5, pp. 4605-4612, Sept.-Oct. 2019.
- [212] J. Hong, S. Wang, Y. Sun and H. Cao, "An Effective Method With Copper Ring for Vibration Reduction in Permanent Magnet Brush DC Motors," in *IEEE Transactions on Magnetics*, vol. 54, no. 11, pp. 1-5, Nov. 2018.
- [213] Z. Yang, S. Wang, Y. Sun and H. Cao, "Vibration Reduction by Magnetic Slot Wedge for Rotating Armature Permanent Magnet Motors," in *IEEE Transactions on Industry Applications*, vol. 56, no. 5, pp. 4882-4888, Sept.-Oct. 2020.
- [214] S. Xia and S. Wang, "Reduction of Switching Frequency Vibration of Induction Machines by Auxiliary Winding With Capacitors," in *IEEE Transactions on Energy Conversion*, vol. 37, no. 1, pp. 367-376, March 2022.
- [215] N. Kurihara, J. Bayless, H. Sugimoto and A. Chiba, "Noise Reduction of Switched Reluctance Motor With High Number of Poles by Novel Simplified Current Waveform at Low Speed and Low Torque Region," in *IEEE Transactions on Industry Applications*, vol. 52, no. 4, pp. 3013-3021, July-Aug. 2016.

Reference

- [216] T. Hara, T. Ajima, K. Hoshino and A. Ashida, "Carrier Electromagnetic Vibration of DC Voltage Fluctuation in Permanent-Magnet Synchronous Motor With Distributed Winding," in *IEEE Transactions on Industry Applications*, vol. 56, no. 5, pp. 4623-4631, Sept.-Oct. 2020.
- [217] F. Duan and R. Živanović, "Condition Monitoring of an Induction Motor Stator Windings Via Global Optimization Based on the Hyperbolic Cross Points," in *IEEE Transactions on Industrial Electronics*, vol. 62, no. 3, pp. 1826-1834, March 2015.
- [218] Q. He, H. Song and X. Ding, "Sparse Signal Reconstruction Based on Time–Frequency Manifold for Rolling Element Bearing Fault Signature Enhancement," in *IEEE Transactions on Instrumentation and Measurement*, vol. 65, no. 2, pp. 482-491, Feb. 2016.
- [219] H. Yu, K. Wang and Y. Li, "Multiscale Representations Fusion With Joint Multiple Reconstructions Autoencoder for Intelligent Fault Diagnosis," in *IEEE Signal Processing Letters*, vol. 25, no. 12, pp. 1880-1884, Dec. 2018.
- [220] J. Wang, F. Cheng, W. Qiao and L. Qu, "Multiscale Filtering Reconstruction for Wind Turbine Gearbox Fault Diagnosis Under Varying-Speed and Noisy Conditions," in *IEEE Transactions on Industrial Electronics*, vol. 65, no. 5, pp. 4268-4278, May 2018.
- [221] J. Sun, S. Liu, F. Zhang, A. Song, J. Yu and A. Zhang, "A Kriged Compressive Sensing Approach to Reconstruct Acoustic Fields From Measurements Collected by Underwater Vehicles," in *IEEE Journal of Oceanic Engineering*, vol. 46, no. 1, pp. 294-306, Jan. 2021.
- [222] K. Yamaguchi et al., "Experience-Based Lecture for Vibration Engineering Using Dual-Scale Experiments: Free Vibration of an Actual Seismic Building and Controlling the Vibration of Scale-Down Experimental Model," in *IEEE Access*, vol. 8, pp. 94767-94779, 2020.
- [223] Q. Li, S. Liu and Y. Hu, "Vibration Characteristics of Permanent Magnet Motor Stator System Based on Vibro-Inertance Matrix Method," in *IEEE Transactions on Energy*

Reference

Conversion, vol. 37, no. 3, pp. 1777-1788, Sept. 2022.

[224] Wu, Yuankai & Zhuang, Dingyi & Labbe, Aurelie & Sun, Lijun. (2020). Inductive Graph Neural Networks for Spatiotemporal Kriging.

[225] Y. Dai, F. Gieseke, S. Oehmcke, Y. Wu and K. Barnard, "Attentional Feature Fusion," in 2021 IEEE Winter Conference on Applications of Computer Vision (WACV), Waikoloa, HI, USA, 2021 pp. 3559-3568

[226] Shifat, Tanvir Alam & Hur, Jang-Wook. (2021). ANN Assisted Multi Sensor Information Fusion for BLDC Motor Fault Diagnosis. IEEE Access. 9. 9429-9441.